2011

Analysis of amyloid beta (A [beta]) peptides by capillary electrophoresis and laser-induced fluorescence anisotropy detection

Ryan Andrew Picou
Louisiana State University and Agricultural and Mechanical College

ANALYSIS OF AMYLOID BETA (Aβ) PEPTIDES BY CAPILLARY ELECTROPHORESIS AND LASER-INDUCED FLUORESCENCE ANISOTROPY DETECTION

A Dissertation
Submitted to the Graduate Faculty of the
Louisiana State University and
Agricultural and Mechanical College
in partial fulfillment of the
requirements for the degree of
Doctor of Philosophy

in

The Department of Chemistry

by
Ryan Andrew Picou
B.S., Nicholls State University
December 2011

DEDICATIONS

I dedicate this dissertation to my Angels – **Aubrey**, **Briana** & **Sarah**.

ACKNOWLEDGMENTS

To my Wife, Catherine Prosperie Picou, you are my best friend. You have lived through the ups and downs of graduate school with me, and I could have not done this without you. I always have and always will appreciate that you really listen. I thank you for being patient with me as we worked on completing this degree. As we grow as a couple and as parents, I look forward to a lifetime of happiness with you.

To my parents, Vickie and Bryce Picou, I want to thank you for the countless sacrifices, which have helped me get where I am today. Thank you for the continuing care that you give Catherine, the kids and me.

I would like to thank Dr. Gilman for his guidance as I journeyed through the graduate program. Observing your work ethic has greatly influenced my own. I will never forget the lengthy meetings when you would lecture us on being efficient in the lab and how you would break down the number of hours on campus versus number of hours working and getting things done. That was painful to sit through but still a valuable thing to hear. Perhaps your greatest talent, if I may, is your ability to recruit talented students. This brings me to my final acknowledgment.

To my dear friends Dr. Yohannes Rezenom and Dr. Rattikan Chantiwas (Jin), I thank both of you for being mentors to me especially in my early years of graduate school. We spent many hours together and have had great conversations (mostly not work-related) over many cups of coffee, and I look forward to our next cup.

TABLE OF CONTENTS

ABSTRACT

The goal of the research presented in this dissertation is to develop laser-induced fluorescence anisotropy (LIFA) detection for detecting and characterizing amyloid beta (Aβ) peptide aggregates separated by capillary electrophoresis (CE). Senile plaques composed primarily of aggregated Aβ (1-40) and Aβ (1-42) peptides have been found in the brains of Alzheimer's disease patients. These peptides are thought to be responsible for the disease pathology. A CE method using UV absorbance detection was developed for the quantification of Aβ (1-40) monomer and testing of Aβ monomer preparations for undesired aggregates (Chapter 2). Analyses of both Aβ (1-40) and Aβ (1-42) monomer and aggregate samples were performed by CE-UV (Chapter 3). The CE-UV experiments demonstrated that the CE method can separate Aβ monomers from aggregated Aβ. A lab-constructed CE-LIFA instrument was built to separate and detect individual Aβ fibrils using Thioflavin T (ThT) in the separation buffer as a fluorescent probe (Chapter 4). Separating and detecting individual Aβ aggregates opens the door to a better understanding of amyloid aggregation, which is normally studied with bulk methods, i.e. all aggregates measured at once. Individual Aβ aggregates detected by the CE-LIFA instrument were shown to exhibit fluorescence anisotropy, but all of the aggregate peaks exhibited similar anisotropy values using ThT as a fluorescent probe. Plots of fluorescence anisotropy vs. time did not produce peaks as expected. A data treatment method to facilitate visualization of peaks in CE-LIFA data was developed (Chapter 5). Thioflavin T spectroscopy in the presence of polystyrene spheres was studied to address potential false positives observed in preliminary experiments from Chapter 4 using ThT as a fluorescence probe for Aβ aggregate detection (Chapter 6). It was found that polystyrene spheres can enhance ThT fluorescence similar to Aβ. A CE-LIFA study of Aβ peptides covalently labeled with a fluorophore was performed to

overcome the apparent limitations of ThT. Aggregation of two different preparations of Aβ was studied as a function of time. Different forms of Aβ were separated and detected using CE-LIFA, and peaks resulting from different forms of Aβ exhibited different fluorescence anisotropy values.

CHAPTER 1

INTRODUCTION

1.1 Amyloid Proteins and Amyloidogenesis

There are over 20 amyloid-forming proteins that are known to be associated with human diseases [1]. Several amyloid proteins and their associated diseases are listed by Rambaran et al., Rochet et al. and Ecryod et al. [1-3]. Briefly, some diseases and their associated amyloid proteins include Type II diabetes (IAPP, or amylin), Parkinson's disease (α-synuclein), Huntington's disease (Huntingtin), Creutzfeldt-Jakob disease (prion protein) and Alzheimer's disease (beta amyloid (Aβ)).

Amyloid proteins misfold and self-assemble under physiological conditions to form aggregates. This aggregation process is referred to as amyloidogenesis. Ecroyd et al. have suggested that all proteins are capable of undergoing amyloidogenesis, but the amino acid sequence of the protein highly dictates a protein's predisposition to adopt amyloid aggregate structures [2]. Amyloid proteins are soluble prior to self-assembly but become more insoluble as aggregation progresses, eventually leading to mature, fully-formed fibrils. Not all proteins that self-assemble can be characterized as amyloidogenic. Proteins are characterized as "amyloid" by the cross β-sheet structure that they form as a result of aggregation. Amyloidogenesis is complex, and many transient and metastable intermediate aggregates existing between monomers and fibrils. It is believed that the term "amyloid" was derived from "corpus amygdaloideum", which is latin for "amygdale". Amygdala is the name of neurons located in the brain's temporal lobe that have an effect on memory.

The nucleation-dependent polymerization pathway is a theory that explains the mechanism of amyloid fibril formation [4]. According to this theory, monomers self-assemble in

solution to form a nucleus, i.e. “nucleation”. Remaining free monomers in solution add to the nucleus and extend its dimensions, i.e. polymerization. The nucleation-dependent polymerization reaction follows first-order kinetics, with nucleation being the rate-limiting step followed by the thermodynamically favored polymerization step [4,5].

Research has shown that the process of monomers aggregating to form fully-formed fibrils produces several complex intermediate and transient structures that exist between monomers and fibrils [6-8]. Each intermediate aggregate and fully-formed fibril will potentially be unique in size, shape and structure. Intermediates can be in the form of oligomers, i.e. dimmers, trimers, tetramers, etc., or protofibrils, which are structures intermediate in size between oligomers and fully-formed fibrils. Takahashi et al. schematically illustrated the aggregation process from monomers to fibrils in a recent article [9]. Aβ species in solution have been shown to reach a dynamic equilibrium with a reproducible end point of approximately 1 μM unpolymerized monomer [10]. Different amyloid proteins do not have similar primary sequences or monomer structures, but the aggregates they form have common structural features. For example, β-sheet secondary structures and rod-shaped 3D structures that can be up to microns in length and roughly 10 nm in diameter. The overall size and shape between aggregates formed from the same amyloid protein can vary drastically [11,12].

1.2 Amyloid Beta (Aβ) Peptides and Alzheimer’s Disease

As previously mentioned, amyloid aggregation has been linked to human diseases [1]. The research covered in this dissertation focuses on the Amyloid beta (Aβ) peptide. The Aβ peptide has been found to be the major protein in the extracellular neuritic plaques of people who have Alzheimer’s disease (AD) [13,14]. Alzheimer’s disease is a form of senile dementia named after the German Physiologist Alois Alzheimer who originally described the pathology of AD

based on analyzing slices of neuronal tissue using microscopy in 1906. Alzheimer's disease is the most common form of dementia [15]. There are no biological markers to diagnose a living person with AD, and the greatest risk factor is age [15]. The main symptoms of AD are loss of memory and cognitive skills [15]. Diagnoses of AD can be accomplished through eliminating other potential sources of AD-like symptoms [15]. It is not clear if genetics plays a role in predisposing a person to AD, but genetics does appear to play a role in the timing of the disease onset [15].

The Aβ peptide is cleaved from the Amyloid precursor protein (APP) by the proteases α, β and γ secretases [16]. The APP found in neurons is a type 1 transmembrane glycoprotein that contains 695 amino acids and is abundantly expressed in neuronal tissues [17,18]. α secretase cleaves APP between amino acids 16 and 17, and produces a nontoxic soluble form of Aβ [16]. β secretase first cleaves off the extracellular domain of APP. The remaining transmembrane domain APP is then cleaved by γ secretases, which produces the form of Aβ that becomes neurotoxic [15,16,18].

Proteolysis of APP can produce different length Aβ peptides from 39 to 43 amino acids in length. The primary sequence of Aβ is shown below as the Aβ (1-43) amino acid isoform. Shorter isoforms of Aβ have the same primary sequence minus amino acids from the C-terminus of the peptide chain. The molecular weight of Aβ is about 4 kDa, depending on the isoform.

1 5 10 15 20
D A E F R H D S G Y E V H H Q K L V F F A
25 30 35 40
E D V G S N K G A I I G L M V G G V V I A T

The Aβ (1-40) and (1-42) peptides are the most abundant isoforms produced from APP cleavage. The cleaved Aβ segments from APP are released into the extracellular matrix and exist in human plasma and cerebrospinal fluid even in normal subjects [15,17]. The concentration of

Aβ in the cerebrospinal fluid is estimated to be in the low nanomolar range [19]. The secreted concentration of Aβ (1-42) is about 5 – 15% of Aβ (1-40) [20]. Interestingly, Aβ (1-42) is the most abundant form found in senile plaques of AD patients [21-24]. Aβ (1-42) is more neurotoxic relative to Aβ (1-40) [25]. Aβ (1-40) is found in association with blood vessels [21].

Under physiological conditions, the Aβ peptide accumulates in the brain, and, through aggregation, deposits as amyloid plaques [17]. The accumulation of Aβ plaques can be observed decades before the AD symptoms [20]. The amyloid hypothesis describes the accumulation of Aβ in the brain, the imbalance of Aβ production and clearance from neuronal tissue and how these events could be critical in AD pathology [13]. Aβ is protease-resistant due in part to racemization of aspartyl and seryl residues and cyclization of N-terminal glutamyl resides [24]. Additionally, racemization from the L-amino acids to D-amino acids could have an impact on the aggregation rate of Aβ peptide [26].

Fully formed Aβ fibrils have been found during autopsies performed on the brains of people who were diagnosed with AD. This is likely the reason that researchers initially targeted Aβ fibrils to prevent or treat AD. Small molecules and small designer-peptides that can potentially dismantle Aβ aggregates or inhibit their formation have been tested [16,27,28]. For example, Curcumin (Yang 2005), phenol-related compounds [29] and pixantrone and mitoxantrone [30] have been shown to inhibit Aβ aggregation in vitro. An effective disruptor of Aβ aggregates for clinical use must be necessarily small in order to cross the blood-brain barrier while still being specific enough to bind only neurotoxic Aβ. Small molecular inhibitors satisfy the former but can suffer from non-specific binding [28]. Designer-peptide inhibitors have the advantage of increased binding specificity, relative to small molecules [28,31]. Peptide-based inhibitors can be designed with specific chirality and level of hydrophobicity, both of which can

contribute to preventative and disruptive aggregation [28,31]. The central hydrophobic core of Aβ, amino acids 16 – 20, is known to play a critical role in Aβ oligomer production and is therefore a popular target for developing agonist of aggregation [32,33]. Other than small molecules and peptide inhibitors that target the Aβ peptide for prevention or disassembly of the aggregation, some researchers have investigated ways to treat AD by more indirect methods. One such method is the regulation of the proteolytic secretases that are responsible for cleaving APP and producing Aβ [34].

The previous paragraph discussed ways to treat, manage or prevent AD by dismantling or inhibiting Aβ aggregation. Arguably, the biggest challenge in developing methods to treat, manage or prevent AD is that there is no clearly defined neurotoxic Aβ aggregate. One hypothesis is that AD neurotoxicity is related to Aβ aggregate size, but this does not imply that there is a direct relationship between size and neurotoxicity. Large fibrils were initially suspected to be the toxic species of AD [32]. More recently, researchers have shown that smaller Aβ oligomers are also toxic and could be more toxic than larger Aβ aggregates [13,27,35,36]. One method to determine the cytotoxic potency of Aβ peptides is to monitor the cellular concentration of 3-(4,5-dimethyl-2-yl)-2,5-diphenyltetrazolium bromide (MTT) as a function of Aβ peptide exposure [37]. Normal cells reduce MTT and peptide-treated cells do not reduce MTT. By monitoring the concentration of MTT using absorbance spectroscopy at 570 nm, cytotoxic potency can be ascertained [37]. MTT assays have also been used to test inhibitors of aggregation [38]. It is possible that if smaller Aβ aggregates, such as oligomers are more neurotoxic relative to larger aggregates, disrupting or dismantling fully-formed aggregates in vivo could produce oligomers thus leading to enhanced AD neurotoxicity.

1.3 Preparation of Synthetic Aβ Peptides

The lack of analytical tools to characterize the plethora of sizes, shapes and structures of Aβ, from monomers to fully-formed fibrils, makes designing treatments for AD a major challenge. While synthetic Aβ monomer peptides are commercially available as lyophilized powders, no analytical standards for aggregates exist that can be used to develop analytical methods to characterize and quantify Aβ aggregates. Because no analytical standards of Aβ aggregates exist, developing methods to characterize Aβ aggregates relies heavily on the ability to reproducibly prepare high quality synthetic Aβ samples [39]. Reproducibility of Aβ samples is a major challenge because the final product is extremely sensitive to small preparation variations. Chapter 2 demonstrates this clearly. Several Aβ monomer samples were prepared by the same scientist using the same method, and some samples were found to contain unwanted Aβ aggregates while others were found to contain only Aβ monomers. There are several potential sources of Aβ preparation variability [40]. Briefly, some of these include the commercial source of the peptide, initial aggregation state and aggregation conditions including solvent polarity, pH, ionic strength and incubation temperature [40,41]. Moreover, errors associated with solid phase peptide synthesis of Aβ can be a potential source of irreproducible Aβ aggregation [42].

Methods have been developed that can provide reproducible Aβ preparations [42-44]. The first step in preparing synthetic Aβ samples from the lyophilized monomer is treating the lyophilized monomer with a solvent that will disaggregate any preformed aggregates that could act as seeds. Seeds are known to accelerate aggregation and increase polydispersity [11,44]. Pre-formed aggregates could be a result of synthetic impurities or improper storage conditions. An effective solvent to dismantle preformed aggregates should break down H-bonding between aggregates and be easily removable. Solvent removal can be performed under a stream of

oxygen-free and inert gas. Oxygen-free gas is important so that amino acids are not oxidized. Trifluoroacetic acid (TFA), hexafluorpisopropanol (HFIP), or a combination of the two, are common solvents used to initially treat the lyophilized monomer to dismantle pre-formed aggregates. For aggregation studies, incubation temperature is critical because the velocity of amyloid formation is highly dependent on temperature [4]. The velocity of amyloid formation at 25° C is reported to be only 10% of that at 37° C [4]. High ionic strength buffers and pH between 4 and 7 promote aggregation [40].

1.4 Analytical Methods for Studying Aβ Monomers and Aggregates

An ideal method for studying Aβ aggregation could monitor Aβ monomers, fibrils and all aggregates in between with a single technique that would provide size, structure and concentration information of each species detected in real time during aggregation. No single method is capable of this; however, several methods are routinely used that provide some of this information. Quantifying Aβ monomer has been achieved by UV absorbance spectroscopy [17,45]. The peptide bonds between the amino acids absorb in the low UV radiation range (~190 – 254 nm). To accurately quantify Aβ monomer in solution using UV absorbance, a linear concentration curve should be developed that has been calibrated to the exact protein concentration by amino acid analysis (AAA). The procedure of AAA involves hydrolysis of the peptide bonds followed by separation, detection and quantitation of the amino acids. A benefit to AAA is that any preexisting aggregates are also broken down to monomers and subsequently amino acids. This means that all of the peptide is accounted for, which results in a more accurate determination of the peptide concentration. Amino acid analysis can also provide relative amino acid composition of a protein to help verify the identity of the protein.

It is not clear that UV absorbance spectroscopy can accurately determine the concentration of Aβ aggregates. Because aggregates are made up of Aβ monomer subunits, one might expect that an aggregate's absorbance would scale with *n* monomer units. No literature was found to support or dispute this. It is unknown how molar absorptivity scales with aggregation. Moreover, unlike monomers, large aggregates will significantly scatter light in addition to absorbing it. A UV detector would not differentiate between scattered light and absorbed light, so this could obviously lead to unreliable concentration results. Further complicating quantification of aggregates by UV absorbance is that, unlike a solution of monomers, a solution of aggregates is polydispersed, i.e. each aggregate is potentially unique. UV absorbance spectroscopy is a powerful tool, but it can suffer from if the sample is not pure since many unwanted analytes can potentially absorb at the same wavelengths being used to quantify Aβ monomers.

Circular dichroism (CD) is a qualitative spectroscopic method that can detect secondary structures of proteins. The method relies on the differential absorption of left and right circularly polarized radiation. The conversion of Aβ monomers to aggregates in solution is accompanied by a conversion of random coil and α-helix structures to β-sheet structures [40]. This conversion can therefore be monitored be CD. Circular dichroism is particularly useful in kinetic studies of Aβ aggregation and screening inhibitors and disruptors of Aβ aggregates. Because CD is based on an absorbance measurement it can suffer from light scattering from larger aggregates similar to UV absorbance spectroscopy [44].

As mentioned above, light scattering from aggregates is a potential source of interference in absorbance-based measurements, but if aggregates are of interest, light scattering (LS) detection is a useful tool. Aggregated Aβ has been suggested to be a more reliable target for AD

diagnoses compared to soluble Aβ monomers [23]. The power of light scattering detection is that the diffusion coefficients, D, of particles in solution undergoing Brownian motion can be determined [46,47]. Light scattering detection works well to study Aβ aggregates in solution because they behave similarly to particles in solution. Lomakin et al. describe in detail how a particle's diffusion coefficient can be used to determine that particle's size, i.e. its hydrodynamic radius, R_h, using the Stokes-Einstein equation [47]. While the aggregate's shape has to be assumed to relate the D to R_h, no other method was found that can determine an aggregate's R_h. R_h is most accurately related to D when (1) the solution is dilute so that local viscosity does not affect D and (2) when the aggregate's length is not greater than 150 nm [46,47]. Light scattering detection may not work well for determining R_h of fully-formed fibrils because they are greater than the approximate 150 nm length threshold. The hydrodynamic radius of low molecular weight Aβ, however, has been determined to be 1.5 – 2.0 nm based on quasielastic light scattering measurements [48]. Furthermore, LS detection is not a useful method for monitoring Aβ monomer because monomers do not scatter light.

Mass spectrometry (MS) is another valuable tool for quantifying Aβ monomer in solution. Mass spectrometry can identify different monomeric isoforms of Aβ, e.g. 1-40, 1-42, 1-43, based on their mass differences. Thompson et al. demonstrated that electrospray ionization (ESI) MS could be used to identify different Aβ monomeric forms based on their m/z values after being chromatographically separated [49]. Using matrix-assisted laser desorption ionization (MALDI) with MS imaging (MSI), Stoeckli et al. were able to map different isoforms of Aβ in post-mortem mouse brain tissue, which demonstrates the power of MS analysis [50]. Mass spectrometry, however, cannot be used to analyze Aβ aggregates directly because they are too large to get into the gas phase [51]. Typically, if aggregates are to be analyzed by MS, the

aggregates are first disaggregated to monomers and then analyzed. A report by Teplow and coworkers discusses that when monomers build on each other, the m/*z* remains constant, which means that normal MS would not be able to differentiate between a monomer and any higher order oligomer [42]. The authors discuss that ion mobility mass spectrometry (IM-MS) can differentiate between monomers and higher order oligomers because the technique can resolve ions of different masses even if the m/*z* values are the same [42]. For a recent review on IM-MS, see Uetrecht et al. [52].

For structural information of aggregates, imaging methods, such as transmission electron microscopy (TEM) have been used [39]. Transmission electron microscopy can quantify dimensions of a single Aβ aggregate and is commonly used to identify the presence of aggregates in a solution of Aβ. Non-imaging techniques, such as solid-state nuclear magnetic resonance (SSNMR) and hydrogen-deuterium exchange mass spectrometry (HDXMS), do not provide images attainable by imaging techniques. TEM requires that the sample be removed from solution, spotted onto a surface and dried prior to analysis. It is likely that the dried aggregate is not in the exact confirmation as it was in solution. Also, only aggregates large enough to interact with the beam of the electrons from the TEM source will be imaged. Monomers and low molecular weight oligomers are too small to be resolved by TEM [53]. Atomic force microscopy (AFM) is another imaging technique that has been used to obtain structural information of Aβ aggregates, but like TEM, the sample is spotted on a surface and dried [54,55]. One advantage of AFM over TEM is that TEM provides 2 dimensional images and AFM provides 3 dimensional information.

Ryu et al. have also demonstrated the use of surface plasmon resonance (SPR) spectrometry to study Aβ peptide [56]. Like TEM and AFM, SPR measurements are made with

the analyte on a surface. The surface in SPR is a dielectric material that resonates with an incident beam of radiation at a specific angle, called the SPR angle. As the mass on the surface increases due to Aβ accumulation, i.e. aggregation, the SPR angle shifts. The shift in SPR angle is therefore indicative of aggregation. A limitation to SPR is that the monomeric Aβ is bound to the dielectric surface prior initiating aggregation [56]. While this provides an anchor on which aggregation can proceed, it is not known how anchoring the peptide affects polymerization. SPR is a non-quantitative method. Moreover, like AFM and TEM, SPR can be used to determine if aggregation has occurred. Unlike AFM and TEM; however, SPR is incapable of providing an image of the aggregates.

Solution-based methods that are capable of providing structural information of proteins are: X-ray crystallography, MS and nuclear magnetic resonance (NMR) spectroscopy. Unfortunately, Aβ fibrils do not form crystals or ordered repeat structures, which limits the use of X-ray crystallography for structural analysis of larger aggregates [57]. Mass spectrometry coupled with hydrogen/deuterium exchange (HDX) has been used to probe structural information of aggregates [58]. HDX is the process of exchanging amide hydrogens on the peptide for deuterons in solution. Structural information can be obtained using HDX based on the idea that hydrogens involved in hydrogen bonding and those embedded more deeply in the aggregate's core will exchange for deuterium more slowly relative to hydrogens on the surface of an aggregate [51,58]. After the HDX process, the back exchange of deuterium for hydrogens is quenched, the aggregates are dismantled and the number of deuterons acquired by an aggregate can be measured by MS based on the increase in mass [51,58]. It is critical to perform the MS analysis quickly to minimize loss of HDX information due to back exchange of hydrogens for deuteriums [58]. Using HDX-LC-MS, Kheterpal et al. were able to demonstrate that about 50%

of the amide hydrogens of Aβ are protected from exchange after Aβ has aggregated [59].

Another challenge of studying Aβ aggregates is that aggregates become increasing insoluble as they get larger. This limits the size of Aβ aggregates that are analyzable by solution-based NMR because the aggregates precipitate out of solution. Smaller oligomers are more soluble relative to larger aggregates. Moreover, oligomers are short lived relative to larger aggregates. This means that oligomers are likely to change structure and size before, after or during the measurements. NMR is limited to proteins approximately 30 kDa [60], which is approximately equal to 6- or 7-*mer* oligomers. NMR also requires approximately 1 – 10 mM of protein, which is a concentration that would certainly promote aggregation and precipitation [61].

Fluorescence spectroscopy is a very common method for studying and assaying Aβ aggregation. For a protein to be intrinsically fluorescent, it must contain aromatic amino acids. Tryptophan (abbreviated Trp or W), Tyrosine (abbreviated Tyr or Y) and Phenylalanine (abbreviated Phe or F) are the three fluorescent aromatic amino acids of the 22 amino acids. Tryptophan is by far the most fluorescent amino acid with a molar absorptivity (ε) of 5600 $M^{-1}cm^{-1}$ and a quantum yield (Φ) of 0.20 [61]. This is compared to Tyr (ε = 1400 $M^{-1}cm^{-1}$ and Φ = 0.14) and Phe (ε = 200 $M^{-1}cm^{-1}$ and Φ = 0.04) [61]. Of these aromatic amino acids, Aβ contains 0 Trp, 1 Tyr and 3 Phe. Aβ does not have strong native fluorescence in part because it lacks Trp and only contains 1 Tyr.

While Aβ does not exhibit strong native fluorescence, researchers have used covalent and noncovalent fluorescent labeling techniques to study Aβ. Fluorescently labeled Aβ monomeric isoforms are commercially available. One example is carboxyfluorescein (FAM) labeled Aβ, which is used in Chapter 7 to fluorescently probe Aβ aggregation. Another labeling technique

involves using Aβ aggregate antibodies that are covalently bound to fluorescent dyes. Funke et al. used fluorescent labeled antibodies (6E10-Alexafluor-488 and 19H11-Alexafluor-633) to fluorescently detect single aggregates by fluorescence correlation spectroscopy [23].

Other fluorescence probes for Aβ aggregates are amyloid dyes. The most widely used amyloid dyes are Congo Red and Thioflavin T (ThT); although, derivatives of these dyes have been used. Thioflavin T is perhaps more widely used compared to Congo Red. Amyloid dyes are fluorogenic according to IUPAC's definition because their fluorescence is enhanced in the presence of Aβ aggregates. The research presented in Chapters 2 and 4 of this dissertation employed ThT as an amyloid dye to study aggregation of Aβ. Chapter 6 covers research on studying the spectral properties of ThT in the presence of polystyrene beads. Because ThT was a used in several areas of research for this dissertation, the next section is devoted to covering background information of ThT.

1.4.1 Thioflavin T

Thioflavin T (ThT) is a water soluble benzothiazole dye that binds to the β-sheet architecture formed by amyloid aggregates. Molecules of ThT align parallel to the long axis of the Aβ fibrils [62]. Upon binding to Aβ aggregates, ThT undergoes a excitation:emission spectral shift from 385:445 nm to 450:482 nm [12,63]. Moreover, ThT fluorescence can increase by several orders of magnitude when bound to Aβ fibrils compared to unbound ThT [12]. By monitoring the ThT fluorescence near 450:482 nm, the presence of Aβ aggregates can be detected. The spectroscopy of ThT in the presence of Aβ has been characterized in detail by LeVine and Naiki [63-65]. An EEM of ThT in the presence and absence of Aβ (1-40) aggregates is presented in Chapter 6.

Thioflavin T assays are well-documented and easy to use to determine amyloid

aggregation kinetics, especially for Aβ (1-40). For kinetic studies of Aβ aggregation with ThT as the fluorescent marker, an initial lag phase is observed where the ThT fluorescence is weak for a period of time. This lag phase is presumably during the formation of the Aβ nucleus according to the nucleation/polymerization theory. The lag phase is followed by a rapid increase in the ThT fluorescence, which eventually plateaus at a maximum ThT fluorescence. Chapter 2 illustrates bulk ThT measurements of an aggregating mixture of Aβ (1-40). The rate and extent of Aβ aggregation is dependent on the starting Aβ monomer concentration. It is interesting that there are cases where the ThT signal, after reaching its maximum value, begins to decrease as a function of time. Nilsson et al. have suggested that this is due to the formation of mat-like assemblies of Aβ fibrils, which could lack ThT binding sites [39].

The structure of ThT is shown below. Researchers have suggested that the free rotation of the benzylamine and benzothiole rings around their shared carbon-carbon bond quenches the excited state of ThT, which reduces the Φ of free ThT [12].

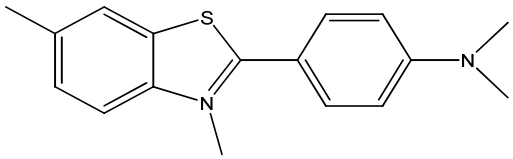

Figure 1.1. Structure of Thioflavin T

It has been suggested that the binding of ThT to the β-sheet of Aβ immobilizes the free rotation about this carbon-carbon axis, which enhances the Φ of ThT relative to free ThT [12]. This means that the rotation of the ring structure of ThT could be the source of the fluorogenic property of ThT. Stsiapura et al. investigated the rotation about the shared carbon-carbon bond of the benzylamine and benzothiole rings and how the angle between the rings relates to the observed Φ enhancement observed in ThT measurements [66]. At a torsional angle, ψ, of 90° and 270°, the highest occupied molecular orbital (HOMO) and the lowest unoccupied molecular

orbital (LUMO) overlap the least [66]. This means that when the benzylamine and benzothiole rings of ThT are perpendicular to each other, ThT is nonfluorescent because there is little to no charge transfer from the ground electronic state to the excited state. On the other hand, $\psi = 0°$ or 180° could provide the most overlap of the HOMO and LUMO, hence, the largest Φ. When the two ring structures are in the same plane, the fluorescence is greatest. Stsiapura et al. demonstrated that increasing the viscosity of the ThT microenvironment lead to an increase in Φ, presumably due to preventing the ThT rings from adopting the perpendicular configuration [66]. It was not described by Stsiapura et al. and it is not clear why a viscose solution would prevent only the perpendicular configuration and not the parallel configuration.

Another interesting property of ThT is that it forms micelles [67]. Some data suggest that ThT micelles bind to Aβ fibrils rather than free ThT [67]. The critical micelle concentration is debatable but has been suggested to be between 4 – 30 μM [67,68].

1.4.2 Fluorescence Anisotropy

Fluorescence anisotropy is a focal point of the research presented in this dissertation. Chapter 4 demonstrates a novel use of ThT for fluorescence anisotropy measurements of Aβ aggregates. Chapter 5 presents a data treatment method that was developed to extract fluorescence anisotropy peaks from separations of Aβ aggregates. In Chapter 7, fluorescence anisotropy measurements of FAM-labeled Aβ monomers, intermediate aggregates and fibrils are presented. This section will cover background information of fluorescence anisotropy.

Fluorescence anisotropy (FA) is based on the photoselective excitation of a fluorophore using a polarized source. A polarized source means that the electric field vector oscillations have a particular orientation, i.e. they are not randomly oriented. Photoselective excitation means that only those fluorescent species whose absorption dipoles are oriented with the polarization of the

excitation source are excited. The probability of a fluorophore absorbing a photon whose electric field vector lies in the z-axis is proportional to the $\cos^2\theta$, where θ is the angle between the z-axis and the absorption dipole of the fluorophore [69].

For simplicity, ignoring the fundamental anisotropy, which will be discussed below, the fluorescence emission of a fluorescent species, excited by a polarized source, will have the same polarization as that of the polarized source. If the emission polarization is altered relative to that of the excitation polarization, e.g. through rotational diffusion of the fluorescent species, this can be measured as the fluorescence anisotropy.

The fluorescence anisotropy, then, is a measure of the degree of fluorescence depolarization. A major source of fluorescence depolarization is rotational diffusion [69]. According to anisotropy theory, slower rotational diffusion rates result in larger fluorescence anisotropy values and larger rotation diffusion rates result in smaller fluorescence anisotropy values. This relationship is described by the Perrin Equation, which is discussed in Chapter 4 (Equation 4.2). A fluorescent species's rotational diffusion rate, hence its fluorescence anisotropy, will be affected by its shape and size. For Aβ species, size and shape can change drastically as a function of aggregation.

Fluorescence anisotropy is a calculated value based on measurements of the parallel and perpendicular fluorescence intensities relative to the excitation source (see Chapter 4 Equation 4.1). The fluorescence anisotropy is independent of the total fluorescence emitted by the fluorophore because the difference between the parallel and perpendicular intensities is normalized to the total fluorescence intensity. It is worth noting that fluorescence anisotropy was preceded by fluorescence polarization, which does not normalize the difference between the parallel and perpendicular fluorescence intensities to the total fluorescence [69].

Each fluorophore has an intrinsic fundamental anisotropy, r_0. The fundamental anisotropy is the anisotropy in the absence of any depolarization. The fundamental anisotropy is described in Equation 1.1, where β is the angle between the absorption and emission dipoles. For collinear dipoles, β = 0° and r_0 = 0.4. This means that the maximum anisotropy is 0.4. When β > 54.7°, r_0 becomes negative reaching a maximum negative value of -0.2 for β = 90° (Lakowicz 3rd Ed).

$$r_0 = \frac{2}{5}\left(\frac{3cos^2\beta - 1}{2}\right) \qquad (1.1)$$

1.5 Methods for Separating Various Forms of Aβ Peptides

Section 1.4 highlighted some of the more common analytical approaches for studying Aβ with a focus on fluorescence and fluorescence anisotropy. It is clear that no one method can detect, quantify and characterize the range of Aβ species between monomers and fibrils. Many detection methods for studying Aβ rely on bulk-based measurements, i.e. the results are population averages. The difficulty with bulk-based measurements is that the larger species tend to dominate the signal. As mentioned, there is growing consensus that smaller Aβ aggregated species may be more cytotoxic compared to very large fibrillar aggregates. There is an obvious need for detecting and characterizing smaller aggregates independent of monomers and fibrils. To accomplish this, separation methods are needed to effectively characterize Aβ monomers and aggregates.

Several liquid-based separation methods have been used to study Aβ. Separation methods like high performance liquid chromatography (HPLC) and size-exclusion chromatography (SEC) use columns that are packed with small particles that serve as a stationary phase. Stationary phases have the potential to disrupt amyloid aggregates due to shear force as the aggregates are forced through the stationary phase at high pressures. The mechanism of separation is based how much time the analytes spend in the mobile phase versus the stationary phase. Analytes that

spend more time in the mobile phase pass through the column faster than those that spend more time in the stationary phase. For HPLC, the affinity of an analyte for the stationary phase versus the mobile phase determines how much time the analyte will spend on the column. For SEC, the analyte does not interact chemically with the stationary phase like HPLC. Instead, the stationary phase particles are porous, and the analytes that can physically fit into the particles' pores have more volume of solvent to pass through compared to an analyte that is too large to fit into the pore volume. Size exclusion chromatography thus separates analytes based on size. For amyloid aggregates, it is assumed that shape also affects how the aggregate passes through an SEC column. HPLC is typically only used to separate monomers of various isoforms of Aβ [49]. Researchers have successfully separated Aβ oligomers from monomers using SEC [70].

Gel-based separations are another approach used for Aβ separations. Klafki et al. optimized an SDS-PAGE separation method to separate synthetic Aβ (17-40), Aβ (1-40) and Aβ (1-42) monomers [71]. Gel electrophoresis has also been used successfully for separating smaller oligomeric forms of Aβ [25,72]. Gel-based separations certainly offer the advantage of simplicity over HPLC and SEC while still achieving separations of monomer and oligomers. A disadvantage of gels is that large fibrillar aggregates may not be able to traverse the gel because they are too large to enter the pore-sizes of the gel material. This means that fibrillar aggregates may not be easily analyzable by gel-based separation methods. Hartley et al. were able to use SDS-PAGE with western blotting employing the Aβ antibody R1282 to analyze monomers, protofibrils and fibrils, but the fibrils showed little to no movement through the gel [53]. Agarose gels can provide large intrinsic pore sizes relative to sodium dodecyl sulfate gels and may be more suitable for analyzing larger fibrils [73].

While HPLC, SEC and gels are popular separation platforms for amyloid studies,

stationary phases have the potential to disrupt amyloid aggregates on-column. Alternative to stationary phase-based separations, field-flow fractionation (FFF) and capillary electrophoresis offer stationary-free separations. The analytes are separated based on their diffusion coefficient and hydrodynamic size [74]. Field-flow fractionation can separate macromolecular complexes ranging from 1 nm to 100 μm [74]. Rambaldi et al. demonstrated the use of FFF with UV/Vis absorbance detection and multiangle light scattering (MALS) detection for the size characterization of soluble and insoluble Aβ (1-42) aggregates [75]. While FFF has not gained significant attention for Aβ separations, Silveira et al. demonstrated the utility of FFF to separate aggregates of another aggregate-forming peptide, PrP-res [74].

1.5.1 Capillary Electrophoresis (CE)

Open tubular capillary electrophoresis, also known as capillary zone electrophoresis (CZE), has been shown to be a powerful separation method to study Aβ monomers and aggregates [76,77]. Capillary electrophoresis was extensively used in this research, and CE theory and applications will be discussed in this section. Some features of CE that are advantageous for Aβ studies are (1) no stationary phase that can potentially disrupt aggregates on column, (2) small volumes (nL) of sample can be analyzed, (3) the ability to separate individual particle-like structures and (4) many types of on-column detection methods are possible. Moreover, commercial CE instruments are available. Additionally, laboratory-constructed CE instruments are simple in design and can be easily constructed. For the work presented in this dissertation, a commercial CE instrument and a laboratory-constructed CE instrument were used. Figure 1.2 illustrates the basic components of a CE instrument.

Capillary dimensions, i.e. length, inner diameter (i.d.) and outer diameter (o.d.), will vary depending on the application. For the work in this dissertation, typical dimensions were

approximately 60 cm in length with i.d. and o.d. of 50 μm and 360 μm, respectively. The silanol groups of the fused silica capillary are ionizable, and at pH values above 3, they become negatively charged. When the capillary is filled with buffer, the negatively charged silanol surface attracts positively charged ions from the buffer, and an ionic double layer is formed at capillary wall. Under an applied voltage, cations in the double layer migrate to the cathode. Because these cations are hydrated, they pull bulk solvent toward the cathode. This phenomenon is called electroosmotic flow (EOF), which will be discussed below.

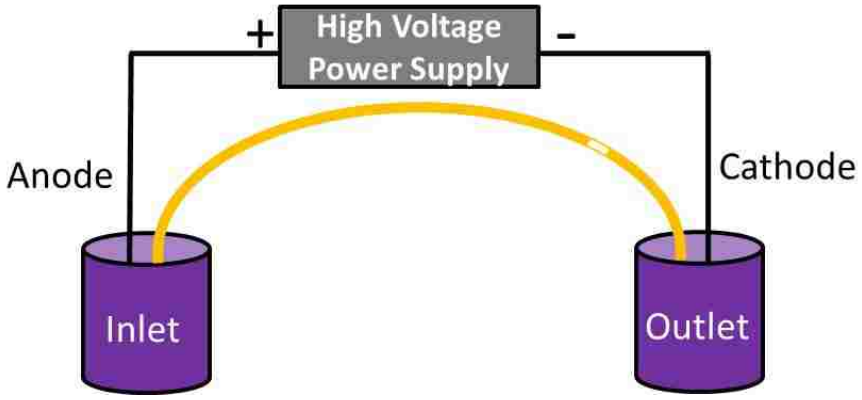

Figure 1.2. Schematic diagram of a capillary electrophoresis instrument.

The EOF is extremely important in CE separations because it is the pumping mechanism of CE [78]. Having control of the EOF is equivalent to having control of the pump in HPLC. Two main factors to consider with EOF are direction and velocity. The direction of the EOF will depend on whether electrophoresis is performed in negative or positive polarity. For example, in the Figure 1.2, applying a positive voltage (positive polarity) causes the electrode on right to become negatively charged, i.e. the cathode. As a result, the EOF would flow from left to right. The direction of the EOF can be reversed by applying a negative polarity, which would cause the electrode on the left to become the cathode, and the EOF would flow from right to left.

The velocity of the EOF should be fast enough to drag all analytes past the detector, even

anions. The general order of elution in normal CE is cations, neutrals and anions. The EOF velocity can be controlled based on the buffer ionic strength and pH. Buffer cations are attracted to the negatively charged silanol groups of the capillary surface, which forms an electric double layer at the capillary surface. The double layer thickness (δ), is dependent on the molar concentration of the buffer (*c*), dielectric constant of the eluent (ε_r), the permittivity of a vacuum (ε_0), the universal gas constant (R), temperature (T) and the Faraday constant (F) according to Equation 1.2 [78]. The formation of the double layer produces a potential called the zeta potential, ζ. The ζ is highest at the capillary surface and falls off exponentially moving away from the surface toward the center of the capillary [79]. Equation 1.3 relates the ζ to the δ, where σ is the surface charge density [78]. Equation 1.4 shows the Smoluchowski equation, which relates the linear velocity of the EOF, u_{eo}, to ζ, where E is the electric field and η is the solvent viscosity [78].

$$\delta = \sqrt{\frac{\varepsilon_r \varepsilon_0 RT}{2cF^2}} \tag{1.2}$$

$$\zeta = \frac{\delta\sigma}{\varepsilon_r \varepsilon_0} \tag{1.3}$$

$$u_{eo} = \frac{\varepsilon_r \varepsilon_0 \zeta E}{\eta} \tag{1.4}$$

Increasing the ionic strength of the buffer, i.e. *c*, results in a decreased δ (see Equation 1.2). This results in a decrease in ζ (see Equation 1.3), which results in a decrease u_{eo} (see Equation 1.4). For high pH values, more silanol groups on the capillary surface are ionized, which increases the surface charge density, σ. This results in an increase in the ζ (see Equation 1.3) and an increase in u_{eo}.

Ionic strength also plays a considerable role in Joule heating, which increases peak broadening [78]. This has a negative impact on peak resolution. Joule heating is generated from

the resistance of the current flowing through the ions of the buffer. Joule heating can be reduced by reducing the ionic strength of the buffer and/or reducing the applied voltage. Thermostatting the capillary and/or using a capillary with higher surface to volume ratios, i.e. capillaries with smaller inner diameters, are other ways to effectively remove heat from the capillary. Joule heating has the potential to alter Aβ and is known to have an effect on the spectroscopy of ThT [66]; therefore, measures were taken in this work to reduce Joule heating by using low ionic strength buffers (10 mM Tris), small i.d. capillaries (50 μm) and capillary thermostatting when available.

To perform a CE separation, analytes are injected into a buffer filled capillary by positioning the inlet end of the capillary into the sample vial, and a voltage is applied across the capillary for a short time. This type of injection is called electrokinetic injection. The injection time and voltage applied depend on the application. Hydrodynamic injection and gravity injections are other injection techniques that use pressure and gravity, respectively, instead of voltage to transfer the analytes into the capillary. After the analytes have been injected into the inlet of the capillary, the inlet is positioned into the inlet buffer reservoir. A voltage is then applied across the capillary via a high voltage power supply, which induces the EOF.

During electrophoresis, analytes separate according to their electrophoretic mobilities. Chapter 2 describes equations that govern electrophoretic mobility (Equations 2.1 and 2.2). For protein separations, the net charge on the protein will be a function of the solution pH. The isoelectric point, pI, is the pH at which the net charge on the protein is zero. For example, monomeric Aβ (1-40) has a pI of 5.1, therefore, in buffers of pH < 5.1, Aβ has a net positive charge and in buffers of pH > 5.1, Aβ has a net negative charge.

For CE separations, analytes migrate at different rates based on their electrophoretic

mobilities. For example, using a positive polarity, cations will pass the detector at a faster rate than anions. This is unlike liquid chromatography, where analytes pass the detector at a constant velocity dictated by the mobile-phase flow rate. This point is discussed here because in Chapter 2, the CE-UV peak areas are divided by the corresponding migration times of the peaks [80]. This was done to normalize the peaks' areas for varying migration rates. Slower migration rates produce wider peaks, and faster migration rates produce narrower peaks for analyte zones of the same physical dimensions migrating at different rates. This is not to be confused with band broadening. Band broadening is the longitudinal diffusion of a zone of analyte and should not have a major impact on peak area. In other words, as a zone broadens, the peak gets wider and the peak height reduces, so the peak area is not changed.

Another benefit of CE for Aβ separations is that CE can separate particles based on size without the need for a stationary phase. This is ideal for Aβ fibrils, which will migrate similarly to particles in solution. Chapter 4 demonstrates the separation and detection of individual Aβ aggregates by CE and discusses how peak widths of aggregates are defined and how it differs from how peak widths of monomers are defined. The electrophoretic migration of particles is covered in great detail by Radko and coworkers [81]; however, because of the complexity of particle separations by CE and the similarities of particles to Aβ fibrils, in terms of size, a brief discussion explaining how particles separate by CE will be covered next.

A particle in an electrolyte solution will develop an electric double layer that forms due to the electrostatic interaction of counterions in the buffer with charges on the particle's surface. The thickness of a particle's double layer, κ^{-1} is a function of the ionic strength of the solution, I ($\kappa \sim I^{1/2}$) [81]. In CE experiments, when a voltage is applied, a particle's motion is dependent on the magnitude of the charge of the particle, the magnitude of the charge of the counterions in the

double layer (which moves opposite to that of the particle) and the viscous drag of the double layer [81]. Adding to the complexity of translational motion of a particle in CE is the effect of double layer distortion, which is called the relaxation effect. The relaxation effect describes how when a particle is displaced in solution, its double layer lags behind, which has been shown to decrease particle mobility [81].

Spherical particles of the same size with very narrow size distributions have been shown to have slightly different electrophoretic mobilities, referred to as electrophoretic heterogeneity [82]. Electrophoretic heterogeneity could be a result of ζ heterogeneity [81]. As discussed above, ζ is the potential that arises due to the formation of an electric double layer. Recall that peak widths of particles passing a detection zone are defined by their electrophoretic mobilities. This means that electrophoretic heterogeneity can result in various peak widths for particles of the same size due to differences in the particles' ζ potentials. Another factor to consider is that non-spherical particles, such as Aβ fibrils, can be oriented in an electric field, which can affect their electrophoretic mobilities [81].

1.6 Goals of This Research

Amyloid beta (Aβ) proteins have been linked to Alzheimer's disease (AD). Some of the challenges studying Aβ are discussed above. To reiterate a few of these challenges, (1) aggregating mixtures of Aβ are heterogeneous with various Aβ species ranging in size from monomers to micron-sized aggregates, (2) detection methods that work well for smaller Aβ species tend to not work well for larger Aβ species and vice versa and (3) most detection methods are based on bulk measurements that do not provide information regarding individual Aβ aggregates. The overall goal of this research is to develop analytical methods for studying and characterizing Aβ species from monomers to fully-formed fibrils.

Chapter 2. A CE-UV method is developed to analyze Aβ (1-40) peptide samples. Chapter 2 demonstrates that CE-UV can be used to quantify monomeric Aβ (1-40) and can separate monomeric and aggregated Aβ (1-40). The CE conditions established in Chapter 2 lay the foundation for the CE conditions in later chapters were fluorescence detection is used.

Chapter 3. One of the goals in Chapter 3 was to confirm that the additional non-monomeric peaks observed in the electropherograms from Chapter 2 were due to aggregated Aβ. Samples of Aβ (1-40) monomers, fibril and seed and Aβ (1-42) monomers and fibrils were prepared for this study. These samples were carefully prepared at nearly equal monomeric-equivalent concentrations to minimize difference between the electrophoretic profiles that could be a result from differences in Aβ concentration. The results of Chapter 3 confirmed that the two main electrophoretic peaks observed in Chapter 2 were due to monomer and aggregate. Chapter 3 also demonstrates some additional sharp electrophoretic UV peaks in samples that were prepared to contained fibrils. These peaks were thought to be due to individual Aβ fibrils and were further investigated in Chapter 4.

Chapter 4. In Chapters 2 and 3, the UV detector on the commercial-based instrument was not fast enough to detect individual Aβ aggregates. For detecting and characterizing individual aggregates, a CE instrument with laser-induced fluorescence anisotropy (LIFA) detection was constructed. The CE-LIFA instrument is shown in Chapter 4 to separate and detect individual aggregates from Aβ (1-40) and Aβ (1-42) samples. The dye thioflavin T was used in the separation buffer to fluorescently label the Aβ aggregates online during the separation. The fluorescence part of the method was validated based on bulk measurements of the same samples using a microplate reader. The anisotropy of the individual aggregates was calculated in an attempt to differentiate one individual aggregate from another, but no clear anisotropy

differences between individual aggregates were observed.

Chapter 5. In Chapter 4, the anisotropy values calculated from the individual Aβ fluorescence peaks were indistinguishable from the anisotropy calculated from the background ThT fluorescence. A data treatment method was developed to extract anisotropy peaks from the anisotropy background. The method is mathematically described using data from experiments in Chapter 4. The benefits and limitations of the method are discussed in the chapter.

Chapter 6. Thioflavin T is a powerful tool for detecting amyloid aggregates. It is widely used in the literature and was used in this dissertation for Aβ detection. While ThT is branded as an amyloid specific dye, preliminary CE-LIF data using ThT in the electrophoresis buffer to label and detect Aβ aggregates suggested that ThT was binding to non-amyloid species and producing false-positives. This observation initiated a spectroscopic investigation of ThT in the presence of non-amyloid particles, polystyrene spheres. Chapter 6 confirms that polystyrene spheres can enhance ThT spectroscopy similar to that of Aβ. Several concentrations and sizes of polystyrene spheres are analyzed to demonstrate the enhancement.

Chapter 7. In Chapter 7, we investigated if Aβ monomers, intermediate aggregates and fibrils could be differentiated based on their fluorescence anisotropy values using a FAM-labelled Aβ instead of ThT as in Chapter 4. By using a covalently labeled fluorescent Aβ monomer to perform the study, all forms of Aβ could be detected independent of size. Unlike other Aβ analysis by CE in this dissertation, the Aβ samples were analyzed at different time points during the aggregation process. The main reason for this was to attempt to detect any transient intermediate Aβ species. Additionally, Arctic Aβ was mixed with normal Aβ, which has been shown to stabilize oligomeric/protofibril structures [83].

CHAPTER 2
ANALYSIS OF MONOMERIC Aβ (1-40) PEPTIDE BY CAPILLARY ELECTROPHORESIS*

2.1 Introduction

Protein aggregation to form amyloid fibrils is closely linked to many diseases including Parkinson's disease, type II diabetes, Huntington's disease, prion diseases and Alzheimer's disease [1,84-86]. Peptides that are seemingly unrelated in terms of size and sequence aggregate to form structures that are very similar in size and shape – amyloid fibrils. A major component of senile plaques found in the brains of patients suffering from Alzheimer's disease is the β-amyloid (Aβ) peptide, and this peptide is thought to be responsible for the disease pathology [1,84,86]. The amyloid core of these plaques contains interwoven fibrils that are composed of 40 and 42 amino acid residue peptides denoted as Aβ (1-40) and Aβ (1-42), respectively. Figure 2.1 shows a transmission electron microscopy (TEM) image of Aβ (1-40) fibrils produced *in vitro* for this work. These fibrils typically are 10 – 12 nm in diameter and can be 10^2 – 10^3 nm long.

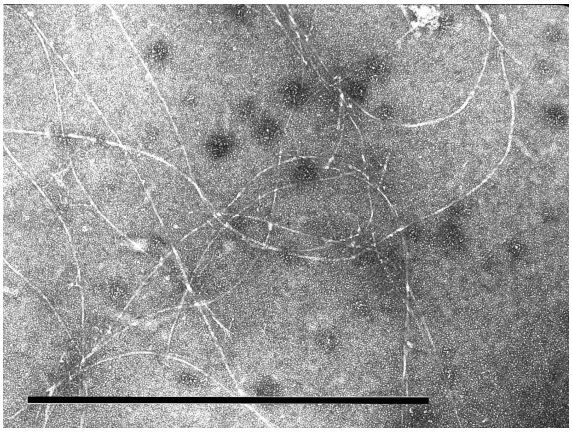

Figure 2.1. TEM of Aβ (1-40) fibrils. The monomer equivalent concentration of this sample was 31 μM. Scale bar is 1 μm. Data for this sample are also presented in Figures 2.2b and 2.4b.

* *Reproduced by permission of The Royal Society of Chemistry*

Due to the link between Aβ aggregation and Alzheimer's disease, the aggregation mechanism and kinetics of Aβ aggregation are the focus of intense study [86,87]. *In vitro* studies of Aβ fibril formation have demonstrated that this process occurs via a complex multi-step nucleated polymerization mechanism [4,41,86,88]. Preparing consistent monomeric Aβ samples, free from aggregates and at known concentrations, is critical for kinetic and mechanistic studies of Aβ aggregation, and it is a significant technical challenge. Complex protocols are used in an attempt to prepare Aβ monomer solutions free of aggregates that might influence both aggregation kinetics and the aggregation mechanism [40,42-44]. Studies have shown that sample preparation significantly influences aggregation kinetics and the aggregate structures formed [40-42,44,89,90].

In this work, we present a capillary electrophoresis (CE) method with UV absorbance detection for characterizing Aβ preparations and quantifying Aβ monomer. Capillary electrophoresis has been used to separate and detect Aβ peptides and aggregates, and most of this work has been qualitative [77,91-93]. Alper et al. showed a calibration curve for Aβ (1-40) monomer based on CE-UV peak areas in the Supplementary Material of a recent publication [17]. Our initial goal for this work was to develop an alternative method to HPLC for quantifying Aβ monomer solutions prior to using them for aggregation studies [17,43,44]. During the development of this method, Aβ peaks in addition to the major monomeric Aβ peak were observed. We investigated differences in aggregation kinetics relative to the presence and absence of these additional aggregate peaks in monomer preparations.

2.2 Experimental

2.2.1 Chemicals

Tris (hydroxymethyl) aminomethane hydrochloride (Tris-HCl), sodium phosphate

monobasic, trifluoroacetic acid (TFA), thioflavin T (ThT) and hexafluoroisopropanol (HFIP) were purchased from Sigma (St. Louis, MO). Sodium hydroxide was purchased from Fisher (Pittsburgh, PA). All solutions were prepared in 18 MΩ water obtained from a Modulab water purification system (United States Filter Corp.; Palm Desert, CA). Chemically synthesized Aβ (1-40) peptide was purchased from Biosource International, Inc (Camarillo, CA).

2.2.2 Aβ Monomer and Fibril Preparation

Monomer samples were prepared as described previously [43]. Briefly, Aβ peptide was treated with TFA/HFIP to remove any pre-existing aggregates. The solvent was evaporated off, and the peptides were dissolved stepwise in equal volumes of 2.0 mM NaOH and 2× phosphate buffered saline (PBS) at pH 7.4, containing 0.1% sodium azide. The PBS was prepared with sodium chloride. Alternate to the PBS preparation, a fraction of the sample was dissolved in 10.00 mM Tris buffer at pH 7.8. Centrifugation (~50,000 g) for a minimum of 10 hr at 4 °C was carried out to remove any aggregates. The supernatant monomer concentration was determined using CE as described below, and the quantification of the peptide monomer was confirmed by amino acid analysis. Fibril samples were prepared by incubating the Aβ samples in 1× PBS without agitation at 37 °C for approximately 7 days. Thioflavin T fluorescence was used to monitor fibril growth.

2.2.3 Capillary Electrophoresis

All CE separations were performed using a Beckmann Coulter P/ACE^{TM} MDQ CE system. The instrument was equipped with a photodiode array (PDA) detector. Fused-silica capillaries (50 μm i.d., 353 μm o.d.; 60 cm total length, 50 cm to detector) were used (Polymicro Technologies, Phoenix, AZ). A new capillary was pretreated by flushing with 1.0 M NaOH for 30 min followed by rinsing with water for 20 min and the separation buffer

(10.00 mM Tris buffer, pH 7.8). Between runs, the capillary was flushed with water (20 psi, 2.0 min) and separation buffer (20 psi, 2.0 min). Hydrodynamic injections were used (1.0 psi, 5.0 s), and the applied separation potential was 30.0 kV (500 V/cm) for 6 min. The instrument was thermostatted at 20.0 °C. Data were acquired using 32 Karat™ Software Version 5.0 from Beckman Coulter at a scan rate of 4 Hz. Quantification was based on integrated peak areas corrected for the migration time for each individual CE run as discussed by Hjerten et al [94].

The electropherograms were plotted as as a function of electrophoretic mobility rather than migration time due to variablility in migration times between runs. This is commonly observed in CE separations of peptides and biological samples due to changes in electroosmotic flow (EOF) caused by adsorption of sample components to the capillary surface. For the CE experiments presented in this work, the RSD for migration times (intraday) ranged from 1-5 % although it was below 2% for all but one day. The changes in EOF can be corrected by using a neutral marker peak to measure the average EOF rate [95]. In these experiments, there was a reproducible neutral system peak in the electropherograms at about 150 s. This peak was confirmed to be neutral by adding mesityl oxide to the sample, which co-migrated with this peak. The electrophoretic mobilities, μ_{ep}, of the peaks were calculated by subtracting the electroosmotic mobility, μ_{eo}, from the apparent mobilities, μ_{app}, of the peaks (Equation 2.1). Equation 2.2 shows how μ_{eo} can be calculated based on experimental data where L_d is the length of capillary from the inlet to the detection window (cm), L_t is the total length of the capillary (cm), V is the applied voltage (V) across the capillary, t_m is the migration time of the analyte peak (s) and t_{eo} is the migration time of the neutral marker peak (s).

$$\mu_{ep} = \mu_{app} - \mu_{eo} \quad (2.1)$$

$$\mu_{ep} = \frac{L_d L_t}{V}\left(\frac{1}{t_m} - \frac{1}{t_{eo}}\right) \quad (2.2)$$

2.2.4 Thioflavin T Fluorescence

The aggregation progress, or fibril formation, of Aβ samples was monitored using ThT fluorescence. The change in fluorescence is linear with an increase in protein concentration of the amyloid fibrils [57]. Samples were incubated at 37 °C in PBS, and representative aliquots were taken daily to measure the ThT fluorescence. Each aliquot was transferred to a well of a 96-well plate, containing 200 µL PBS and 2 µL of 1.5 mM ThT ($[ThT]_{final}$ = 15 µM). The sample volumes were adjusted to give a final peptide mass of 1.00 – 1.25 µg per well. Fluorescence excitation was at 450 nm, and the emission was measured at 482 nm using a BMG Lab Technologies FLUOstar 430 microplate reader (Offenburg, Germany).

2.2.5 Amino Acid Analysis

A Dionex Direct Amino Acid Analysis System (Sunnyvale, CA) was used to perform the amino acid analysis (AAA) with an internal standard correction to determine the Aβ monomeric concentration of each sample. The technique involved hydrolyzing the peptide, separating the amino acids on an anion-exchange column by a stepwise salt and pH gradient, detecting the amino acids by integrated pulsed amperometric detection and calculating the amino acids' peak areas, which allow the determination of each amino acid's concentration and the original peptide concentration. The concentration of each Aβ sample determined by AAA was used as the starting concentration of the stock solution to quantify the Aβ monomer by CE-UV.

2.2.6 Transmission Electron Microscopy

Transmission electron microscopy images of the aggregated Aβ samples were obtained with a JEOL 100CX (Tokyo, Japan). TEM analyses are routinely performed by spotting the sample on a carbon coated mesh grid, allowing the sample to rest for several minutes, wicking the excess solvent from the grid, applying 2% uranyl acetate to the grid, wicking off excess solvent and imaging.

2.3 Results and Discussion

2.3.1 Separations of Aβ Monomer Samples

The initial goal of this research was to develop a method based on capillary electrophoresis with UV absorbance detection for quantifying Aβ peptide in preparations of monomeric peptide for studies of Aβ fibril formation. This analysis is commonly carried out by HPLC [17,43,44,89]. Determining the initial concentration of Aβ peptide in a preparation at the start of an experiment is critical in order to obtain reproducible kinetic data or even reproducible aggregate structures [40-42,44,90]. Some loss of peptide during preparation to remove aggregates before the start of an experiment is inevitable and will vary substantially between different experiments or different experimentalists. While satisfactory quantification of Aβ peptide can be obtained by HPLC, CE offers several potential advantages. Very rapid separations consuming only a few nL of sample per injection are possible with CE. Laboratory-constructed CE instruments with UV detectors are common, inexpensive and simple to operate, and more sophisticated commercial instruments with autosamplers are available.

Figure 2.2 presents a typical electropherogram of monomeric Aβ peptide with UV absorbance detection at 200 nm. The monomer peak, *M*, has an electrophoretic mobility of -

1.20×10^{-4} $cm^2V^{-1}s^{-1}$ (migration time of 183 s) in this separation. Just after the main monomer peak there are two small peaks that are consistently present in sequential separations of the same sample and for different Aβ monomer preparations. It is suspected that these peaks are produced by impurities from Aβ synthesis [42,96]. If these peaks were due to Aβ aggregates or impurities from sample preparation, more variability in magnitude would be expected between different preparations.

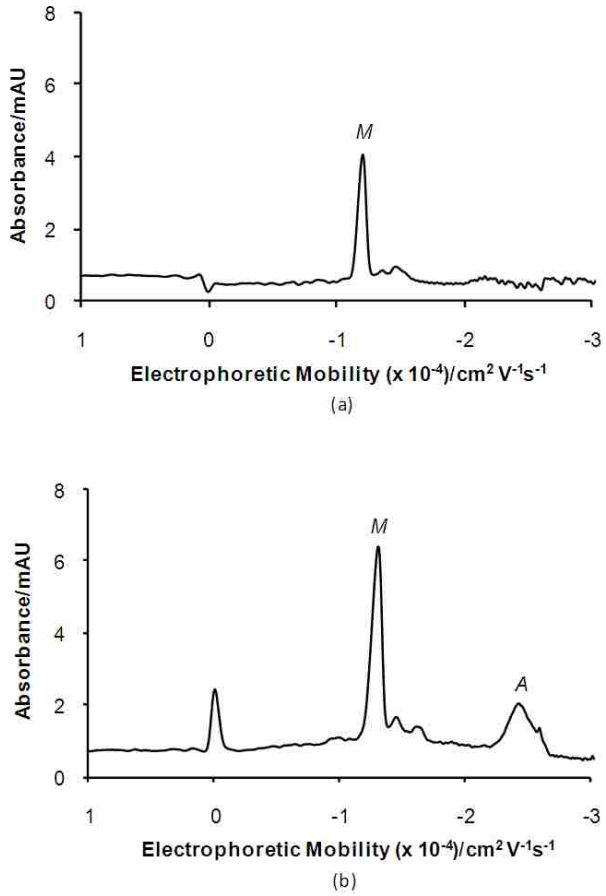

Figure 2.2. Electropherograms of (a) Aβ monomer, *M,* and (b) Aβ monomer, *M*, with aggregate, *A*. The injections were 5.0 s long at 1.0 psi, and the separation potential was 30.0 kV (500 V/cm). The Aβ peptide monomeric-equivalent concentrations for (a) and (b) were determined by AAA to be 26 and 31 μM, respectively. The Aβ preparation used in (b) is the same as that used in Figure 2.1. The same electropherograms plotted vs time are presented in Appendix A Figure A.1.

2.3.2 Quantification of Aβ Monomer

Peptide samples are difficult to prepare at accurate concentrations due to the difficulty of removing water, salts and other impurities from the peptides so that standard solutions can be generated. Quantitative sample preparation is particularly challenging for Aβ peptide due to the extensive procedures used to prepare a monomer solution initially free of aggregates. Amino acid analysis was used to quantify the Aβ monomeric peptide in each stock solution prepared for this work as described in the Experimental section. Analysis with this technique provides the absolute concentration of the peptide as prepared in the sample solution without using a standard of the same peptide at known concetration. After the monomeric equivalent concentrations were determined by AAA, CE-UV was performed on the same stock solutions. The Aβ stock solutions were then serially diluted to generate calibration plots using CE peak areas.

Two plots of peak areas measured by CE with UV absorbance detection vs. Aβ monomer concentration (based on AAA analysis and serial dilution) are shown in Figure 2.3. A linear response is obtained for the range of concentrations studied. Table 2.1 presents linear regression data for calibration curves measured using four different preparations of Aβ monomer (including the two shown in Figure 2.3). The lowest concentration of Aβ monomer injected was 5 μM, resulting in a peak with a S/N of 28. For Aβ monomer, the estimated detection limit (S/N = 3) is 0.5 μM, and the estimated limit of quantitation (S/N = 10) is 1.8 μM. The calculated sample injection volume is 8.8 nL, and the mass LOD and LOQ are 19.1 pg and 68.6 pg, respectively. The LOD for a method used to quantify Aβ in our laboratory based on HPLC with UV absorbance detection is 0.2 μM (5 ng) (unpublished results). It is not unexpected that the plots for the 4 samples are not perfectly superimposable. One source

of error is AAA since each of the fours Aβ monomer samples were prepared seperately, and their concentrations were determined by AAA separately [97]. Another source of error is CE, since different capillaries were used for analysis of different preparations. Any difference in capillary inner diameter (nominally 50 μm) will lead to a different pathlength for absorbance detection.

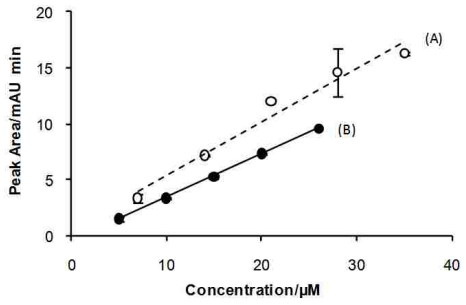

Figure 2.3. Calibration curves for two Aβ monomer preparations. The starting concentration of Aβ monomer for each preparation was determined by AAA to be 35 μM (*open circles/plot* (A)) and 26 μM (*closed circles/plot* (B)). Serial dilutions were performed to generate the standards at lower concentrations. All samples were run in triplicate and the error bars are presented in the figure. Linear regression data for these plots are presented in Table 2.1. The Aβ preparation used to generate plot (B) is the same as that used in Figure 2.2a.

Table 2.1. Concentrations of Aβ monomer and linear regression values from peak areas measured for serial dilutions of 4 Aβ preparations.

Sample ID	Starting Monomer Concentration by AAA (μM)	Linear Regression		
		Slope (mAU min μM^{-1})	Y-intercept (mAU min)	R^2
(A)[a]	35	0.476	0.69	0.97
(B)[b]	26	0.386	-0.47	1.00
(C)	18	0.302	0.69	0.93
(D)	11	0.271	-0.48	0.89

[a,b] *Data shown in Figure 2.3 (A) and (B)*

2.3.3 Aggregate Peaks and Fibril Formation

Figure 2.2b shows an electropherogram that contains an additional peak with an electrophoretic mobility of -2.43×10^{-4} $cm^2V^{-1}s^{-1}$ (migration time = 247 s). This peak was present in the electropherograms for some, but not all of the Aβ monomer samples prepared for this study. One hypothesis is that this peak is due to an aggregated form of Aβ present in those preparations. Unpublished studies in our laboratory showed that Aβ samples containing fibrils or protofibrils result in electropherograms with additional peaks at more negative electrophoretic mobilities compared to monomer peaks. Other studies in the literature also indicate that Aβ aggregates migrate with more negative electrophoretic mobilities (relative to monomer peaks) although those published studies were carried out in different buffers at different pH's [91].

Aggregation studies were carried out using both Aβ monomer samples that contained the putative aggregate peak and samples for which this peak was absent. Fibril formation for these two different types of monomer samples was monitored using Thioflavin T (ThT) fluroescence with excitation at 450 nm and detection of emission at 482 nm. Thioflavin T fluorescence is routinely used to follow the progression of Aβ aggregation [4,41,57,63,89,90]. Thioflavin T fluorescence increases in intensity and shifts spectrally when it selectively binds to amyloid fibrils [4,57,63].

Figure 2.4 presents representative plots of ThT fluorescence from these aggregation studies. The plot in Figure 2.4a is typical for Aβ aggregation from monomer to form fibrils. The fluorescence is relatively low and constant through about Day 5, and then it increases rapidly to a higher values at Day 6 and 7. This lag phase followed by rapid aggregation is typical of Aβ aggregation [41,44,86,89]. The lag phase is reduced for peptides that aggregate

more rapidly to form amyloid fibrils [41,89].

Figure 2.4b shows a representative plot of ThT fluorescence for aggregation studies using a sample with the additional peak present in the CE separation at -2.43×10^{-4} $cm^2V^{-1}s^{-1}$. The ThT fluorescence is relatively high at the initial measurement and remains relatively constant throughout the aggregation study. This indicates that the fibril formation was extremely rapid, and a lag phase was not apparent.

We hypothesize that the presence of aggregates as indicated by the peak with an electrophoretic mobility of -2.43×10^{-4} $cm^2V^{-1}s^{-1}$ is the cause of the abnormally rapid aggregation kinetics shown in Figure 2.4b (no lag phase). We studied the aggregation by ThT fluorescence of six Aβ preparations. Of the six preparations, four contained preexisting aggregates, and the ThT data indicated no lag phase or sustained ThT fluorescence increase over 6-7 days. The other two preparations did not contain aggregates, and they demonstrated typical lag phases and subsequent increases in ThT fluorescence over time as expected. These results are consistent with the hypothesis that monomer preparations that contain preexisting aggregates eliminate the lag phase indicated by ThT fluorescence, and CE with UV absorbance detection is capable of detecting these aggregates in monomer preparations.

We do not believe that the presence of these putative aggregate peaks indicates a limitation of the sample preparation method used in this work [43]. This basic CE method has been used previously in our laboratory to analyze Aβ monomer samples prepared by scientists with more experience using this preparation technique, and the aggregate peaks were never observed (unpublished data). The scientist who prepared Aβ monomer samples for this publication was eventually able to routinely prepare monomer samples without the aggregate peak. It is not known what improvements in technique led to the elimination of the

aggregate peaks in CE, but based on our experience this method can be used to routinely prepare aggregate free monomer preparations.

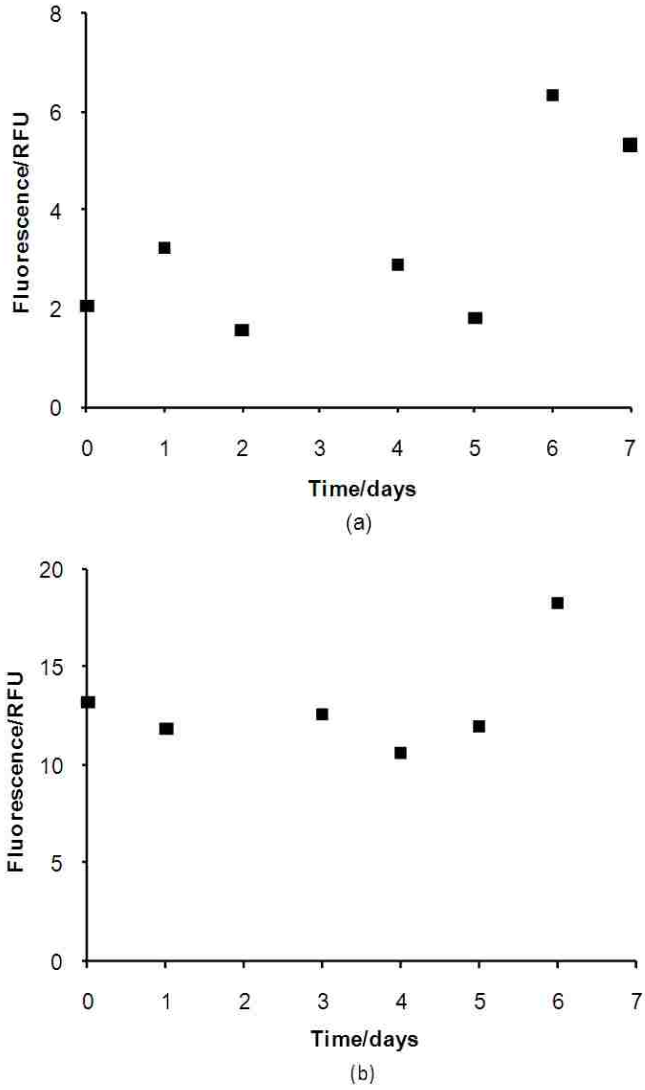

Figure 2.4. Plots of ThT fluorescence of (a) Aβ monomer (26 μM) and (b) Aβ monomer with aggregate (31 μM) vs. time. [ThT] = 15 μM. The Aβ preparation used for (a) is the same as that used for Figure 2.2a (no peak at -2.43×10^{-4} $cm^2V^{-1}s^{-1}$. The Aβ preparation used for (b) is the same as that used for Figures 2.1 and 2.2b (has a peak at -2.43×10^{-4} $cm^2V^{-1}s^{-1}$).

2.4 Conclusions

These results demonstrate that CE with UV absorbance detection is an effective technique for characterizing and quantifying Aβ peptide monomer preparations for studies of amyloid fibril formation. Compared to HPLC methods, CE offers rapid analysis times and reduced sample consumption. Importantly, this study shows that aggregate peaks in CE analysis of Aβ monomer preparations can be used to indicate whether a preparation will exhibit normal or accelerated aggregation kinetics.

CHAPTER 3

ANALYSIS OF Aβ (1-40) AND Aβ (1-42) MONOMER AND FIBRILS BY CAPILLARY ELECTROPHORESIS[†]

3.1 Introduction

Amyloid beta (Aβ) peptides have been identified as the primary peptide component of the neuritic plaques of Alzheimer's disease (AD) patients [13,15,21]. This has led to the hypothesis that Aβ peptide aggregates are the cause of the development and progression of AD. Biologically, monomeric Aβ is formed through the enzymatic cleavage of the transmembrane amyloid precursor protein (APP) [98]. Different length Aβ peptide monomers can be formed from APP through additional enzyme processing [98]. The characteristic plaques of AD patients are composed of both Aβ (1-40) and Aβ (1-42), but Aβ (1-42) is the dominant species [70]. Under physiological conditions, soluble Aβ monomers that have been released into the extracellular fluid can self-assemble to form Aβ aggregates, reaching 10 – 12 nm in diameter and 10^2 – 10^3 μm in length for mature Aβ fibrils. The toxicity of Aβ is thought to be related to aggregate size and structure, and the most toxic species may be an intermediate species between monomer and fibrils [15,36,53,99].

Both Aβ (1-40) and Aβ (1-42) peptides have been the focus of intense research because of their relevance to AD and their potential as therapeutic targets for AD treatment. The characterization of Aβ aggregation is complex and challenging, even when synthetic peptides of only one length (e.g. Aβ (1-40) or Aβ (1-42)) are studied. Preparations of aggregated, synthetic Aβ peptides result in heterogeneous mixtures containing numerous aggregated structures and unaggregated monomer. In order to understand the aggregation process and determine which Aβ aggregate species are toxic, it is necessary to characterize and quantify the different aggregate

[†] *Reproduced by permission of Journal of Chromatography B*

species present in a sample. Few analytical techniques are capable of analyzing Aβ monomer and aggregates with a single experiment. Thioflavin T (ThT) fluorescence, transmission electron microscopy (TEM) and light scattering, for example, are powerful tools for analyzing large Aβ aggregates but are not well suited for studying small oligomeric structures and monomer [44]. Separation techniques such as HPLC, size-exclusion chromatography and gel electrophoresis have been applied to Aβ analysis [44,70]; however, these methods are able to separate Aβ structures only over a limited size range. Their stationary phases have the potential to disrupt aggregates during the separation [100]. An ideal separation method for Aβ analysis would provide rapid and gentle separations of structures ranging in size from monomeric Aβ to mature Aβ fibrils.

Capillary electrophoresis (CE) has been used to analyze species ranging in size from small cations like Na^+ and K^+ to whole cells [101-103]. Capillary electrophoresis with UV absorbance detection (CE-UV) is emerging as a valuable tool for studying Aβ peptides [17,30,45,77,91,93]. In 1993, Sweeney et al. first applied CE-UV to analyze Aβ peptides [77]. Over a decade later, Verpillot et al. produced similar CE-UV results and additionally analyzed Aβ (1-40) peptide from cerebrospinal fluid of an AD patient [93]. De Lorenzi and coworkers analyzed Aβ (1-40) and Aβ (1-42) peptides by CE-UV after performing ultracentrifugation using different molecular weight cut-off filters to determine the sizes of aggregates producing peaks attributed to Aβ aggregates [91]. The antifibrillogenic effectiveness of small molecules on Aβ (1-42) peptides by CE-UV was also studied using a similar approach [30]. Picou et al. recently reported a CE-UV method to characterize and quantify Aβ (1-40) monomer samples and predict whether an Aβ preparation will exhibit normal or accelerated aggregation kinetics [45]. While previous papers have shown that CE-UV has the potential to serve as a powerful tool for

studying Aβ aggregation, such studies are challenging. Small changes in sample preparation can result in large variations in aggregation kinetics and aggregate structures [45,70,90]. In this paper, stringent preparation procedures were used to prepare high quality Aβ monomer and aggregated samples at low concentrations (≤ 25 μM). The Aβ concentrations were determined independently by HPLC with UV absorbance detection (calibration based on amino acid analysis (AAA)), and the aggregated samples were characterized by TEM. This study assesses the potential of CE-UV to distinguish the aggregate types present in different Aβ samples.

3.2 Experimental

3.2.1 Chemicals

All solutions were prepared in 18 MΩ water obtained from a Modulab water purification system (United States Filter Corp.; Palm Desert, CA) unless otherwise noted. Tris(hydroxymethyl)aminomethane (Tris) and methanol (99.8%) were purchased from Fisher Scientific (Fair Lawn, NJ). Tris buffer was prepared at 10.00 mM, and the pH was adjusted to 7.79 with 1.0 M HCl and filtered through a 0.2 μm filter (Whatman; Hillsboro, OR). This Tris buffer was used for all experiments as the electrophoresis buffer unless otherwise noted. Mesityl oxide (MO) was purchased from Alfa Aesar (Ward Hill, MA), and solutions of MO were prepared in Tris buffer at a concentration of 0.2 % (v/v) MO. Formic acid was obtained from Acros Organics; (Geel, Belgium). α-Cyano-4-hydroxycinnamic acid (CHCA) was prepared in acetonitrile/H_2O (50:50, v/v) containing 1.0 % trifluoroacetic acid (TFA) with a final concentration of 10 mg/mL.

3.2.2 Aβ Peptide Sample Preparation

Aβ (1-40) was purchased from the W.M Keck Foundation Biotechnology Research Laboratory (Yale University; New Haven CT), and Aβ (1-42) peptides were purchased from

rPeptide (Bogart, GA). The Aβ (1-42) sequence is shown below, and the Aβ (1-40) sequence is identical except the two amino acids at the C terminus, isoleucine (I) and alanine (A), are not present.

Aβ (1-42)

1 5 10 15 20
D A E F R H D S G Y E V H H Q K L V F F A
25 30 35 40
E D V G S N K G A I I G L M V G G V V I A

Five sample types were prepared for this work: Aβ (1-40) monomer, Aβ (1-40) mature fibrils, Aβ (1-40) seed prepared by ultrasonicating mature fibrils, Aβ (1-42) monomer and Aβ (1-42) mature fibrils. The samples were prepared as described previously by O'Nuallian et al. and Picou et al. [44,45]. Briefly, Aβ peptides were treated with TFA/hexafluoroisopropanol (HFIP) to remove any preexisting aggregates. For Aβ monomer samples, the solvent was evaporated off, and the peptides were dissolved in 10.00 mM Tris at pH 7.79. For Aβ (1-40) aggregate samples, the TFA/HFIP was evaporated off, and the peptides were dissolved stepwise in equal volumes of 2.0 mM NaOH and 2× phosphate buffered saline (PBS) containing 22.8 mM phosphate, 274 mM NaCl, 5.4 mM KCl and 0.1% NaN_3 at pH 7.4. The samples were centrifuged at 50,000 g for a minimum of 10 hr at 4 °C. The supernatant was incubated at 37 °C for 7 d. Fibril formation was monitored using HPLC-UV and ThT fluorescence as described previously [44]. The seed sample was prepared by ultrasonicating a mature fibril sample for 30 s with a Branson Digital Sonifier Microtip (Model 450) and then placed on ice for 1 min. The ultrasonication process was repeated 5×. Prior to CE analysis, the fibril and seed samples were buffer exchanged from PBS to electrophoresis buffer, 10.00 mM Tris at pH 7.79 as described previously [59].

The Aβ (1-42) monomer and fibril samples were prepared using the same procedure with the following exceptions: (1) the Aβ (1-42) monomer sample was centrifuged for 30 min at 20,000 g and 4 °C instead of 10 hr at 50,000 g and 4 °C, and (2) the Aβ (1-42) fibril sample was incubated for 2 days to form mature fibrils. These method changes were due to the faster aggregation kinetics for Aβ (1-42) peptide compared to Aβ (1-40) peptide.

3.2.3 Characterization and Quantification of Aβ Samples

The Aβ concentration for each sample was determined with a Shimadzu HPLC-UV instrument with detection at 215 nm. The concentration of Aβ standards for calibration was determined independently by AAA, as described previously [10]. For aggregate-free samples, the monomer concentration was determined using peak areas and the standard curve for Aβ. For aggregate-containing samples, the Aβ monomer-equivalent concentration was determined by (1) disassembling the aggregates to form monomers by treatment with 70% formic acid and (2) determining the resulting monomer concentration by HPLC-UV. The monomer-equivalent concentrations of the samples used in this work are reported in Table 3.1. Mature fibrils and seed were characterized by TEM and ThT fluorescence assays [4].

Table 3.1. Monomeric-equivalent concentrations determined by HPLC-UV

Peptide Type	Sample ID	Monomeric Equivalent Concentrations by HPLC-UV (μM)
(1-40)	Monomer	20
	Fibril	25
	Seed	20
(1-42)	Monomer	22
	Fibril	22

3.2.4 Aβ Analysis by MALDI-MS

Mass spectrometry experiments were performed on an Applied Biosystems Voyager DE-PRO™ MALDI-TOF MS, equipped with a 20 Hz repetition rate nitrogen laser (337 nm). The instrument was controlled by Voyager Version 5.0 Software with Data Explorer™ and was operated in linear mode. The CHCA matrix was prepared as described in Section 3.2.1. The CE separation buffer for these experiments was 10 mM Tris-HCl at pH 8.0, and a Beckman Coulter CE-MDQ was used for CE experiments. Fractions were collected from 30 consecutive CE separations and combined with an equal volume of matrix. This sample was spotted on a 100 well stainless steel MALDI sample plate for MS analysis. The laser power was adjusted for each sample spot with 200 shots acquired per spectrum.

3.2.5 Aβ Analysis by CE-UV

Capillary electrophoresis with UV absorbance detection was performed with a Beckman Coulter P/ACE MDQ CE system equipped with a diode array detector (DAD) (Brea, CA) [45]. All electropherograms were plotted at 190 nm. The instrument and data collection were controlled with Beckman Coulter 32 Karat™ Software Version 5.0. Fused-silica capillaries were purchased from Polymicro Technologies (Phoenix, AZ). The capillary (ID = 50 μm, OD = 366 μm) was cut to 63.0 cm total length with a window created 53.0 cm from the inlet end using a window maker (MicroSolv Technology Corp.; Eatontown, NJ). The capillary was conditioned by flushing with 1.0 M NaOH (20.0 psi for 1.0 h), 18 MΩ water (20.0 psi for 1.0 h) and Tris buffer (20.0 psi for 30 min).

All samples were dissolved or buffer exchanged (see Section 3.2.2.) into electrophoresis buffer prior to CE in order to eliminate conductivity and composition differences between the sample buffer and electrophoresis buffer. The Tris electrophoresis buffer has a low ionic strength

compared to PBS, and the high conductivity of PBS results in a high electrophoretic current and poor results due to excessive Joule heating. Samples (50 μL) were placed in 200 μL thermowell polypropylene vials (Corning Incorporated; Corning, NY). Prior to each run, the sample was removed from the MDQ and vortexed briefly to resuspend any aggregates that settled to the bottom of the sample vial. For each run, MO was injected for 2.0 s at 0.3 psi prior to the Aβ sample injection. The Aβ sample was then injected for 5.0 s at 0.5 psi. The calculated Aβ injection volume was 4.2 nL. Because MO migrated faster than all forms of Aβ, injection of MO first minimized potential on-column interaction between MO and Aβ. The capillary was thermostatted at 20 °C. The applied separation voltage was 25.0 kV (397 V/cm), and the current was 5.0 μA. The detection scan rate was 32 Hz (maximum allowed), and the run time was 10 min.

All electropherograms were plotted as a function of electrophoretic mobility, μ_{ep}, instead of migration time to correct for any electroosmotic flow (EOF) variations, which is a common problem for CE [45,95].

3.3 Results and Discussion

The goal of the studies presented here was to determine if CE-UV could be used to separate and characterize monomeric and aggregated samples of Aβ (1-40) and Aβ (1-42) peptides for carefully prepared and well-characterized samples. In this study, samples of Aβ (1-40) monomer, mature fibrils and seed (ultrasonicated fibrils) and Aβ (1-42) monomer and fibrils were analyzed using CE-UV. The equivalent monomer concentrations of all samples, as measured by HPLC-UV, were kept at low concentrations between 20 and 25 μM Aβ, to minimize structural differences resulting from Aβ concentration differences [104]. Each sample was quantified independently by HPLC-UV and characterized by TEM. Mass spectrometry was

used to confirm that selected peaks in the electropherograms were due to Aβ peptide.

3.3.1 Aβ (1-40) Monomer, Fibril and Seed Analysis by CE-UV

A representative electropherogram with UV absorbance detection (plotted at 190 nm) of an Aβ (1-40) monomer sample is presented in Figure 3.1a. Monomeric Aβ (1-40) was dissolved directly in electrophoresis buffer (10.00 mM Tris at pH 7.79) and analyzed by CE-UV. The CE conditions are summarized in Table 3.2. All electropherograms are plotted as absorbance vs. electrophoretic mobility, where the neutral marker (NM) has $\mu_{ep} = 0$ cm^2/Vs. The principal peak at a mobility of -1.082×10^{-4} cm^2/Vs in Figure 3.1a is Aβ (1-40) monomer (M). The electrophoretic mobility of the main monomer peak is consistent with that from our previous studies (-1.2×10^{-4} cm^2/Vs) [45]. Figure 3.1a does not indicate the presence of aggregates, which is expected for unaggregated samples. Furthermore, the electrophoretic peak pattern of the Aβ (1-40) monomer sample is similar to that observed by Sabella et al. for Aβ (1-40) at a higher Aβ concentration (100 μM) dissolved in 20 mM phosphate at pH 7.4 and electrophoretically separated using 80 mM phosphate buffer at pH 7.4 [91]. The small peaks near the principal monomer peak are thought to be minor impurities from the peptide synthesis [45]; however, other researchers have hypothesized that peaks with similar mobilities could be due to different oligomerization states of Aβ monomers ranging from 3000 to 50000 Da [91]. Attempts to identify these minor peaks by dilution-based experiments provided inconclusive results *(data not shown)*.

In related experiments, Aβ (1-40) monomer was analyzed by MALDI-TOF MS to confirm the identity of the main monomer peak based on its measured molecular mass. Figure 3.2 shows a mass spectrum for the Aβ (1-40) monomer peak. Fractions at the migration time of the monomer peak were collected from 30 CE runs (see Figure 3.2 inset) and spotted on a

MALDI target for MS analysis. The main MS peak corresponds to the molecular ion, $[M+H]^+$, of the Aβ (1-40) monomer (m/z of 4330.5 Da), and this supports the identification of the main peak in Figure 3.1a as Aβ (1-40) monomer. The weak MALDI MS signal is not surprising since the sample volume injected for each CE run was only a few nanoliters.

An electropherogram of the Aβ (1-40) fibril sample is presented in Figure 3.1b. This sample was prepared to contain mature fibrils by allowing an aliquot of Aβ (1-40) monomer to aggregate for 7 days. Incubation for 7 – 10 d is common to produce mature fibrils [44,45,105]. Figure 3.1b shows two main peaks at -1.071×10^{-4} cm^2/Vs and -2.39×10^{-4} cm^2/Vs in addition to the neutral marker peak. The peak at -1.071×10^{-4} cm^2/Vs is identified as monomer based on its electrophoretic mobility. Detecting a small monomer peak is not surprising since 0.7 – 1.0 μM residual monomer remains unaggregated at equilibrium with fibrils [10]. While the monomer equivalent concentrations of the Aβ (1-40) monomer and fibril samples are similar (20 and 25 μM, respectively, Table 3.1), the monomer peak area in Figure 3.1b is reduced relative to that in Figure 3.1a, 2.2 mAU·s and 15.2 mAU·s, respectively. This is expected because Aβ monomer is aggregating to form fibrils, which migrate at different times relative to monomer. The monomer concentration in the Aβ (1-40) fibril sample is estimated to be 3.5 μM based on its peak area (2.2 mAU·s). This is four to five-fold greater than the residual monomer concentration reported by O'Nuallian, et al. by HPLC [10].

Table 3.2. Summary of Capillary Electrophoresis Conditions

Capillary Dimensions (L_T, L_D, i.d.)	63.0 cm, 53 cm, 50 μm
Separation Buffer (concentration, pH)	10.00 mM, 7.79
Aβ Injections (t_{inj}, pressure)	5 s, 0.5 psi
Applied Electric Field	397 V/cm
Electrophoretic Current	5.0 μA
Electroosmotic Flow Velocity (n = 5)*	0.25 ± 0.01 cm/s
Thermostated Capillary Temperature	20 °C

*The EOF is averaged from the 5 electropherograms shown in Figures 3.1 and 3.3.

Figure 3.1. Electropherograms of Aβ (1-40) samples. Absorbance plotted at 190 nm. *(a)* Aβ (1-40) monomer, *(b)* Aβ (1-40) fibril and *(c)* Aβ (1-40) seed. The neutral marker, NM, has an electrophoretic mobility of 0 cm^2/Vs. A monomer peak, M, was detected in all Aβ (1-40) samples at $\mu_{ep} = -1.077$ ($\pm$ 0.006) $\times 10^{-4}$ cm^2/Vs (n = 9). An aggregate peak, A, was detected in the fibril and seed samples at $\mu_{ep} = -2.37$ ($\pm$ 0.02) $\times 10^{-4}$ cm^2/Vs (n = 6). The TEM insets confirm the presence of aggregates observed in the electropherograms (scale bar = 1 μm).

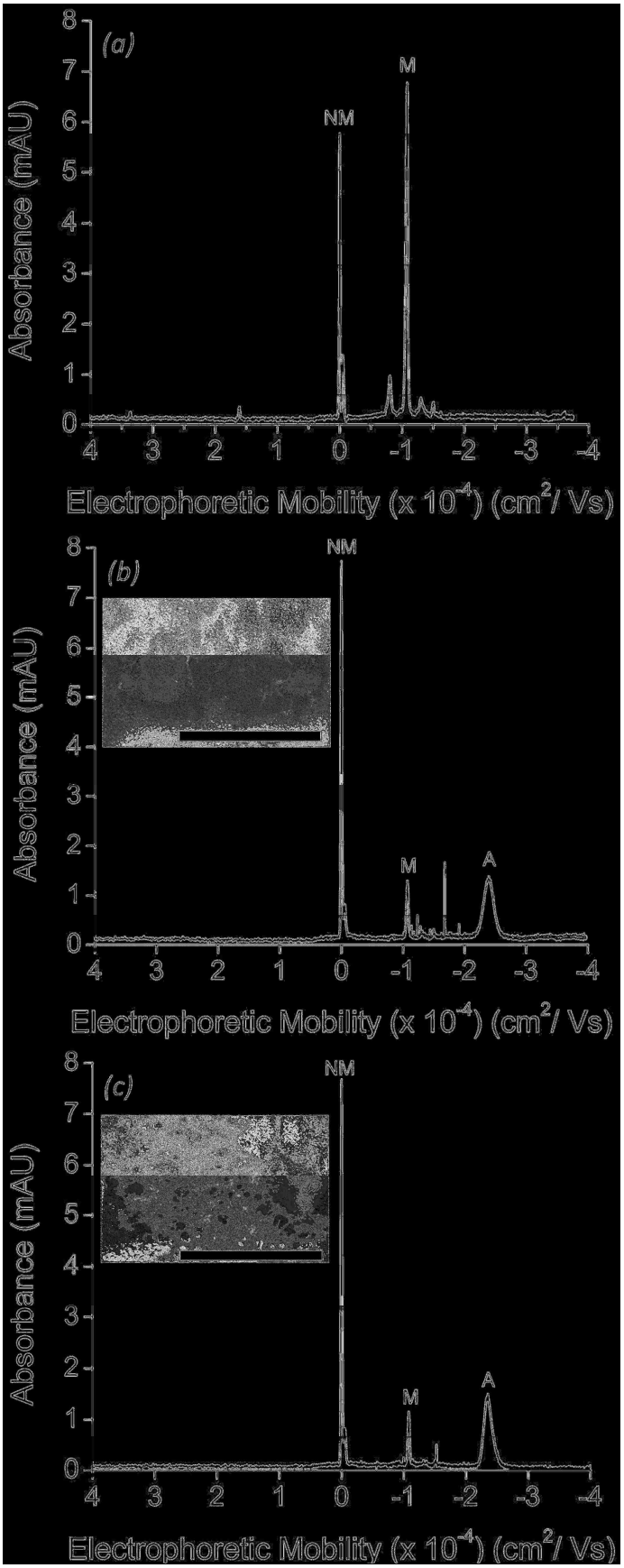
(a)
NM
M
Absorbance (mAU)
Electrophoretic Mobility (x 10^{-4}) (cm^2/ Vs)
(b)
NM
M
A
Absorbance (mAU)
Electrophoretic Mobility (x 10^{-4}) (cm^2/ Vs)
(c)
NM
M
A
Absorbance (mAU)
Electrophoretic Mobility (x 10^{-4}) (cm^2/ Vs)

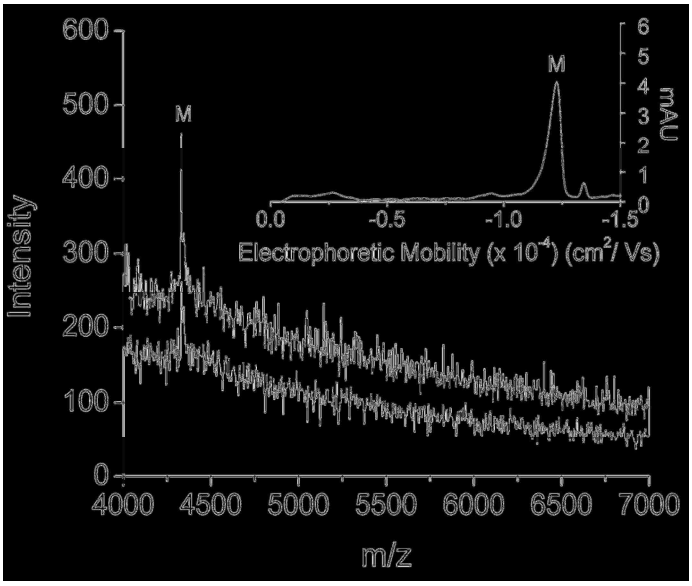

Figure 3.2. MALDI-TOF mass spectrum of collected CE fractions of Aβ (1-40) monomer, M. The Aβ was mixed 1:1 (v/v) with α-cyano-4-cinnamic acid matrix prior to MS. MS data were collected in linear mode. Inset: CE-UV (λ = 200 nm) electropherogram of Aβ (1-40) monomer sample in 10.0 mM Tris-HCl at pH 8.00. The main electrophoretic peak at μ_{ep} = -1.2 × 10^{-4} cm^2/Vs is monomer, M. Fractions were pooled from 30 consecutive CE runs to obtain the mass spectrum.

The broad peak (FWHM = 18.70 s) at -2.39 × 10^{-4} cm^2/Vs in Figure 3.1b is attributed to Aβ (1-40) aggregates (A). In previous work, we analyzed several Aβ (1-40) monomer preparations by CE-UV absorbance [45]. In that work, some preparations produced only a monomer peak in the CE-UV electropherogram; however, other samples contained an additional broad peak at -2.4 × 10^{-4} cm^2/Vs. These samples also exhibited accelerated aggregation kinetics based on ThT fluorescence studies, suggesting that the additional peak was due to Aβ (1-40) aggregates [45]. Analyses of the Aβ (1-40) aggregate peak by CE-UV and MALDI-TOF MS confirmed that the electrophoretic peak at μ_{ep} = -2.4 × 10^{-4} cm^2/Vs in mature fibril preparations produced a MS peak at m/*z* of 4330 Da *(data not shown)*, similar to that shown in Figure 3.2. This confirms that the CE peak at -2.4 × 10^{-4} cm^2/Vs contained Aβ (1-40) peptide. The presence

of full-length, mature fibrils in the sample studied in Figure 3.1b was verified by TEM *(Inset, Figure 3.1b)*.

An interesting observation in Figure 3.1b is the detection of several sharp peaks (FWHM ~0.25 s) with electrophoretic mobilities between those of the monomer and aggregate peaks. These peaks were consistently observed for injections of the Aβ (1-40) fibril sample, but they were not observed for injections of the Aβ (1-40) monomer sample (Figure 3.1a). The exact electrophoretic mobilities of these peaks and the number of peaks were quite variable for consecutive injections of the Aβ (1-40) fibril sample compared to the mobility and appearance of the monomer peak and peak A. We hypothesize that these peaks are due to individually detected, large Aβ aggregates. They are similar in appearance to the sharp peaks detected in previous reports for Aβ (1-43) and Aβ (1-42) analyses by CE-UV [30,77,91]. If these sharp peaks are due to individually detected aggregates, then the peak widths will be defined by the migration rate of the aggregate through the detection zone [82]. The optical aperture used in the capillary cartridge defines the detection zone for this work, which is 0.08 cm. The calculated migration rate of the sharp peak in Figure 3.1b at -1.7×10^{-4} cm^2/Vs is 0.179 cm/s, which was determined by dividing the length of the capillary to the detection window (53.0 cm) by the peak's migration time (295.50 s). The predicted peak width, calculated by dividing the detection zone length by the migration rate of the peak, is 0.5 s. This value is consistent with the measured baseline peak width of 0.45 s. To put this into context, the FWHM and baseline width for the monomer peak in Figure 3.1b are 2.25 s and 3.81 s, respectively. For the work in this paper, the instrument's maximum data sampling scan rate was 32 Hz, which means that the 0.45 s peak was represented by about 14 points. Therefore, a scan rate much less than 32 Hz would be insufficient to accurately represent peaks from individual aggregates migrating at the rate described above,

based on a minimum of 10 points to define a peak [82,106].

The results in Figure 3.1a and 3.1b clearly show that the electrophoretic mobility of Aβ peptide changes as it aggregates from monomer to mature fibrils. Both the broad aggregate peak and the sharp peaks have more negative electrophoretic mobilities (i.e. slower migration times) relative to that of the monomer peak. Ideally, the relative sizes of aggregates could be determined by their relative electrophoretic mobilities. Based on the relative migration of the monomer peak and peak A, one might expect that Aβ monomer would be detected first (smaller negative electrophoretic mobility), followed by the broad aggregate peak labeled A (intermediate negative electrophoretic mobility) and finally the sharp peaks due to mature fibrils (largest negative electrophoretic mobility). However, the sharp peaks migrate between monomer and peak A. For molecules, it is known that electrophoretic mobility is proportional to the ratio of an analyte's charge, z, to hydrodynamic radius, R_h, but it is not known how the ratio z/R_h scales as Aβ aggregates. Additionally, the electrophoretic mobilities of larger Aβ aggregates will depend on more than just their size. Aggregate shape, counter ion double layer and surface zeta potential have been shown to be important for electrophoresis of polystyrene spheres of dimensions similar to mature Aβ fibrils [107]. Because standards for Aβ aggregates do not exist, interpreting separations of Aβ aggregates based on CE and other techniques (e.g. size-exclusion chromatography and field flow fractionation) is quite challenging [42,75].

Seeds are aggregated amyloid peptides that can be added to an unaggregated peptide solution, e.g. a solution of Aβ monomer, to accelerate aggregation to form amyloid fibrils [108]. Seeds reduce the lag phase of Aβ aggregation in a concentration-dependent manner [10,89,108]. An Aβ seed sample was prepared by ultrasonicating mature fibrils as described in the Section 3.2.2. Ultrasonication breaks apart mature fibrils into smaller pieces. The TEM inset of Figure

3.1c confirms the presence of aggregates after ultrasonication. The Aβ (1-40) seed sample was analyzed by CE-UV, and the electropherogram is shown in Figure 3.1c. The electrophoretic profile of the Aβ (1-40) seed closely resembles that of Aβ (1-40) fibril (Figure 3.1b) with two peaks at -1.072×10^{-4} cm^2/Vs and -2.34×10^{-4} cm^2/Vs for monomer and aggregates, respectively. The monomer and aggregate peak areas from the Aβ fibril and seed samples are similar, which is consistent with the samples having similar equivalent monomer concentrations of 25 μM and 20 μM, respectively. For the Aβ (1-40) fibril sample (Figure 3.1b), the average monomer and peak A areas are 2.3 ± 0.1 mAU·s (n = 3) and 20.6 ± 0.5 mAU·s (n = 3), respectively. The sum of the sharp peak areas in Figure 3.1b is 0.6 mAU·s for six peaks. For the Aβ (1-40) seed sample (Figure 3.1c), the average monomer and peak A areas are 1.7 ± 0.1 mAU·s (n = 3) and 18.9 ± 0.7 mAU·s (n = 3), respectively.

Although the electropherograms for Aβ (1-40) fibril and seed are quite similar in most respects, it is interesting to note that the seed sample produced fewer sharp peaks between the mobilities of the monomer and aggregate peaks relative to fibril samples. We hypothesized that the sharp peaks observed in the electropherogram for the Aβ (1-40) fibril sample are due to individually detected mature fibrils. If ultrasonication broke up the mature Aβ fibrils producing the sharp peaks, fewer sharp peaks would be observed.

3.3.2 Aβ (1-42) Peptide Analysis by CE-UV Absorbance

Figure 3.3 presents electropherograms for Aβ (1-42) samples. Like Aβ (1-40), Aβ (1-42) is present in neuritic plaques associated with AD, but it is thought to be more neurotoxic compared to Aβ (1-40). It is well known that Aβ (1-42) peptide aggregates much faster than Aβ (1-40) peptide. The Aβ (1-42) monomer sample (Figure 3.3a) was prepared as described in the experimental section. The sample was analyzed by CE-UV within 6 hr of its initial preparation,

and during that time, the sample was on ice or refrigerated at 4 °C to minimize aggregation before analysis. A large Aβ (1-42) monomer peak at -1.072×10^{-4} cm^2/Vs and a small aggregate peak at -2.29×10^{-4} cm^2/Vs were observed in the electropherogram (Figure 3.3a). The TEM in Figure 3.3a (inset) confirmed that aggregates were present in the Aβ (1-42) monomer sample despite careful sample preparation and low peptide concentration (22 μM).

Other reports of Aβ (1-42) monomer analysis using CE-UV have shown the presence of aggregate peaks but not a monomer peak in contrast to the data shown in Figure 3.3a [30,91]. Several factors may explain these differences: sample concentration, peptide source, sample preparation and handling and buffers. De Lorenzi and coworkers used 100 μM Aβ (1-42), about 5 times the concentration used in this work. Their sample was prepared in 20 mM phosphate buffer at pH 7.4, and 80 mM phosphate buffer at pH 7.4 was used as the electrophoresis buffer. In the work presented here, the sample and electrophoresis buffers were 10.00 mM tris at pH 7.79. Consistent with the electropherogram for Aβ (1-42) monomer in Figure 3.3a, De Lorenzi and coworkers did report a broad peak at a more negative electrophoretic mobility (longer migration time) compared to the peaks they attributed to small (< 50000 Da) Aβ oligomers. The electropherogram in Figure 3.3a indicates that it is possible to prepare and analyze a sample of Aβ (1-42) that contains primarily monomer as indicated by the peak at -1.072×10^{-4} cm^2/Vs, in contrast to the work of De Lorenzi et al.

The electrophoretic mobility of the Aβ (1-42) monomer peak in Figure 3.3a is almost identical to that for the Aβ (1-40) sample presented in Figure 3.1, suggesting that the two additional amino acids in the Aβ (1-42) peptide did not result in a significant mobility shift. The CE method described in this work was not optimized to separate Aβ (1-40) monomer from Aβ (1-42) monomer. Rather, it was designed to separate monomeric Aβ from aggregated Aβ, and it

is successful for both Aβ (1-40) and Aβ (1-42) peptides. Other reports have demonstrated that CE is capable of separating a mixture of different length Aβ peptides, including Aβ (1-40) and Aβ (1-42) [77,93].

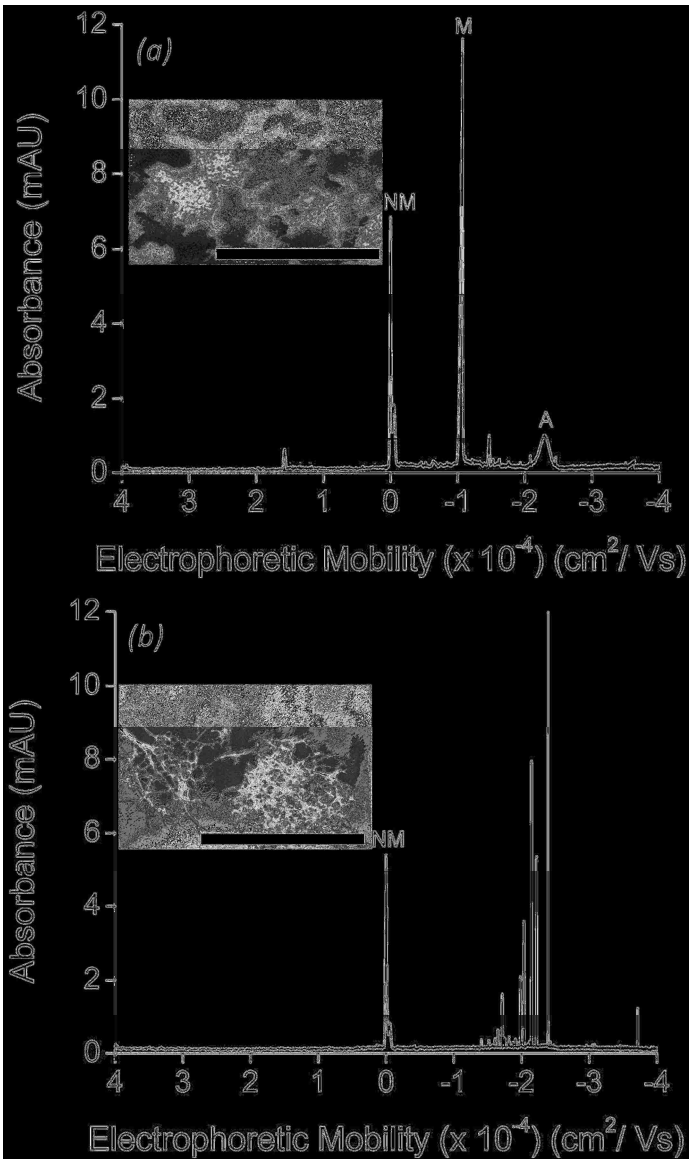

Figure 3.3

Figure 3.3. Electropherograms of Aβ (1-42) samples. Absorbance plotted at 190 nm. *(a)* Aβ (1-42) monomer sample produced a monomer peak, M at μ_{ep} = -1.074 (± 0.003) × 10^{-4} cm^2/Vs (n = 3) and an aggregate peak at μ_{ep} = -2.294 (± 0.002) × 10^{-4} cm^2/Vs (n = 3). *(b)* Aβ (1-42) fibril sample produced many peaks in the mobility range of aggregates. The neutral marker, NM, has an electrophoretic mobility of 0 cm^2/Vs. The TEM insets confirm the presence of aggregates observed in the electropherograms (scale bar = 1 μm).

Figure 3.3b shows an electropherogram for an Aβ (1-42) mature fibril sample. To produce fibrillar Aβ (1-42), this sample was incubated at 37 °C for 2 days in PBS. After incubation, the sample was buffer exchanged to 10.00 mM tris at pH 7.79 as described in Section 3.2.2. Unlike all of the other electropherograms in this work, there is no monomer peak apparent near -1.1×10^{-4} cm^2/Vs. The equilibrium concentration of Aβ (1-42) monomer has been reported as approximately four to five-fold less than Aβ (1-40), which may be below the detection limit for Aβ (1-42) monomer using this method [109]. The TEM for the fibril sample (inset in Figure 3.3b) indicates the presence of fibrils. Unlike the Aβ (1-40) fibril and seed samples, no broad peak is detected at an electrophoretic mobility near -2.4×10^{-4} cm^2/Vs. Instead, there are 17 peaks between -1.4×10^{-4} and -2.9×10^{-4} cm^2/Vs (253–314 s). These peaks all have a FWHM of ~ 0.30 s. Based on these peaks' electrophoretic mobilities and appearance; it is believed that they are due to mature Aβ (1-42) fibrils. Other researchers have reported detecting sharp peaks when analyzing Aβ (1-42) peptide [30]. Colombo et al. analyzed 100 μM Aβ (1-42) peptide in 20 mM phosphate buffer at pH 7.4. In that work, after 24 hr of incubation at room temperature, two main oligomer peaks and a few sharp peaks attributed to micro-precipitation and fibril deposition were observed [30]. No other reports examining Aβ (1-42) by CE-UV have shown a separation similar to that in Figure 3.3b. As discussed in Section 3.3.1 for Aβ (1-40) fibril samples, the length of the detection zone and data sampling rate are critical when detecting peaks due to individual fibrils passing through the detector.

3.4 Conclusions

In this chapter, five distinct monomeric and aggregated samples of Aβ (1-40) and Aβ (1-42) peptides were analyzed by CE with UV absorbance detection. The results showed that the CE-UV method can separate monomeric and aggregated forms of Aβ based on differences in

electrophoretic mobilities. Samples that contained Aβ aggregates, confirmed by TEM, produced a single broad peak, several sharp peaks or both in CE-UV separations. The broad peak is attributed to smaller oligomeric Aβ aggregates, and the sharp peaks are due to larger mature fibrils. Detecting these sharp fibril peaks requires fast data sampling, and faster data collection combined with a narrower detection window should improve the detection of the individual fibrils. Capillary electrophoresis with UV detection is a powerful tool to examine the contents of aggregating Aβ samples containing aggregates ranging from monomers to fibrils, and the method and results described here help lay the foundation for future amyloid analysis by CE.

CHAPTER 4

SEPARATION AND DETECTION OF INDIVIDUAL Aβ AGGREGATES BY CAPILLARY ELECTROPHORESIS WITH LASER-INDUCED FLUORESCENCE DETECTION

4.1 Introduction

Senile plaques composed of neurofibrillary tangles and polymorphic amyloid beta (Aβ) fibrils are hypothesized to be responsible for the neurological degeneration associated with Alzheimer's disease (AD) [36,110]. Aggressive research efforts have focused on developing methods to prevent the formation of or cause the dissociation of amyloid fibrils [9,110]. Effective development of such treatments requires a thorough understanding of the formation and composition of Aβ plaques. Amyloid β peptides (1-40) and (1-42) readily form amyloid fibrils in vitro. The aggregation reaction from soluble monomeric peptide to insoluble fibrils is a complex, multistep process including heterogeneous populations of dynamic polymorphic intermediates [110]. These intermediates have been implicated to be cytotoxic; however, the identity and structure of the cytotoxic species are unknown. These multiple potential therapeutic targets make developing a treatment for AD extremely challenging.

An ideal technique to analyze Aβ peptide aggregation would provide concentration and structural information as a function of time for the entire reaction landscape from monomer to fully-formed fibrils, where all forms of Aβ would be distinguishable. Current analytical techniques are far from this ideal. A variety of techniques has been employed to study static Aβ structures, mainly monomers or fully-formed fibrils. These include imaging techniques such as transmission electron microscopy (TEM), atomic force microscopy and total internal reflection fluorescence microscopy [54,111]. In addition, spectroscopic and spectrometric techniques such as circular dichroism, ThT and Congo red fluorescence, fluorescence correlation spectroscopy,

light scattering techniques, surface plasmon resonance, nuclear magnetic resonance and mass spectrometry have been applied to study Aβ structures [4,23,46,51,56,63,112].

Detecting and distinguishing monomeric Aβ peptides, intermediate oligomeric aggregates and fully-formed fibrils within a sample mixture using one technique is an important challenge that has not been met. Most of the aforementioned techniques can detect larger peptide aggregates, or fibrils, but are incapable of simultaneously detecting smaller aggregated peptide structures. Imaging techniques, for example, have a size threshold, below which the peptide is not detectable. This size threshold also exists for light scattering detection. Thioflavin T (ThT) fluorescence measurements allow the detection of peptide aggregates that have folded into a β-sheet conformation, which is more pronounced as a function of increasing aggregate size. The signal measured by bulk fluorescence is also dominated by larger Aβ aggregates, which mask the signal produced from smaller aggregates. Larger aggregates also dominate bulk light scattering measurements. Although there is no one technique to monitor all forms of Aβ, all of the current techniques are very informative and important within their limitations.

Characterizing the structural pathway from monomeric peptides to fibrillar aggregates involves measuring and characterizing the intermediate oligomeric structures between monomers and fibrils for which little information is available. Separations of Aβ aggregates based on size have been performed using several techniques, including ultracentrifugation, sedimentation velocity analysis, gel electrophoresis, size-exclusion chromatography (SEC) and capillary electrophoresis (CE) [22,26,53,70,71,77,91,92,113-115]. Capillary electrophoresis was first applied to the analysis of Aβ monomer in 1993 by Sweeney et al. [77]. Since this early paper, only a few reports regarding the application of CE to Aβ analysis have been published [26,45,91,92,113,116-118]. Capillary electrophoresis offers fast separations with higher peak

capacities and lower mass detection limits relative to other separation methods applied to study Aβ aggregation. Speed is especially important since some aggregate species will presumably disaggregate when they are physically separated from an aggregating mixture. Another advantage of CE relative to gel electrophoresis and SEC is that it does not require a gel or stationary phase that can disrupt or otherwise alter aggregates due to shear and adsorption. Clodfelter et al. demonstrated that CE is a more gentle technique relative to SEC for separating protein aggregates for another aggregate-forming peptide (C8GLIP) [100].

Laser-induced fluorescence (LIF) is a common on-column detection technique for CE, and CE-LIF has been used to study Aβ peptides [113]. Laser-induced fluorescence anisotropy (LIFA) is a less common detection method for CE, which has been applied to study protein-protein and protein-nucleic acid interactions [119-122]. Fluorescence anisotropy (FA) is a fluorescence phenomenon that is dependent on the size of the fluorescent entity being investigated. Sabaté et al. demonstrated the use of bulk ThT anisotropy to monitor aggregation kinetics of the fungal prion protein HET-s(218-289) [68]. Allsop et al. demonstrated that bulk time-resolved fluorescence anisotropy can be used for monitoring early stages of Aβ aggregation using a fluorescein-labeled Aβ peptide [123]. Capillary electrophoresis with LIFA detection has the potential to be developed into a powerful tool for studying Aβ aggregation. Capillary electrophoresis is capable of resolving different Aβ aggregate species, and LIFA could provide a sensitive on-line detection method that also could provide information about the sizes of the separated species. To the best of our knowledge, there are no reports of the application of CE-LIFA to study aggregation of amyloid forming peptides.

The goal of this work was to separate and detect individual Aβ aggregates labeled with ThT using capillary electrophoresis with laser-induced fluorescence detection. Furthermore, the

potential of laser-induced fluorescence anisotropy to characterize individual Aβ aggregates labeled with ThT was explored.

4.2 Experimental

4.2.1 Chemicals

All solutions were prepared in 18 MΩ water obtained from a Modulab water purification system (United States Filter Corp.; Palm Desert, CA) unless otherwise noted. Tris (hydroxymethyl) aminomethane (Tris) and methanol (99.8%) were purchased from Fisher Scientific (Fair Lawn, NJ). Tris buffer was prepared at 10.00 mM, and the pH was adjusted to 7.79 with HCl. This Tris buffer was used for all experiments unless otherwise noted. The buffer was filtered through a 0.02 μm filter (Whatman; Hillsboro, OR). Mesityl oxide (MO) was purchased from Alfa Aesar (Ward Hill, MA), and working solutions of MO were prepared in Tris buffer at a concentration of 0.2% (v/v). Coumarin 334 was purchased from Acros Organics (Morris Plains, NJ), and a stock solution was prepared at 1.00 μM in methanol. Working solutions of coumarin 334 were prepared at 50 nM in Tris buffer. Thioflavin T was purchased from Sigma (St. Louis, MO). A stock solution of 289 μM ThT solution was prepared in Tris buffer, and working solutions of ThT were prepared at 15.0 μM in Tris buffer.

4.2.2 Aβ Peptide Sample Preparation and Characterization

Aβ (1-40) peptide was purchased from the W.M. Keck Foundation Biotechnology Research Laboratory (Yale University, New Haven, CT), and Aβ (1-42) peptide was purchased from rPeptide (Bogart, GA). Four Aβ sample preparations were studied in this work: Aβ (1-40) monomer, Aβ (1-40) fibril, Aβ (1-42) monomer and Aβ (1-42) fibril. All Aβ samples were prepared as previously described [44,45,118]. Aβ peptides were treated with trifluoroacetic acid (TFA)/hexafluoroisopropanol (HFIP) to remove any preexisting aggregates. For Aβ monomer

samples, the solvent was evaporated off, and the peptide was dissolved in 10.00 mM Tris at pH 7.79. For the Aβ (1-40) fibril sample, the TFA/HFIP was evaporated off, and the peptides were dissolved stepwise in equal volumes of 2.0 mM NaOH and 2× phosphate buffered saline (PBS) containing 22.8 mM phosphate, 274 mM NaCl, 5.4 mM KCl and 0.1% NaN_3 at pH 7.4. The samples were centrifuged at 50,000 g for a minimum of 10 h at 4 °C. The supernatant was incubated at 37 °C for 7 d. The Aβ (1-42) monomer and fibril samples were prepared using the same procedure with the following exceptions: the Aβ (1-42) monomer sample was centrifuged for 30 min at 20,000 g and 4 °C, and the Aβ (1-42) fibril sample was incubated for 2 d to form mature fibrils. These changes were due to the faster aggregation kinetics of Aβ (1-42) peptide compared to that of the Aβ (1-40) peptide.

Fibril growth was monitored using ThT fluorescence and transmission electron microscopy as described previously [4,118]. Depletion of Aβ monomer during fibril formation was monitored using a Shimadzu HPLC-UV instrument with detection at 215 nm as described previously [44,45,118]. Samples were characterized by CE-UV. The CE-UV analysis was performed using a Beckman Coulter P/ACE MDQ equipped with a diode array detector, and the absorbance was monitored at 190 nm as previously described [118]. The capillary (ID = 50 μm, OD = 366 μm) used for CE-UV was cut to 63.0 cm total length with a window created 53.0 cm from the inlet end using The Window Maker™ (MicroSolv Technology Corp.; Eatontown, NJ). The Aβ samples were vortexed prior to every injection to resuspend any aggregates that settled to the bottom of the sample vial.

Prior to CE analysis, fibril samples were buffer exchanged from PBS to 10.00 mM Tris electrophoresis buffer at pH 7.79 [51]. This step eliminated conductivity and composition differences between the sample buffer (PBS, higher conductivity) and electrophoresis buffer

(Tris, lower conductivity). The higher conductivity of PBS would result in high electrophoretic current and poor results due to excessive Joule heating if it were used for electrophoresis. The monomer-equivalent concentrations of all samples were determined by HPLC-UV as previously described [44] and were: Aβ (1-40) monomer, 15.7 μM; Aβ (1-40) fibril, 5.1 μM; Aβ (1-42) monomer, 19.9 μM; Aβ (1-42) fibril, 29.5 μM. For CE analysis, the total sample volume was 50.0 μL, and it was placed in a 200 μL thermowell polypropylene tube (Corning Incorporated; Corning, NY).

4.2.3 Capillary Electrophoresis with Laser-Induced Fluorescence Anisotropy Detection

The Aβ samples were characterized first by CE-UV and then analyzed with the CE-LIFA system on the same day. The samples were not transferred to different vials when switching from the CE-UV instrument to the CE-LIFA instrument. A laboratory-constructed instrument was used for all CE-LIFA experiments. The CE part of the instrument was similar to an instrument described previously [124].

Capillary electrophoresis was performed in an open-tubular capillary (ID = 50 μm, OD 366 μm) cut to 60.0 cm total length. A detection window was created at 23.0 cm from the inlet end. A new capillary was initially conditioned with a manual syringe pump using the following sequence: 400 μL of 1.00 M NaOH, 400 μL of 18 MΩ water and 2 × 400 μL of Tris buffer. The total rinse time was approximately 60 min. The capillary was rinsed twice between sample types with 400 μL of Tris electrophoresis buffer using a manual syringe pump. The fluorescent neutral marker (coumarin 334) was injected for 1.0 s at 25.0 kV prior to the Aβ sample injection for 5.0 s at 25.0 kV. This injection order minimized potential interactions between Aβ and the neutral marker because all forms of Aβ detected migrated slower than the neutral marker. The Aβ samples were vortexed prior to every injection. The electrophoretic potential was applied using a

Spellman CZE1000R high-voltage power supply (Hauppauge, NY) at 25.0 kV (417 V/cm). The electrophoretic current was 5-6 μA. This system was not temperature controlled, unlike the commercial CE-UV system.

Figure 4.1 presents a schematic of the detection system for the CE-LIFA instrument. The light source was a 445 nm diode laser (Model No. LDCU12/7532, Power Technology, Inc; Alexander, AR). The laser produced a continuous beam of polarized radiation, and the measured power was 30.0 mW. The beam was attenuated with a neutral density filter to 3.0 mW and focused onto the capillary window with a plano-convex lens (focal length = 25.4 mm). The fluorescence emission was collected with a 20× microscope objective lens (Numerical Aperture = 0.4) at 90° relative to the excitation beam. The emission was directed through a 441.6 ± 10 nm notch filter (MK Photonics, Inc; Albuquerque, NM) to remove Rayleigh scattered light from the laser and a 490 ± 10 nm bandpass filter (Omega Optical; Brattleboro, VT) to selectively detect amyloid-bound ThT fluorescence. After being spectrally filtered, the emission was spatially filtered with a 1000 μm pinhole. The emission was then separated into its parallel and perpendicular polarized components (relative to the excitation source) with a broadband polarizing cube beamsplitter (10FC16PB.3, Newport Corporation; Irvine, CA). Both emission components were detected simultaneously and equidistant from the capillary by two identical photomultiplier tubes (PMT) (H9306-04, Hamamatsu; Bridgewater, NJ). The PMT collecting parallel emission ($PMT_{\parallel}$) was at 1000 V, while the PMT collecting perpendicular emissions ($PMT_{\perp}$) was at 935 V. The outputs of the PMTs were filtered by 500 Hz low pass RC filters and collected by a National Instrument PCI-6024E DAQ board at a scan rate of 1000 Hz. The CE-LIFA data collection was controlled by a program written with LabView Version 5.0, and the data were analyzed using Origin Pro 7.5, Synaptosoft Minianalysis Programs version 6.0.7 and

Microsoft Excel 2007.

Equation 4.1 was used to calculate the fluorescence anisotropy, r, where $I_{\parallel}$, and $I_{\perp}$, are the measured parallel and perpendicular fluorescence intensities relative to the polarization of the excitation source. The factor *G* corrects the anisotropy for the differences in sensitivities of the two PMTs. For this work, *G* was empirically adjusted to 1 by optimizing the potentials applied to both PMTs so that the responses and sensitivities were equal for a small fluorescent molecule, Lucifer Yellow (Molecular Probes; Eugene, OR), from 250 nM to 1 μM (data not shown).

$$r = \frac{I_{\parallel} - GI_{\perp}}{I_{\parallel} + 2GI_{\perp}} \qquad (4.1)$$

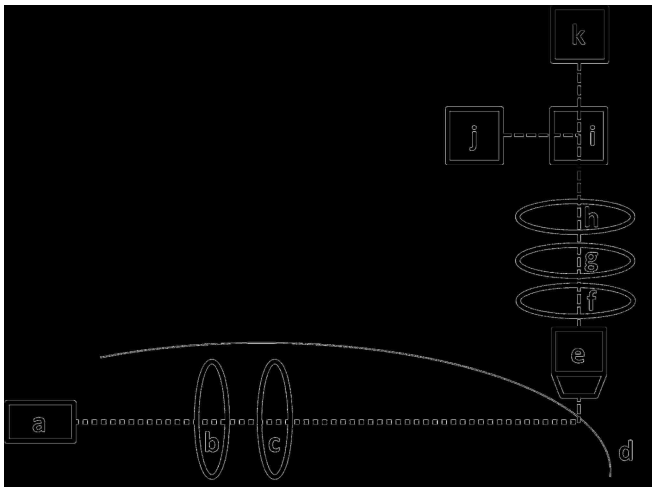

Figure 4.1. Schematic of the fluorescence anisotropy detection system for CE. Components are (a) polarized laser (445 nm), (b) neutral density filter, (c) focusing lens, (d) capillary, (e) microscope objective lens (20×), (f) 440 ± 10 nm notch filter, (g) 490 ± 10 nm bandpass filter, (h) 1000 μm pinhole, (i) polarizing beam splitter cube, (j) $PMT_{\parallel}$, (k) $PMT_{\perp}$.

4.2.4 Microplate Reader Fluorescence

The same samples analyzed by CE-UV and CE-LIF were also analyzed by bulk ThT fluorescence using a BMG Lab Technologies FLUOStar 430 microplate reader (Offenbur, Germany). The instrument and data acquisition were controlled by FLUOstar Software Version 3.02-0. Forty microliters of each sample were transferred from the 200 μL polypropylene tubes

used for CE to separate wells of 96-well Corning, Inc. 3650 black nontransparent microplates. Consistent with the CE experiments, ThT was added at 15 μM to each sample well. The excitation was set to 440 ± 12 nm with a bandpass filter, and the emission was collected at 485 ± 12 with a bandpass filter.

4.3 Results and Discussion

The primary goal of this work was to separate and detect individual Aβ peptide aggregates by CE-LIF using thioflavin T as an amyloid-selective fluorescent label. Thioflavin T (ThT) is a common fluorescence probe used to study Aβ aggregation because it is selective for amyloid aggregates, and its excitation/emission maxima shift from 330/440 nm to 440/490 nm when it noncovalently binds to amyloid aggregates [4,12,63]. Thioflavin T was added to the electrophoresis running buffer to bind to the Aβ aggregates on-column [113]. This approach eliminates the potential for ThT to alter the Aβ aggregates' sizes and shapes during the aggregation process while still being used as an effective fluorescent label for their on-column detection. At the excitation and emission wavelengths used in this work, fluorescence interference from unbound ThT is minimal [63]. The concentration of ThT (15 μM) was chosen based on earlier publications which used 10 and 20 μM ThT for Aβ aggregate detection [45,63]. This is above the critical micelle concentration of free ThT reported by Khurana et al. (3.8 ± 0.5 μM) [67].

The work presented here is distinct from the earlier study by Kato et al. [113] because the instrument used here was designed to detect peaks resulting from individual aggregated Aβ species, which required the use of sufficiently fast data sampling and electronic filters [82,106]. In addition, the ThT fluorescence measured after CE separation was validated by measuring bulk ThT fluorescence for the same samples.

4.3.1 Detection of Individual Aggregates by CE-LIF

The detection system was designed as a two channel (polarization) fluorescence detector in order to evaluate the potential of fluorescence anisotropy to size-characterize individual aggregates (see Experimental for details); however, for the purpose of separating and detecting individual ThT-labeled Aβ aggregates by CE-LIF, two channel fluorescence detection is not required. Data from one fluorescence channel has been plotted in Figures 4.3-4.6 for clarity. The two channel data will be discussed in Section 4.3.3.

Four different Aβ sample types were prepared and used for this work: Aβ (1-40) monomer, Aβ (1-40) fibril, Aβ (1-42) monomer and Aβ (1-42) fibril. The two fibril samples were prepared to contain large mature fibrils that would bind to ThT to produce fluorescence peaks. The Aβ (1-40) monomer and Aβ (1-42) monomer samples were prepared to be free of aggregates and serve as negative controls. A TEM of each sample type is shown in Figure 4.2. The Aβ fibril samples (Figures 4.2B and 4.2D) show clear evidence of fibrillar aggregates and were expected to bind ThT and produce fluorescence peaks. The Aβ monomer samples did not show fibrillar aggregates by TEM (Figures 4.2A and 4.2C). These samples were not expected to produce fluorescence peaks with ThT. Amyloid monomers, unlike amyloid fibrils, do not cause the ThT enhancement [4,12,63].

Figures 4.3A and 4.3B show electropherograms with LIF detection for the Aβ (1-40) monomer sample without and with ThT in the running buffer, respectively. As expected, no peaks were observed in the absence of ThT (Figure 4.3A). In contrast, with ThT a few small, sharp peaks were present (Figure 4.3B). The migration times of these peaks appear to be random for consecutive injections, and approximately the same numbers of peaks were observed in electropherograms of the electrophoresis buffer with thioflavin T for which no Aβ was injected

(data not shown). These peaks are hypothesized to be a result of unfiltered particulate matter (non Aβ particles) in the running buffer that can enhance ThT fluorescence similar to amyloid fibrils. We are currently investigating ThT fluorescence in the presence of synthetic nanoparticles due to their potential to produce false positives in amyloid fibril assays. The Aβ (1-40) monomer sample also was analyzed by a CE-UV method previously developed by Picou et al. [45]. A representative CE-UV electropherogram of the Aβ (1-40) monomer sample is available in Appendix A Figure A.2. This experiment confirmed that the Aβ (1-40) monomer sample does contain Aβ monomer, and it does not indicate that Aβ aggregates are present.

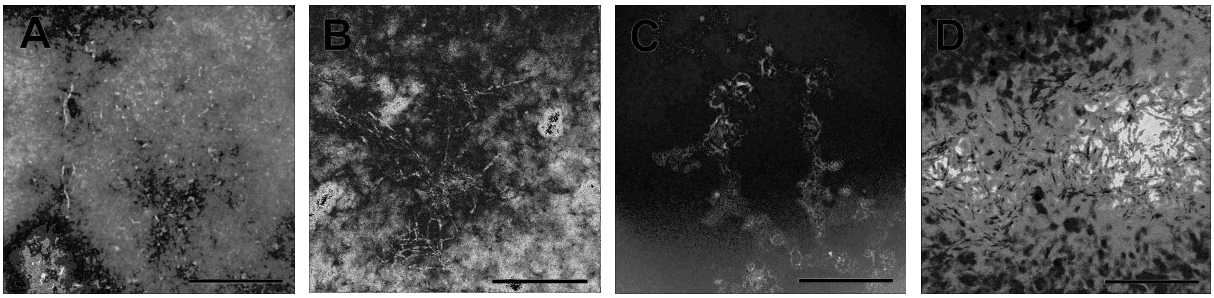

Figure 4.2. TEM images of (A) Aβ (1-40) monomer; (B) Aβ (1-40) fibril; (C) Aβ (1-42) monomer; (D) Aβ (1-42) fibril. Samples were buffer exchanged into 10.00 mM Tris buffer at pH 7.79 prior to imaging (scale bar = 500 nm).

The large, relatively broad peaks at approximately 60 s in Figures 4.3A and 4.3B are the fluorescent dye, coumarin 334, which was used as a neutral marker to determine the electroosmotic flow. The coumarin 334 and Aβ samples were injected consecutively (electrokinetic injection) from separate vials to minimize potential interaction of the neutral marker and Aβ. For these experimental conditions, Aβ has a negative electrophoretic mobility. The coumarin 334 and Aβ sample buffers did not contain ThT. As a result, when they were injected into a capillary filled with ThT, a vacancy zone was created, which caused the fluorescence to decrease as observed at 47 s in Figure 4.3B. No ThT vacancy zone is present in Figure 4.3A because ThT was not included in the running buffer. The vacancy peak in Figure

4.3B gives an indication of the magnitude of the background fluorescence due to unbound ThT and is consistent with reports of ThT background fluorescence in the literature [4,12,63].

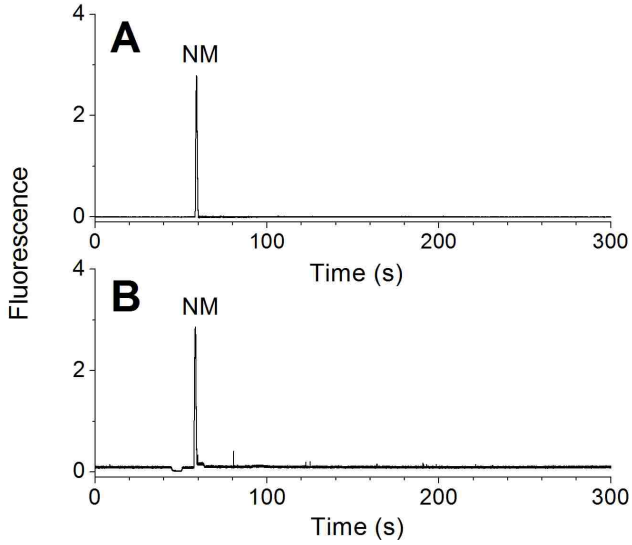

Figure 4.3. Electropherograms with LIF detection for Aβ (1-40) monomer without (A) and with (B) 15 μM ThT in the electrophoresis buffer (10.00 mM Tris at pH 7.79). The peak at 59 s in each electropherogram is the neutral marker (NM), coumarin 334. Coumarin 334 was injected for 1.0 s at 25.0 kV prior to the Aβ sample injection for 5.0 s at 25.0 kV. The separation potential was 25.0 kV (417 V/cm). The dip in the baseline at 47 s in (B) is due to a ThT vacancy zone.

Figures 4.4A and 4.4B show representative electropherograms with LIF detection for the Aβ (1-40) fibril sample without and with ThT in the running buffer, respectively. The Aβ (1-40) fibril sample was prepared by allowing Aβ (1-40) monomer to aggregate for 7 d to produce mature Aβ (1-40) fibrils. Many sharp peaks are observed near 110 s in both Figures 4.4A and 4.4B. Table 4.1 shows that the electropherograms for the Aβ (1-40) fibril sample with ThT in the separation buffer contain approximately 100 of these peaks compared to 10 peaks for the Aβ (1-40) monomer sample (Figure 4.3B). The peaks in Figures 4.4A and 4.4B are hypothesized to be due to individual Aβ (1-40) aggregates passing through the LIF detection zone. The inset of Figure 4.4B is an expanded view showing two individual aggregate peaks in the Aβ (1-40) fibril sample, illustrating their narrow peak widths.

It is extremely challenging to show definitively that these sharp peaks are due to

individual amyloid fibrils. The fundamental limitation is the lack of an analytical standard or surrogate standard for Aβ fibrils. Our laboratory has extensive experience with single particle detection [82,125] and Aβ fibril preparation and analysis [45,51,118]. The peak widths observed are consistent with peaks due to single polymer particles of comparable size observed with a similar CE detector [82]. The expected FWHM of an aggregate passing through a focused laser beam can be estimated by dividing the calculated diameter of the focused laser spot by the measured migration rate of the aggregate [82]. In this case, the calculated diameter of the focused laser beam is 5.7 μm, and the migration rate for species detected at 105.03 s is 0.22 cm/s, which gives a theoretical FWHM for a single aggregate peak of 3 ms. In the inset in Figure 4.4B, the peak at 105.03 s has a measured FWHM of 11 ms, and the peak widths for peaks attributed to individual aggregates ranged from 3–15 ms. The width for the peak in Figure 4.4B is greater than the predicted FWHM of 3 ms, but this is expected due to refraction of the excitation beam at the curved capillary surfaces, which causes the actual spot size to be significantly larger than the calculated spot size [82]. An actual spot size of 24.2 μm would produce the observed peak width of 11 ms. The measured FWHM for coumarin 334 is 1.2 s, which is typical for a CE peak due to large numbers of identical fluorescent molecules.

The presence of large Aβ aggregates in the Aβ (1-40) fibril sample was confirmed by CE-UV, TEM and bulk ThT fluorescence measurements. In the CE-UV electropherogram (Figure 4.4C), the broad peak at 313 s and the sharp peaks from 300-400 s are typical for Aβ samples containing mature fibrils [118]. Bulk ThT fluorescence was higher for the Aβ (1-40) fibril sample compared to the Aβ (1-40) monomer sample (Table 4.2), which is consistent with the presence of large Aβ aggregates in the fibril sample [4,12,63]. Finally, the TEM of this sample (Figure 4.2B) shows that mature Aβ fibrils were present in this sample.

Table 4.1. Number of CE peaks detected with and without ThT. All data are presented as averages with standard deviations from 3 experiments. All peaks with S/N > 3 were included.

Sample	Peaks Detected	
	with ThT	without ThT
Aβ (1-40) Monomer	10 ± 3	1 ± 1
Aβ (1-40) Fibril	99 ± 23	13 ± 4
Aβ (1-42) Monomer	176 ± 27	5 ± 2
Aβ (1-42) Fibril	300 ± 46	300 ± 30

Table 4.2. Comparison of the total signal measured for each sample by CE and bulk fluorescence with a plate reader. All data are presented as averages with standard deviations from 3 trials. Data are normalized to the values for the Aβ (1-42) fibril sample. The CE values were calculated by summing the integration of the peaks detected in the electropherogram.

Sample	Capillary Electrophoresis (CE)		Plate Reader	
	with ThT (RFU)	without ThT (RFU)	with ThT (RFU)	without ThT (RFU)
Aβ (1-40) Monomer	0.1 ± 0.1	0.0 ± 0.0	0.0 ± 0.0	0.0 ± 0.0
Aβ (1-40) Fibril	3.8 ± 0.1	0.9 ± 0.5	8.8 ± 0.1	2.1 ± 0.1
Aβ (1-42) Monomer	5.9 ± 0.6	0.2 ± 0.0	3.2 ± 0.1	0.2 ± 0.0
Aβ (1-42) Fibril	100.0 ± 26.3	12.3 ± 3.0	100.0 ± 0.5	18.9 ± 0.1

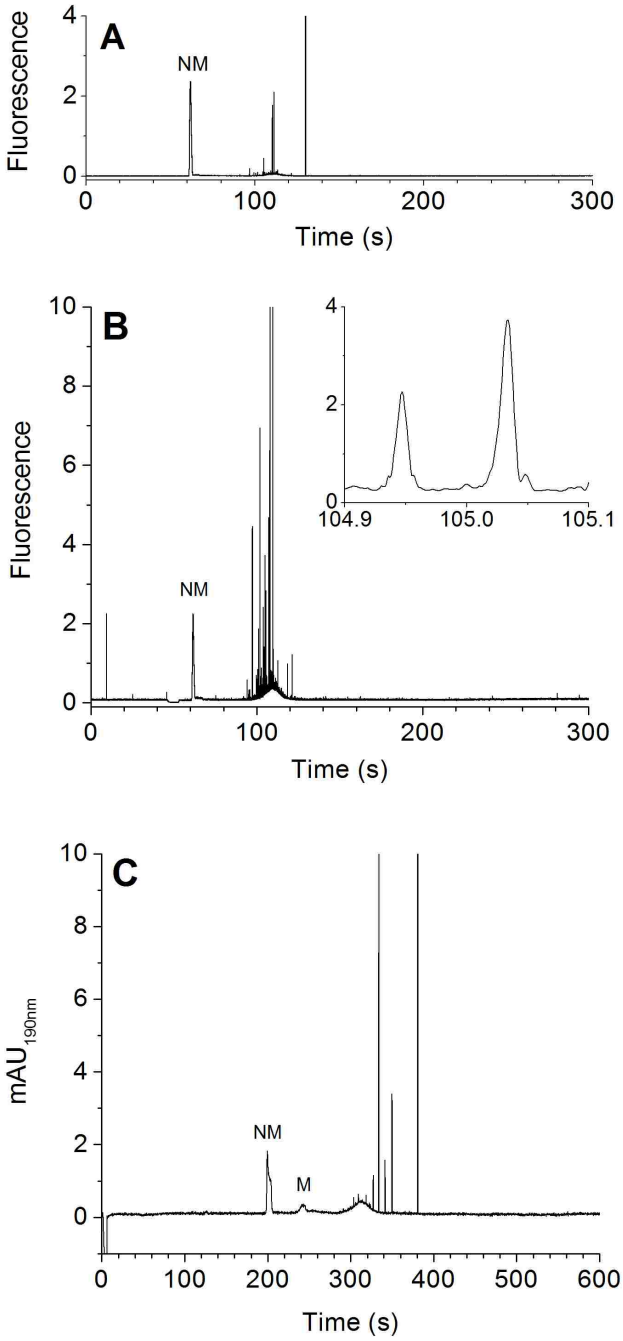

Figure 4.4. Electropherograms with LIF detection of Aβ (1-40) fibril without (A) and with (B) 15 μM ThT in the electrophoresis buffer. The experimental conditions for (A) and (B) are the same as in Figure 3. The inset in (B) is an expanded view (0.2 s) of Aβ (1-40) aggregate peaks. The same sample analyzed by CE with UV absorbance (190 nm) is shown in (C). In (C), the NM was injected for 2.0 s at 0.3 psi followed by the Aβ injection for 5.0 s at 0.5 psi. The separation potential in (C) was 25.0 kV (397 V/cm). The peaks at 200 s and 243 s are due to the neutral marker (NM) and Aβ monomer (M), respectively.

The peaks in Figure 4.4A (Aβ (1-40) fibril without ThT) are hypothesized to be due to scattered light from individual aggregates and are not unexpected. We have previously shown that polystyrene spheres as small as 110 nm diameter can be detected individually by light scattering after CE separation [82], and Aβ fibril samples produce similar peaks in instruments designed to detect scattered light with CE (unpublished results). The peaks in Figure 4.4A were detected despite the use of a 440 nm notch filter and a 490 nm bandpass filter to minimize detection of scattered light and isolate ThT fluorescence. The peaks in Figure 4.4A suggest that aggregates in the mature Aβ (1-40) fibril sample produced a non-negligible light scattering signal in the absence of ThT that will contribute to the apparent fluorescence signal in the presence of ThT. Comparing Figure 4.4A and 4.4B, it is clear that most of the observed signal in Figure 4.4B is due to enhanced ThT fluorescence. The data in Table 4.2 for microplate fluorescence measurements of this sample (without ThT) also produce a higher signal than microplate measurements of Aβ monomer samples both with and without ThT added.

It is important to recognize that the migration times and electrophoretic mobilities for the aggregate peaks in the three electropherograms in Figure 4.4 cannot be directly compared. The differences between the migration times of the aggregate peaks in the CE-LIF and CE-UV electropherograms are mainly due to the difference in capillary length from the inlet to the detection window, L_D, for the two instruments (23.0 cm, Figure 4.4A and 4.4B; 53.0 cm, Figure 4.4C). This will not affect electrophoretic mobilities of the Aβ aggregate peaks, but ThT added to the running buffer in Figure 4.4B can potentially alter the electrophoretic mobilities of Aβ aggregates compared to Figure 4.4A and 4.4C. Finally, the laboratory-constructed CE-LIF instrument used for Figure 4.4A and 4.4B was not thermostatted, but the commercial CE instrument used for Figure 4.4C does control the capillary temperature. Even though the

separation buffers used for all separations were identical, changes in capillary temperature will affect the electrophoretic mobilities of the Aβ species.

Aβ (1-42) peptide samples also were prepared and investigated by CE-LIF. Preparing an Aβ (1-42) monomer sample to be completely aggregate-free is extremely challenging owing to the fast aggregation kinetics of Aβ (1-42) peptide relative to that of the Aβ (1-40) peptide [70]. Figures 4.5A and 4.5B show representative electropherograms of the Aβ (1-42) monomer sample without and with ThT in the running buffer, respectively. Figure 4.5A shows that other than the coumarin 334 peak at 58 s, few peaks (<10) are detected in the Aβ (1-42) monomer sample when no ThT is included in the running buffer (Table 4.1). In contrast, Figure 4.5B shows an electropherogram of the same Aβ (1-42) monomer sample injected with 15 μM ThT in the electrophoresis buffer, and over 150 peaks were detected (Table 4.1). These peaks have FHWMs ranging from 3–15 ms like those attributed to individual aggregates for the Aβ (1-40) fibril sample. Characterization of this sample by CE-UV also indicated that the sample contained aggregates based on the presence of the broad peak at 343 s (Figure 4.5C) [45,118]. The large UV peak at 259 s also demonstrates that this sample contains unaggregated Aβ (1-42) monomer [118].

In the presence of ThT, the Aβ (1-42) monomer sample produced a broad peak (FWHM = 9 s) at 98 s that is separated from most of the peaks attributed to individual aggregates (Figure 4.5B). The Aβ (1-40) fibril sample (with ThT) also produced a broad peak that co-migrated with most of the peaks attributed to individual aggregates (Figure 4.4B). These broad peaks in Figures 4.4B and 4.5B could be due to oligomeric structures, which are too small to produce large distinct peaks for individual aggregates but are large enough to bind ThT and enhance its fluorescence. Biancalana et al. discuss minimal β-sheet requirements for binding and

fluorescence enhancement of ThT using a peptide self-assembly mimic [12], but it is not certain exactly what size Aβ aggregates meet the minimum β-sheet requirements.

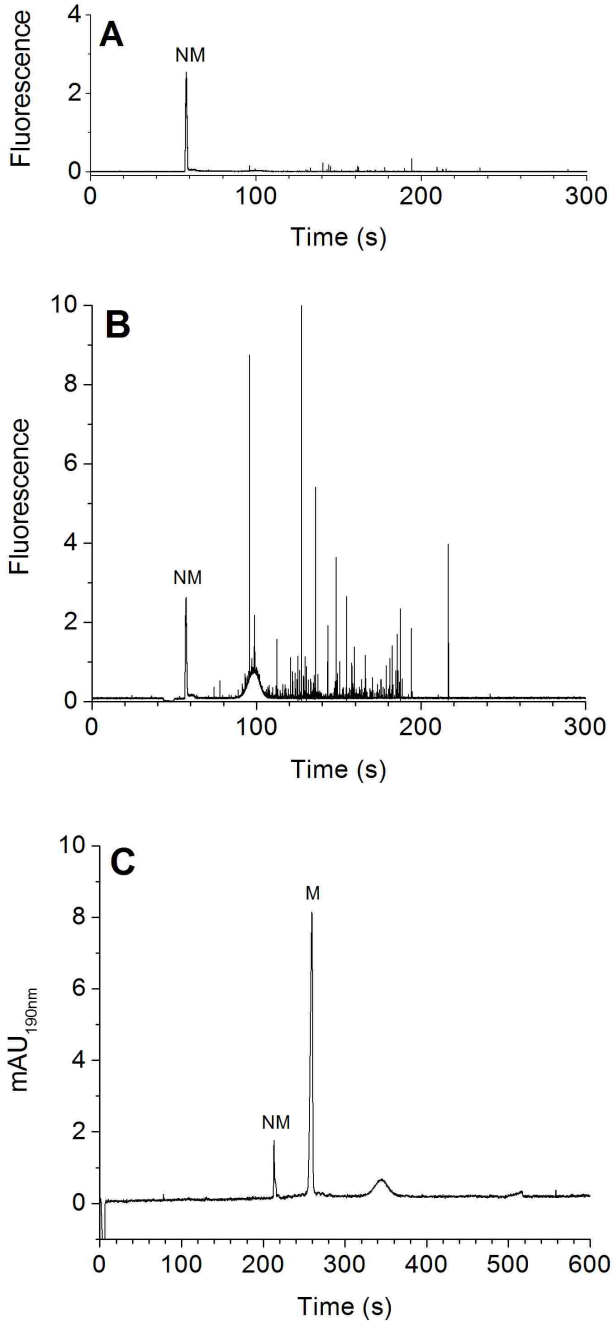

Figure 4.5. Electropherograms with LIF detection of Aβ (1-42) monomer analyzed without (A) and with (B) 15 μM ThT in the electrophoresis buffer. (C) shows the same sample analyzed by CE-UV at 190 nm. The peaks at 213 s and 259 s are due to neutral marker (NM) and Aβ monomer (M), respectively. The experimental conditions for (A–C) are the same as in Figure 4.4(A–C).

A sample containing Aβ (1-42) fibrils also was prepared and analyzed by CE-LIF (Figure 4.6) and CE-UV. The CE-UV electropherogram (Appendix A Figure A.3), bulk ThT fluorescence (Table 4.2) and TEM data (Figure 4.2D) from the Aβ (1-42) fibril sample clearly indicate that large aggregates were present in this sample. Unlike the Aβ (1-40) fibril sample studied in this work (Figure 4.4), the CE-UV data of the Aβ (1-42) fibril sample showed no signs of Aβ monomer (Appendix A Figure A.3). The absence of a monomer peak in the Aβ (1-42) fibril is presumably due to the fast aggregation kinetics and the smaller monomer equilibrium concentration of the Aβ (1-42) peptide relative to that of the Aβ (1-40) peptide [70].

Figures 4.6A and 4.6B are electropherograms of the Aβ (1-42) fibril sample without and with ThT in the running buffer, respectively. Figure 4.6A shows that the Aβ (1-42) fibril sample produced many sharp peaks in the absence of ThT that are believed to be due to scattered light from individual aggregates, similar to the scattering observed in the Aβ (1-40) fibril sample (Figure 4.4A). Table 4.1 shows that an average of 300 peaks were detected for the Aβ (1-42) fibril sample in the absence of ThT, and the peaks were much larger than those observed for Aβ (1-40) fibrils. This is consistent with the microplate measurements for the samples without ThT (Table 4.2). The large peak heights for the Aβ (1-42) fibrils relative to the Aβ (1-40) fibrils, without ThT, suggest that the Aβ (1-42) fibrils are larger.

Adding ThT to the running buffer resulted in an increase in the intensity of the peaks detected for the Aβ (1-42) fibril sample. Most of the peaks were off scale initially, and a neutral density (ND) filter (10.7% transmission) was used to attenuate the emission for the electropherogram shown in Figure 4.6B. The inset of Figure 4.6B highlights a few of the Aβ (1-42) aggregate peaks, which shows that the most peaks are well-resolved from each other. The average values for total peaks presented in Table 4.1 are the same for the Aβ (1-42) fibril sample

with or without ThT, but the peaks are much larger with ThT in the running buffer. The total signal from the Aβ (1-42) fibril sample does increase by a factor of 8 when analyzed in the presence of ThT (Table 4.2).

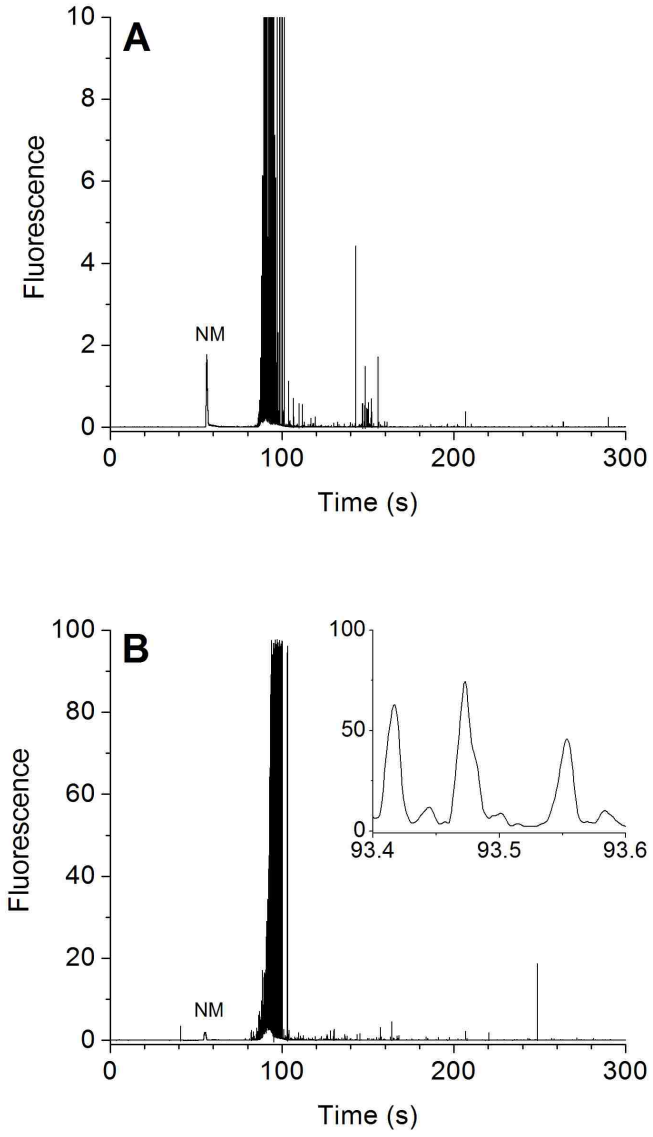

Figure 4.6. Electropherograms with LIF detection of Aβ (1-42) fibrils analyzed without (A) and with (B) ThT in the electrophoresis buffer. A neutral density filter was used in (B) to attenuate the emission (10.7% transmission), and the y-axis in (B) was adjusted to account for this. The inset in (B) shows a 0.2 s segment of the electropherogram showing several of the Aβ (1-42) aggregate peaks. The experimental conditions for (A) and (B) are the same as in Figure 4.3.

4.3.2 Validating CE-LIF Results by Bulk Measurements

Bulk ThT fluorescence measurements are widely used for studying amyloid aggregation [4,10,12,45,63,70]. While the studies presented in Section 4.3.1 and by Kato et al. [113] show that ThT can be used as a label for LIF detection of Aβ aggregates with CE, it is not known if the fluorescence detected as peaks by CE is equivalent to the increase in bulk ThT experiments commonly used to indicate increased Aβ aggregation and to study Aβ aggregation kinetics. To validate the CE results, the total fluorescence detected in electropherograms (summed area of all peaks) has been compared to bulk fluorescence measurements obtained with a microplate fluorometer using the same Aβ samples.

The data for these experiments are presented in Table 4.2. All microplate fluorometer data were normalized to the fluorescence for the Aβ (1-42) fibril sample with ThT, and all of the CE-LIF data were normalized to the total fluorescence for the Aβ (1-42) fibril sample with ThT for CE experiments. The data presented in Table 4.2 demonstrate that the results from the two methods are equivalent. Both methods show almost no signal for Aβ (1-40) monomer both with and without ThT added. Relative to Aβ (1-40) monomer, both techniques indicate a significant increase in signal for the Aβ (1-40) fibril sample without the addition of ThT, suggesting that signal due to scattered light for CE experiments (Figure 4.4A) is also detected by the microplate reader. Upon binding to ThT, the fluorescence signal for Aβ (1-40) fibrils increased by a factor of 4.2 using both techniques. Similarly, both Aβ (1-42) monomer and Aβ (1-42) fibrils show similar signal intensities using both techniques in the presence and absence of ThT.

Overall, the data in Table 4.2 show that the CE-LIF data are consistent with standard bulk fluorescence measurements. The advantage of the CE-LIF technique is that it separates the aggregates in the sample, providing a profile of mobility and intensity data for the Aβ aggregate

population.

4.3.3 Fluorescence Anisotropy of Individual Aβ Aggregates

The results presented in Sections 4.3.1 and 4.3.2 demonstrate that this CE-LIF method can separate Aβ aggregates, providing information about their numbers, electrophoretic mobilities and fluorescence intensity with ThT labeling. While this approach provides a wealth of information about the Aβ aggregate population compared to bulk measurements of ThT fluorescence, it does not allow us to determine the size and shape of an individual aggregate based on CE-LIF peaks. For particles of the size scale of Aβ fibrils, electrophoretic mobility is not a simple function of aggregate size and shape [81,82]. Standards or suitable surrogate standards representative of amyloid fibrils to determine these relationships do not exist. The relationship between aggregate size, shape and structure and ThT fluorescence also is not well understood. This section investigates the potential of characterizing individual aggregates by fluorescence anisotropy with ThT fluorescence.

Fluorescence anisotropy (FA) is a technique capable of providing size-related information about fluorescent analytes. Equation (4.2) shows how fluorescence anisotropy is related to the rotational diffusion coefficient, D, through the Perrin equation, where r_0 is the fundamental anisotropy and τ is the fluorescence lifetime. The fundamental anisotropy is dependent on the angle between the absorption and emission transition dipoles of the fluorophore [69]. It was hypothesized that the differences in size and structure of Aβ aggregates detected by CE would result in differences in fluorescence anisotropy, according to Equation (4.2).

$$r = \frac{r_o}{1 + 6D\tau} \qquad (4.2)$$

For this work, the fluorescence anisotropy detector used two PMTs that simultaneously collected perpendicular and parallel emission relative to the polarization of the excitation source

(Figure 4.1). A pair of data points was collected at each time point, and the emission intensities were used as described in Equation (4.1) to calculate the fluorescence anisotropy, r, as described in Section 4.2.3.

Figures 4.7A–C show three representative 100 ms time segments of the parallel and perpendicular fluorescence signals from the electropherograms of the Aβ (1-42) monomer sample. This sample was chosen to test the potential of fluorescence anisotropy to characterize Aβ aggregates because it produced on-scale peaks in the presence of ThT and no significant signal in the absence of ThT, i.e. minimal scattering signals. These are important attributes for this assessment because peak intensities, which are used in the calculation of fluorescence anisotropy (See Equation 4.1), cannot be determined from off-scale peaks. Moreover, it is known that scattered light from a polarized source is highly polarized and could have a significant impact on the fluorescence anisotropy results [69].

In Figure 4.7A–C, the parallel channel data are plotted as solid lines, and the perpendicular channel data are plotted as dashed lines. Note that the parallel channel data in Figure 4.7A–C are from the same electropherogram shown in Figure 4.5B. It is clear from Figures 4.7A–C that the signal detected in the parallel channel is higher than that detected in the perpendicular channel, indicating fluorescence anisotropy. Coumarin 334, which was used as a neutral marker to measure the electroosmotic flow for these studies, was also used to as a control to assess the performance of the fluorescence anisotropy detection system. The fluorescence anisotropy of coumarin 334 is expected to be near zero because it has a low MW (283.32 g/mol) [69]. The fluorescence anisotropy of coumarin 334 that was injected with the Aβ (1-42) monomer sample in Figure 4.7 was calculated to be 0.007 (coumarin 334 data not shown). This verifies that the detection system was performing properly.

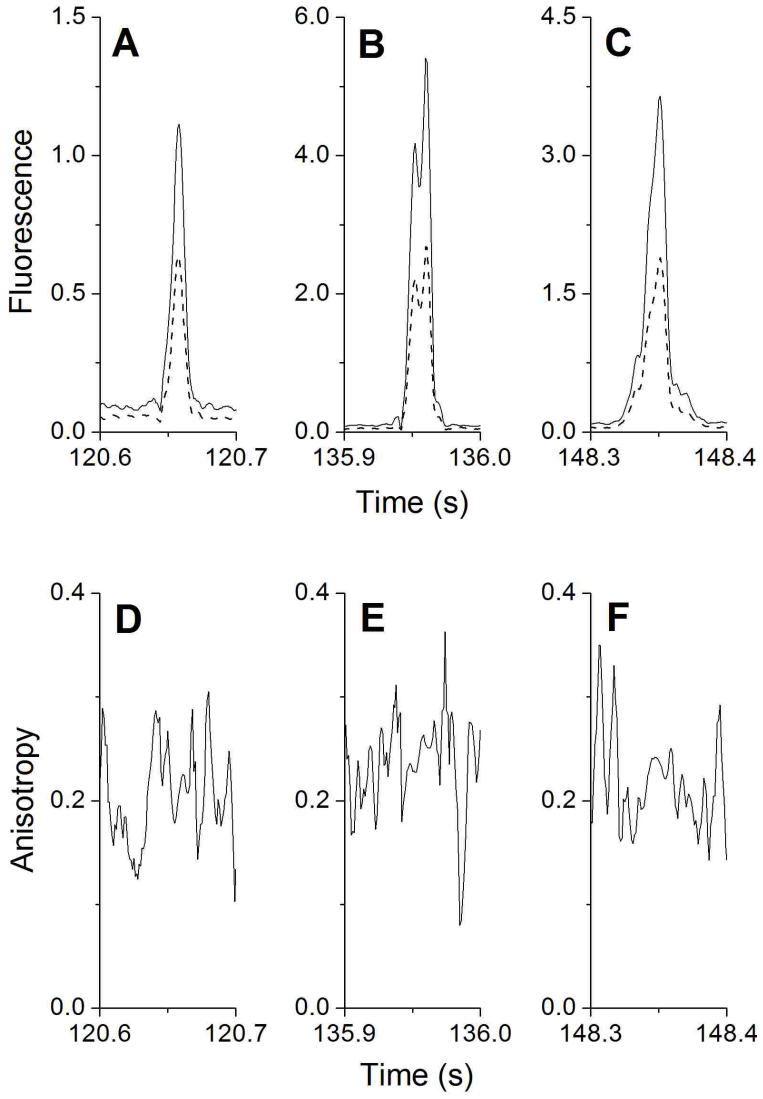

Figure 4.7. Electropherograms of Aβ (1-42) monomer for LIFA detection. Figures A–C are three 0.1 s segments of the electropherogram shown in Figure 4.5B. The parallel and perpendicular fluorescence emissions are shown as solid and dashed lines, respectively. Figures D–F show fluorescence anisotropy electropherograms corresponding to A–C, respectively. The anisotropy data in D–F were calculated using Equation 4.1.

Figures 4.7D–F show fluorescence anisotropy vs. time calculated from the LIF data in Figures 4.7A–C. Figures 4.7D–F show that individual aggregate peaks have non-zero anisotropies, but these anisotropy values are indistinguishable from the anisotropy calculated from the background signal, i.e. no fluorescence anisotropy peaks were observed in Figures

4.7D-F. It was hypothesized that plots of fluorescence anisotropy vs. time for an Aβ aggregate sample would result in distinguishable fluorescence anisotropy peaks and that the intensity of these peaks might provide information about the relative sizes of the aggregates. Protein-protein affinity interaction studies by CE-LIFA included plots of fluorescence anisotropy vs. time with distinct peaks [121]. Sabate and Saupe reported an increase in ThT fluorescence anisotropy due to aggregation of a fungal prion protein (HET-s(218-289) [68]. A study by Khurana et al. reported anisotropy values near 0.3 for ThT without any protein aggregates present in the solution [67]. While ThT clearly produced enahanced fluorescence for Aβ aggregates in this study, fluorescence anisotropy did not appear to increase significantly relative to background levels. In order to effectively use CE with fluorescence anisotropy detection to characterize individual aggregates, the fluorescence anisotropy of Aβ aggregates must be distinct from that of the background anisotropy.

4.4 Conclusions

This work shows that CE with LIF detection can be used to analyze samples of aggregated Aβ (1-40) and Aβ (1-42) using ThT, a dye that fluoresces upon binding to the amyloid fibrils, in the running buffer. This study distinguishes itself from an earlier study [113] by demonstrating the ability to separate and detect individual aggregates and by validating the CE-LIF data using direct comparison with bulk thioflavin T fluorescence measurements, which are widely used to study aggregation kinetics of amyloidogenic peptides. Compared to bulk ThT fluorescence measurements, CE-LIF provides a profile of the aggregate population based on electrophoretic mobilities, fluorescence intensities and numbers of individual aggregate peaks. The studies presented here focus on analysis of Aβ aggregates, but they should be applicable to studies of other amyloidogenic peptides.

Initial studies of CE-LIFA to characterize individual Aβ aggregates yielded encouraging results, but significant improvements must be made to effectively apply this to study Aβ aggregation.

CHAPTER 5

A DATA TREATMENT METHOD FOR DETECTING FLUORESCENCE ANISOTROPY PEAKS IN CAPILLARY ELECTROPHEROGRAMS

5.1 Introduction

Fluorescence anisotropy (FA) is a measure of the degree of emission depolarization of a fluorescent molecule after being excited with a polarized excitation source [69]. A major cause of emission depolarization is molecular rotational diffusion during the excited state lifetime of the fluorophore. In general, molecules with smaller rotational diffusion rates, i.e. slower rotation in solution, exhibit larger fluorescence anisotropy. Similarly, molecules that have large rotational diffusion rates exhibit smaller fluorescence anisotropy.

Laser-induced fluorescence anisotropy (LIFA) has been demonstrated as an on-column detection technique for capillary electrophoresis (CE) for studies of biomolecular interactions, e.g. protein-protein or oligonucleotide-protein interactions [119-122,126,127]. Chapter 4 demonstrates the separation and detection of individual Aβ peptide aggregates by CE-LIF using ThT in the running buffer as the fluorescent probe. It was hypothesized that fluorescence anisotropy differences between aggregates could indicate relative size differences between separated aggregates (see Chapter 4). Plots of fluorescence anisotropy vs. time showed that fluorescence anisotropy due to aggregates and the ThT background [67] were indistinguishable; i.e. no fluorescence anisotropy peaks were observed although there were obvious peaks in plots of fluorescence vs. time. In order to evaluate if CE-LIFA can be used to differentiate individually detected Aβ aggregates, it is important that the fluorescence anisotropy of the aggregates be easily distinguishable from the background anisotropy.

A close examination of the few CE-LIFA papers available indicated that most papers did not include plots of fluorescence anisotropy vs. time [119,121,122,126]. This hinted that other

researchers using fluorescence anisotropy for separation detection may have faced the same issues that we encountered when plotting fluorescence anisotropy vs. time, i.e. clear fluorescent peaks, low background fluorescence, high fluorescence anisotropy background and no observed fluorescence anisotropy peaks. We then set out to understand why our anisotropy plots did not produce peaks like some examples in the literature [120,127] and how we could better visualize the peaks in plots of fluorescence anisotropy vs. time that are evident in the raw fluorescence data.

A simple data treatment method is described here that enables differentiation of anisotropies due to fluorescent peaks (peptide aggregates here) and background signals. This data treatment method effectively extracts anisotropy peaks from fluorescence anisotropy electropherograms that were originally embedded in the background fluorescence anisotropy noise. This method allows simple visualization of anisotropy peaks vs. time.

5.2 Experimental

5.2.1 Chemicals and Peptide Samples

The chemicals, solutions and sample preparations used in this study have been described in detail in Chapter 4. Tris (hydroxymethyl) aminomethane (Tris) was purchased from Fisher Scientific (Fair Lawn, NJ). Thioflavin T (ThT) was purchased from Sigma (St. Louis, MO).

The electropherograms presented in this work were performed using 10.00 mM Tris buffer at pH 7.79. Thioflavin T (15 μM) was included in the running buffer to detect Aβ (1-42) aggregates [113]. The Aβ (1-42) peptide sample was prepared as previously described [45,118]. The monomer-equivalent concentration of the Aβ (1-42) was measured to be 5.1 μM by HPLC-UV [44]. Analysis of the sample by TEM, CE-UV and CE-LIF confirmed that the sample contained Aβ (1-42) aggregates (see Chapter 4).

5.2.2 Capillary Electrophoresis

Capillary electrophoresis was performed in a fused-silica capillary (ID = 50 μm, OD 366 μm; Polymicro Technologies, Phoenix, AZ) cut to 60.0 cm total length with a window created at 23.0 cm from the inlet. The electrophoretic potential was applied across the capillary using a Spellman CZE1000R high-voltage power supply (Hauppauge, NY) at 25.0 kV (417 V/cm), which produced an electrophoretic current of 5-6 μA. Sample injections were performed for 5 s at 25.0 kV. Prior to each injection, the sample was vortexed to suspend any aggregates that could have settled to the bottom of the sample vial.

5.2.3 Laser-Induced Fluorescence Anisotropy Detection System

The fluorescence anisotropy detection system used here has been described in detail previously (see Chapter 4 Figure 4.1). This detector is based on the design reported by Whelan et al. [120] and has been modified for the detection of narrow peaks (3-15 ms) due to individual aggregates. The beamsplitter cube (10FC16PB.3, Newport Corporation; Irvine, CA) separates the fluorescence emission into parallel and perpendicular components relative to the polarization of the 445 nm diode laser excitation source (Model No. LDCU12/7532, Power Technology, Inc; Alexander, AR). Both emission components were spectrally filtered by a 490 nm bandpass filter and 440 nm notch filter. Then the emissions were detected simultaneously and equidistant from the capillary by two identical photomultiplier tubes (PMT) (H9306-04, Hamamatsu; Bridgewater, NJ). The outputs of the PMTs were filtered by 500 Hz low pass RC filters and collected by a National Instrument PCI-6024E DAQ board at a scan rate of 1000 Hz. The CE-LIFA data collection was controlled by a program written in LabView 5.0, and the data were analyzed using Origin Pro 7.5 and Microsoft Excel 2007.

Equation 5.1 was used to calculate the fluorescence anisotropy, r, where $I_{\parallel}$, and $I_{\perp}$, are

the measured parallel and perpendicular fluorescence intensities relative to the polarization of the excitation source. The factor *G* corrects the anisotropy for the differences in sensitivities of the two PMTs. For this work, *G* was empirically adjusted to 1 by optimizing the potentials applied to both PMTs so that the responses and sensitivities were equal for a small fluorescent molecule, Lucifer Yellow (Molecular Probes, Eugene, OR) over range of concentrations (data not shown). The applied potentials for $PMT_{\parallel}$ and $PMT_{\perp}$ were 1000 and 935 V, respectively.

$$r = \frac{I_{\parallel} - GI_{\perp}}{I_{\parallel} + 2GI_{\perp}} \qquad (5.1)$$

5.3 Results and Discussion

The aggregation of Aβ peptides has been linked to Alzheimer's disease. The data presented here are from a capillary electrophoretic separation of a mixture of Aβ (1-42) peptide aggregates. The peptides are non-covalently labeled with the amyloid dye, Thioflavin T (ThT). The peaks in the electropherograms presented here are due to individual Aβ (1-42) aggregates.

Figure 5.1 presents parts of three electropherograms for a sample containing Aβ (1-42) aggregates. The individual parallel and perpendicular fluorescence signals are plotted in the lower part of the figure (left y-axis), and the fluorescence anisotropy calculated from these signals (Equation 5.1) is plotted in the top part of the figure (right y-axis). The fluorescence peak in Figure 5.1 is due to an individual Aβ (1-42) aggregate with ThT noncovalently bound to it (refer to Chapter 4 for more details). The binding of ThT to Aβ causes an excitation and emission spectral shift and enhancement at the wavelengths being using for excitation and detection (440 and 490 nm) [12,63]. Figure 5.1 shows only 1 of the 178 aggregate peaks that were detected for this injection of Aβ (1-42) aggregates. Figure 5.1 shows that the anisotropies of the fluorescence due to Aβ aggregates and due to background fluorescence of ThT [67] are indistinguishable, i.e. no fluorescence anisotropy peaks are apparent in the plot of fluorescence anisotropy vs. time

although fluorescence peaks for $I_{\parallel}$, and $I_{\perp}$ and their different heights are obvious. The slight difference in the background fluorescence signals for ThT is also apparent in Figure 5.1.

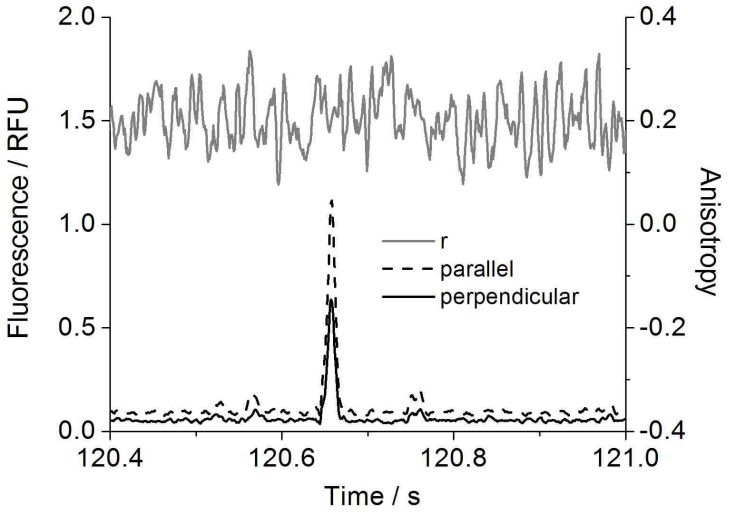

Figure 5.1. Bottom two plots are electropherograms with LIF detection showing an individual Aβ (1-42) aggregate peak at 120.65 s (left axis). The dashed plot and dark solid plot are the parallel and perpendicular fluorescence emissions, respectively. The lighter solid plot is the fluorescence anisotropy, r, calculated from the parallel and perpendicular emissions using Equation 5.1 (right axis).

Based on reports in the literature, we expected that fluorescence peaks resulting from the Aβ (1-42) aggregates would produce distinguishable peaks in a plot of fluorescence anisotropy vs. time [120]. Whelan et al. demonstrated the use of CE-LIFA for affinity assays to monitor the fluorescence anisotropy of $G_{\alpha i1}$ protein complex formation with BODIPY-GTPγS (BGTPγS) [120]. In that work, the fluorescent probe, BODIPY, was included in the electrophoresis buffer, similar to ThT in this paper [120]. As shown in Figure 4 of Whelan et al. [120], the parallel and perpendicular fluorescence signals of the $G_{\alpha i1}$/GTPγS complex were approximately 40 and 25 RFU above background signals of 35 RFU for both the parallel and perpendicular channels [120]. A fluorescence anisotropy peak was clearly observed in plots of fluorescence anisotropy vs. time for the $G_{\alpha i1}$/GTPγS complex with an intensity of approximately 0.08 above a background fluorescence anisotropy of approximately 0.00 [120].

An important difference between the data reported by Whelan et al. and that presented here is the heights of the analyte peaks relative to the fluorescence background signal. In Figure 5.1 of this manuscript for example, the ratios of the Aβ aggregate peak heights to the intensity of the background signals for the parallel and perpendicular channels are 11.2 and 10.3, respectively. The equivalent ratios observed by Whelan et al. for the $G_{\alpha i1}$/GTPγS complex were about 1.1 and 0.7 [120].

It was hypothesized that uniformly adding an artificial background signal to the data for both fluorescence channels, $I_{\parallel}$, and $I_{\perp}$, prior to calculating the anisotropy might enable differentiation of the anisotropies of the aggregate peaks and background, resulting in the visualization of anisotropy peaks. This would greatly facilitate visualizing and interpreting differences between fluorescence anisotropy of Aβ aggregates and that of the background. Adding an artificial signal to all fluorescence data points would have the same effect on the data as if ThT were producing a high fluorescence background signal similar to the BODIPY background signal observed in the work of Whelan et al. [120].

Figure 5.2A shows plots of the original fluorescence data (bottom two traces) and the fluorescence data after adding an artificial signal, z, of 0.5 to the original data (top two traces). In Figure 2, the ratio of the fluorescence intensity of the Aβ aggregate peak at 121.8 s to that of the background for the parallel and perpendicular channels are 7.0 and 8.4, respectively. The added value of 0.5 RFU produced a ratio of Aβ peak height:background signal of 1.1 and 0.7, which are the same ratios of analyte signal:background signal observed by Whelan et al. [120].

Figure 5.2B shows the fluorescence anisotropy before and after the addition of the 0.5 RFU background signal. In Figure 5.2B, the upper trace is the anisotropy calculated from the original fluorescence data, and the lower trace is the anisotropy calculated from the modified

fluorescence data. As hypothesized, the addition of the artificial background signal results in a relative enhancement of the anisotropy of the aggregate peaks relative to the background anisotropy. It is clear that the fluorescence anisotropy peaks correspond in time to the fluorescence peaks in Figure 5.2A.

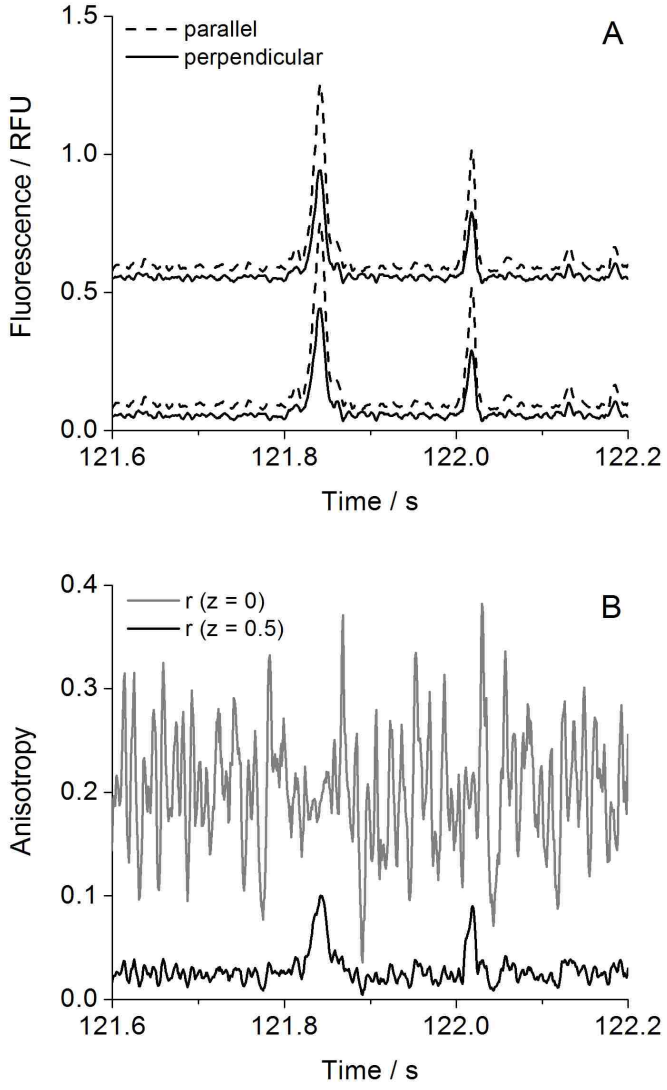

Figure 5.2. (A) Electropherograms with LIF detection showing peaks due to two individual Aβ (1-42) aggregates at 121.84 s and 122.02 s. The dashed plot and solid plot are the parallel and perpendicular fluorescence emissions, respectively. The bottom two plots are LIF emissions without any addition of z, and the top two traces are the LIF emissions after the additions of z = 0.5. (B) Anisotropy calculated from (A) using Equation 5.1. The lighter solid plot was calculated from the unadjusted parallel and perpendicular LIF emissions (lower two traces in (A)). The lower darker solid plot was calculated from the parallel and perpendicular LIF emissions after the addition of z = 0.5 (upper two traces in (A)).

This result can be explained mathematically starting with the Equation 5.1, where *r* is the original anisotropy, i.e. the anisotropy before the fluorescence signals are artificially adjusted. Equation 5.1 is used to calculate the anisotropy data plotted in the upper trace of Figure 5.2B. Recalling that this method adds a constant artificial signal, z, to all the fluorescence data, the modified anisotropy, r_m, can be described by Equation 5.2, which can be reduced to Equation 5.3. Equation 5.3 can be used to calculate the modified anisotropy data, which is plotted vs. time in the lower plot in Figure 5.2B. Subtracting Equation 5.3 from Equation 5.1 gives Equation 5.4, which is useful for considering the differences observed between the two plots in Figure 5.2B.

$$r_m = \frac{(I_{\parallel} + z) - (I_{\perp} + z)}{(I_{\parallel} + z) + 2(I_{\perp} + z)} \tag{5.2}$$

$$r_m = \frac{I_{\parallel} - I_{\perp}}{I_{\parallel} + 2I_{\perp} + 3z} \tag{5.3}$$

$$r - r_m = \left[\frac{I_{\parallel} - I_{\perp}}{I_{\parallel} + 2I_{\perp}}\right] - \left[\frac{I_{\parallel} - I_{\perp}}{I_{\parallel} + 2I_{\perp} + 3z}\right] \tag{5.4}$$

Only the second term on the right side of Equation 5.4 is dependent on z. For lower fluorescence intensities, the z term is more important, and greater differences will result between the original and modified anisotropies. Conversely, adding z to higher fluorescence intensities, e.g. like those produced by aggregates, has less of an impact on the second term of Equation 5.4, which translates to smaller differences between the original and modified anisotropies.

In general, the anisotropy of the background fluorescence is reduced to a greater extent relative to the anisotropy of the Aβ aggregate peaks. After addition of an artificial background signal, our data resembles the data obtained by Whelan et al., and peaks become apparent in a plot of anisotropy vs. time as shown in Figure 5.2B. The natural background fluorescence in our data is due to the fluorescence of unbound ThT, and this fluorescence does have a fluorescence

anisotropy value of about 0.2 at the ThT concentrations used in this work. If the background fluorescence did not exhibit fluorescence anisotropy, the plot of fluorescence anisotropy vs. time would be similar to the upper plot in Figure 5.2B, except it would be centered at 0.0 instead of 0.2. The high noise in the plot of fluorescence anisotropy vs. time would still largely mask the fluorescence anisotropy peaks observed after data modification (bottom plot in Figure 5.2B) [67]. The modified fluorescence anisotropy values are not equal to the true (original) anisotropy values. Our goal here was to develop a data treatment method that allows better visualize fluorescence anisotropy peaks in a plot of fluorescence anisotropy vs. time. Once the peaks of interest have been identified with the help of this method, the true anisotropy values can be easily calculated using Equation 5.1 for data points at the migration times of interest.

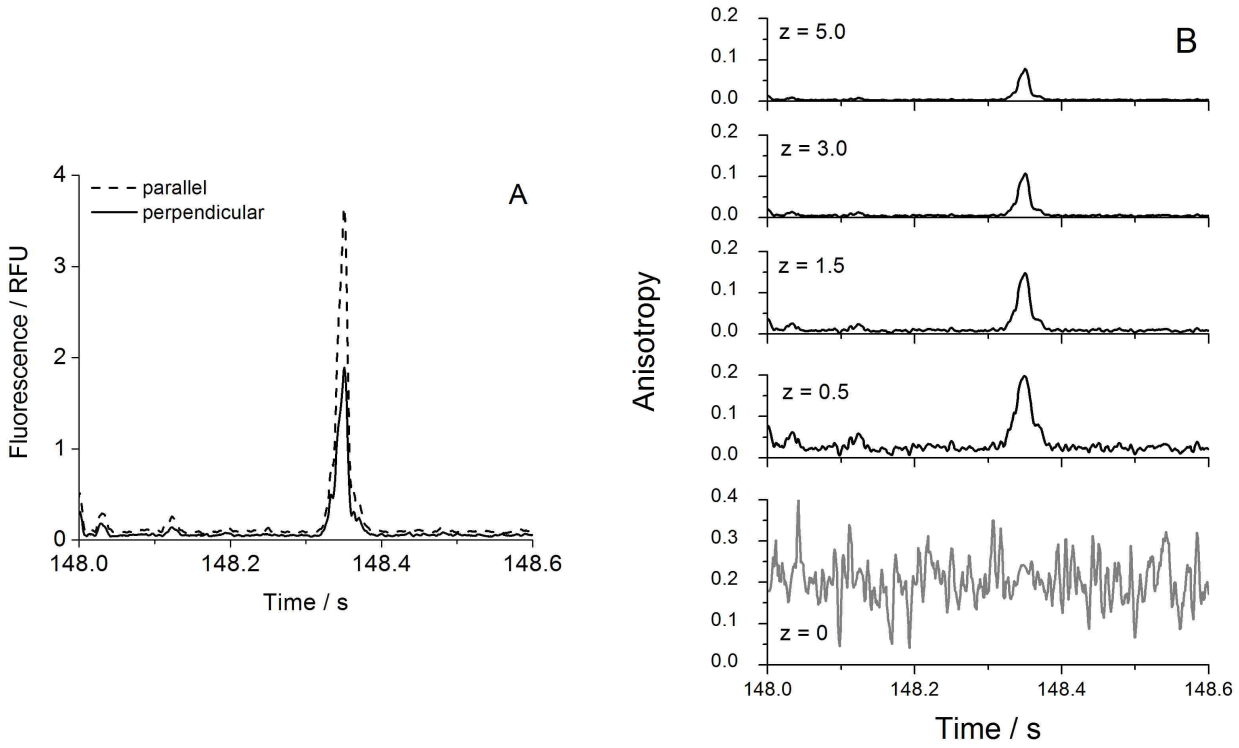

Figure 5.3. (A) Electropherogram with LIF detection showing an individual Aβ (1-42) aggregate at 148.35 s. The dashed plot and solid plot are the parallel and perpendicular fluorescence emissions, respectively. (B) Anisotropy plots at varying levels of z (0, 0.5, 1.5, 3.0 and 5.0) added to the LIF emissions. Note that all the y-axis in Figure 5.3B are the same except in the plot where z = 0.

The impact of the magnitude of z on the adjusted fluorescence anisotropy was investigated. Figure 5.3A shows another time segment of parallel and perpendicular fluorescence data from the same electropherogram shown in Figures 5.1 and 5.2. Figure 5.3B shows five plots of fluorescence anisotropy vs. time, which were calculated from the fluorescence data in Figure 5.3A using several values of z (z = 0, 0.5, 1.5, 3.0 and 5.0 RFU). Consistent with Equation 5.3 and the discussion above, larger z values result in lower fluorescence anisotropy values, and fluorescence anisotropy peaks become apparent in the electropherograms.

The S/N of some of the fluorescence anisotropy peaks were analyzed as a function of the magnitude of z. Figure 5.4 shows a plot of the fluorescence anisotropy S/N vs. z for selected peaks from the same electropherogram. The S/N values are also presented in Table 5.1.

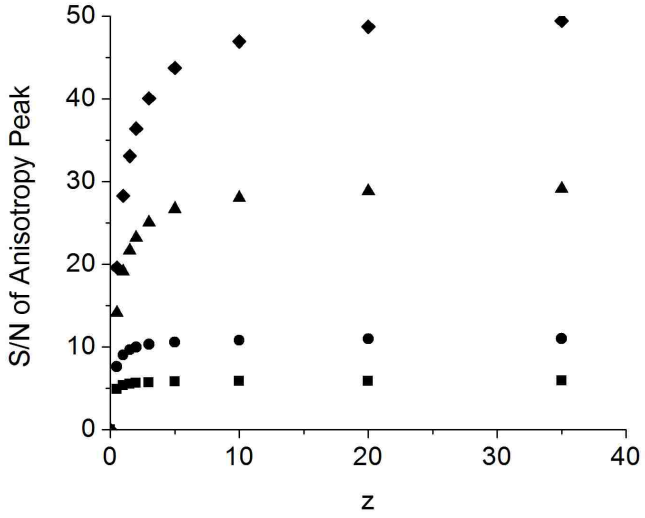

Figure 5.4. S/N of four individual Aβ aggregate anisotropy peaks plotted as a function of z. The anisotropy values were derived from fluorescence peaks with various S/N values. The diamonds, triangles, circles and squares are are anisotropy S/N values from a fluorescence peaks whose parallel fluorescence peaks' S/N values were calculated to be 127, 65, 30 and 15, respectively. The S/N values plotted here are tabulated in Table 5.1.

The peaks in Figure 5.4 were selected based on the S/N of their corresponding fluorescence peaks prior to any data treatment (S/N = 15, 30, 65, and 127). In general, the S/N

values of the anisotropy peaks initially increase as z increases before approaching a limiting value. For the peaks examined here, the S/N values of the anisotropy peaks plateau at a maximum S/N when z is approximately 10 RFU. The plots in Figure 5.4 show that the maximum anisotropy S/N was greater if the corresponding fluorescence peak had a greater S/N. For z = 20 RFU, the anisotropy S/N values are 5.9, 11.0, 28.8, 48.7 and 142.7 for fluorescence peaks that had S/N values of 15, 30, 65, 127 and 323, respectively. The data treatment method resulted in a relatively large increase in fluorescence anisotropy S/N.

Table 5.1. S/N of anisotropy peaks as a function of z (z = 0.5, 1, 1.5, 2, 3, 5, 10, 20 and 35). Data shown for 5 different aggregate peaks, whose fluorescence peaks S/N values varied (15, 30, 65, 127 and 323). All data are plotted in Figure 5.4 with the exception of the data from the fluorescence peak with a S/N of 323.

		z								
		0.5	1	1.5	2	3	5	10	20	35
S/N of Fluorescence Peaks	15	4.9	5.3	5.5	5.6	5.7	5.8	5.9	5.9	5.9 (1.2)
	30	7.6	9.0	9.6	10.0	10.3	10.6	10.8	11.0	11.0 (1.4)
	65	14.1	19.1	21.7	23.2	25.0	26.7	28.0	28.8	29.1 (2.1)
	127	19.6	28.3	33.1	36.4	40.1	43.7	46.9	48.7	49.4 (2.5)
	323	29.0	48.7	63.3	74.3	90.4	109.1	129.4	142.7	149.3 (5.1)

5.4 Conclusions

A simple and effective data treatment method was described for visualizing fluorescence anisotropy peaks in a plot of fluorescence anisotropy vs. time for capillary electrophoresis separations of Aβ (1-42) peptide aggregates. The data treatment method revealed fluorescence

anisotropy peaks that were masked by the high anisotropy noise of the background signal prior to the data treatment. Although this method did alter the fluorescence anisotropy values in the peaks, true fluorescence anisotropy values could be easily calculated once peaks of interest had been identified and considered. While this data treatment method was applied to CE separations with laser-induced fluorescence anisotropy detection, it is equally applicable to other separation techniques using fluorescence anisotropy detection.

CHAPTER 6
FLUORESCENCE ENHANCEMENT OF THIOFLAVIN T BY POLYSTYRENE BEADS

6.1 Introduction

Thioflavin T is a benzothiozole fluorescent dye that has been used extensively to study amyloid aggregation. After binding to amyloid aggregates, ThT undergoes a red shift for both the excitation and emission λ_{max} and an increase in fluorescence signal relative to unbound ThT [64,65]. These two characteristics of ThT are often referred to in the literature as "ThT enhancement". Because ThT enhancement has been observed in the presence of several amyloid proteins, it is believed that the β-sheet structural motif, which is common to amyloid aggregates, is the binding site of ThT.

The exact cause of ThT enhancement is not well understood. Related hypotheses have been that ThT enhancement depends on the torsional angle between the benzylamine and benzylthiol rings [12,66]. The underlining idea is that when ThT is bound, the torsional angle between its ring structures is rigid and small, i.e. the rings are more coplanar relative to when ThT is unbound. This can reduce the HOMO/LUMO gap, resulting in a red shift observed in ThT enhancement. This is plausible, and if it is accurate, it is also plausible that ThT enhancement could be observed in the presence of other structures that can bind and stabilize the coplanar ThT. In fact, bacteria, which can grow readily under the conditions used for Aβ aggregation, can bind ThT and produce false positives [39].

Thioflavin T was used to label and detect hundreds of individual Aβ (1-40) and (1-42) aggregates that were separated by capillary electrophoresis (CE) (see Chapter 4). This was accomplished by including ThT as a component in the electrophoresis buffer. While establishing a baseline, the buffer (with ThT in it) showed irreproducible sharp peaks that mimicked Aβ/ThT

peaks. These false-positive peaks could not be deconvoluted from Aβ/ThT. After filtering the ThT buffer through a 0.02 μm filter, the number of peaks in the buffer reduced to nearly zero and the few random peaks remaining were far less intense. Because filtering reduced the number of peaks, it is assumed that the peaks were either due to bacterial growth in the buffer or the accumulation of dust particles.

Importantly, these peaks were not observed in buffer that did not include ThT even before filtering. This suggested that whatever was causing the peaks was not itself fluorescent, but it could have bound ThT and produced a fluorescent signal. Although we nearly eliminated the false positive peaks by filtering, we wanted to develop a better understanding of ThT enhancement in the presence of non-amyloid particles because of the potential they have to produce false-positives in amyloid studies using ThT.

This work is a fluorescence spectroscopic study of ThT enhancement by polystyrene (PS) beads. Polystyrene beads are ideal analytes for this study because they are uniform in size and the concentrations are controllable (unlike amyloid aggregates). Moreover, many sizes of PS beads are commercially available.

6.2 Experimental

6.2.1 Chemicals

Polystyrene (PS) beads of different sizes (1072 ± 19, 771 ± 25, 535 ± 10, 356 ± 14, 202 ± 10, 108 ± 4.5 nm) were purchased from Polysciences (Warrington, PA). Thioflavin T (ThT) was purchased from Sigma (St. Louis, MO). Tris(hydroxymethyl) aminomethane (Tris) was purchased from Acros (Geel, Belgium) and hydrochloric acid (HCl) was purchased from Fisher Scientific (Pittsburgh, PA). 10.00 mM Tris buffer was prepared in ultrapure water (>18 MΩ cm) from a Modulab water purification system (United States Filter; Palm Desert, CA) and adjusted

to pH 7.80 with HCl. The solutions of PS beads were prepared by mixing required volume of stock solution with the 10.00 mM Tris buffer at pH 7.80 filtered twice with a 0.02 μm syringe filter (Fisher Scientific; Pittsburgh, PA). All stock solutions were homogenized by vortexing prior to use. Dilutions of bead stock solutions were performed directly in microplate well for plate reader studies and in cuvette for fluorometer study.

6.2.2 Plate Reader Study

Fluorescence of the samples was measured using a BMG Lab Technologies FLUOstar 430 microplate reader (Offenberg, Germany). Measurements were made from the top of a black 96 well plate (Corning 3650) (Corning incorporated; Corning, NY) with excitation wavelength 440±12 nm and emission wavelengths 485± 12 nm. A 60 s orbital shaking of the plate was performed prior to the measurement to mix and homogeneous samples.

Measurements were performed in well mode. Each measurement was the average intensity from 100 flashes. Three measurements were made from each well before moving on the next well. Each well that contained PS beads with ThT had a corresponding well with the same concentration of PS beads without ThT. This allowed any scattered light from PS beads to be subtracted from the fluorescence signal.

6.2.3 Spectrophotometry and Spectrofluorometry

Absorbance spectra (200 - 800 nm) of all samples and blank solutions in 10.00 mM tris buffer at pH 7.80 were determined with a Cary 50 UV-Vis spectrophotometer (Varian; Palo Alto, CA) using a 1 cm quartz cuvette. A slit width of 1 nm was used for data collection. Absorbance spectra were collected at room temperature, and the blank was subtracted from each spectrum.

Excitation-emission spectra and EEMs of the samples were determined using a SPEX Fluorolog-3 spectrofluorometer (model FL3-22TAU3; HORIBA Jobin Yvon; Edison, NJ)

equipped with a 450 W Xenon lamp and R928P photomultiplier tube (PMT) detector. Both excitation-emission spectra and EEMs were performed at room temperature using a 1-cm quartz cuvette and adjusting both excitation and emission slit widths to 5 nm. For the determination of EEMs the excitation wavelength was varied from 250 nm to 500 nm in 5 nm intervals, while the emission spectra were collected from 350 nm to 600 nm in 2 nm intervals. For the determination of excitation spectrum, the emission wavelength was fixed (at 435 or 490 nm) and excitation was scanned from 250 nm to 500 nm. Similarly, for the determination of emission spectrum, the excitation wavelength was fixed (at 332, 405, or 440 nm) and emission was scanned from 350 nm to 600 nm. The scanning was at the interval of 1 nm for both excitation and emission spectra.

For data processing, an inner-filter effect correction was performed on the data for both PS bead without ThT and PS bead with ThT. This was accomplished using Equation 6.1, where the F_c is the corrected fluorescence, F_{obs} is the observed fluorescence, i.e. the raw measured fluorescence, Ab_{em} is the absorbance measured at the emission λ and Ab_{ex} is the absorbance measured at the excitation λ. After the inner filter correction, the scattering was subtracted from the fluorescence. The contour plots of EEM data and excitation-emission spectrum were plotted using OriginPro 7.5 (Origin Lab; Northapton, MA).

$$F_c = F_{obs}\frac{(Ab_{em} + Ab_{ex})}{2} \qquad (6.1)$$

6.3 Results and Discussion

6.3.1 Effect of Bead Diameter on ThT Fluorescence

The interaction of ThT with PS beads is thought to be dependent on the surface area of the PS beads similarly to the ThT interaction with the β-sheet motif of the protein aggregates. The concentration units, therefore, are reported here as PS bead surface area per volume of solution, i.e. μm^2/mL. The data in Table 6.1 and Equations 6.2–6.4 demonstrate how these values

were determined. The 108 nm PS beads will be used to briefly explain the equations. For the 108 nm PS beads, the surface area per bead, A_b, was calculated using Equation 6.2, where $\boldsymbol{\phi}$ is the PS bead diameter. The number of beads per volume, N_v, was determined using Equation 6.3, where w is the grams of polymer per mL of solution (provided by PS bead manufacturer), ρ is the density of the polymer (g/mL) (provided by PS bead manufacturer), V is the volume of PS bead solution prepared. Equation 6.4 is used to convert from number of beads per mL to total surface area per mL, A_T.

Table 6.1. Volume of beads needed to obtain a PS bead concentration of 1.26×10^8 μm^2/mL for each PS bead.

Bead Diameters, ϕ (nm)	**Surface Area per Bead, A_b (μm^2)**	**Number of Beads per Volume, N_V (N/mL)***	**Total Surface Area per Volume, A_T (μm^2/mL)**	**Volume of Bead Solution Used (μL) ‡**
108	3.67×10^{-2}	3.75×10^{13}	1.38×10^{12}	2.3
202	1.28×10^{-1}	5.78×10^{12}	7.41×10^{11}	4.2
356	3.98×10^{-1}	1.09×10^{12}	4.33×10^{11}	7.2
535	9.00×10^{-1}	3.17×10^{11}	2.85×10^{11}	10.9
771	1.87	1.04×10^{11}	1.94×10^{11}	16.6
1072	3.61	3.90×10^{10}	1.41×10^{11}	23.5

* *Based on manufacturer's percent weights.*
‡ *This was the volume used of a 100-fold dilution of the manufacturer's stock solution to obtain 1.26×10^8 μm^2/mL in a total of 250 μL for the plate reader study.*

$$A_b = 4\pi\left(\frac{\phi}{2}\right)^2 \qquad (6.2)$$

$$N_V = \frac{6w10^{12}}{\rho\phi^3\pi V} \qquad (6.3)$$

$$A_T = A_b \times N_V \qquad (6.4)$$

Figure 6.1 demonstrates the effect of PS bead diameter on ThT fluorescence for two different concentrations, 1.26×10^9 μm^2/mL (A) and 1.26×10^8 μm^2/mL (B). Six PS bead

diameters were tested, and first column in Table 6.1 lists the bead diameters used.

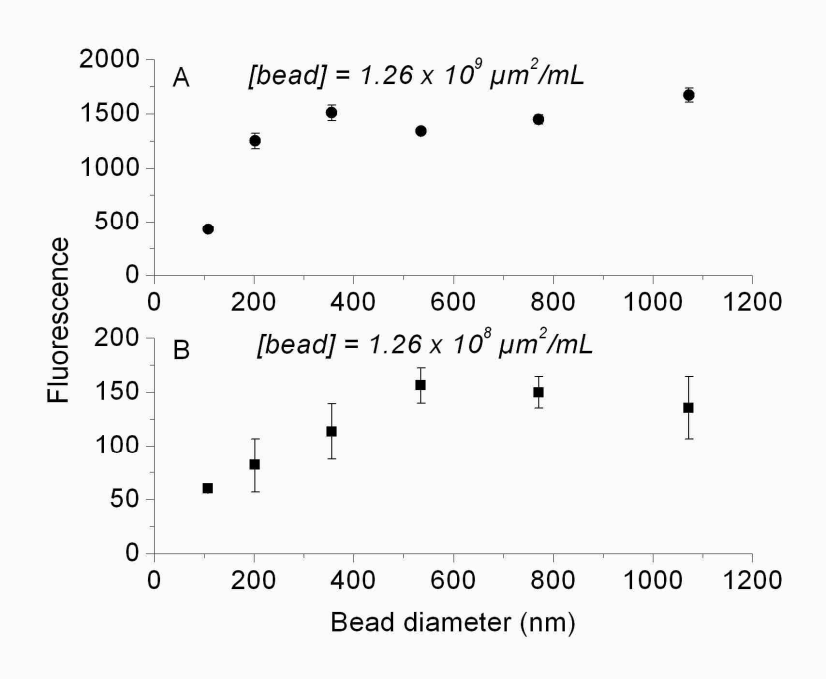

Figure 6.1. Fluorescence of 15 μM ThT in the presence of PS beads of different sizes. The fluorescence was measured using a plate reader and a 96-well plate (excitation: 440 nm, emission: 485 nm). Two graphs are for two different PS bead concentrations (1.26×10^9 μm^2/mL and 1.26×10^8 μm^2/mL). Concentrations are reported as bead surface area per mL.

A maximum fluorescence is reached that appears to be related to bead diameter and concentration. For both concentrations, the intensity of the maximum fluorescence is approximately 3-fold that of the intensity of the smallest bead size tested. The bead diameter at which the maximum fluorescence is reached is 202 nm for 1.26×10^9 μm^2/mL (Figure 6.1A) and 535 nm for the 1.2×10^8 μm^2/mL (Figure 6.1B). More smaller beads are needed to attain the same μm^2/mL compared to larger beads. For example, 8.63×10^{10} beads/mL of the 108 nm beads are needed to attain a surface area per volume of 1.26×10^8 μm^2/mL, while 3.46×10^9 beads/mL of the 535 nm beads are needed to attain the same 1.26×10^8 μm^2/mL. A higher number of beads/mL could result in the beads being packed more closely together. Also, the greater number of beads/mL could cause the beads to aggregate in solution. Either of these

possibilities could effectively reduce the available surface area of the beads for binding ThT and would explain the lower ThT fluorescence intensity for the smaller beads relative to larger beads. Larger beads will not pack so tightly, so more bead surface area is available for binding ThT. A related effect has been suggested to explain the decrease in ThT intensity in the presence of Aβ fibril formation that is followed by the initial ThT increase and plateau [39]. It is suggested that Aβ fibrils can stack on top of each other forming a mat-like motif, which effectively reduces the binding sites available for ThT binding; hence, a reduction in ThT intensity is observed [39].

6.3.2 Effect of Bead Concentration on ThT Fluorescence

The data in Figure 6.1 show that the overall fluorescence intensity is approximately 1 order of magnitude greater for the 1.26×10^9 μm^2/mL concentration versus the 1.2×10^8 μm^2/mL concentration. This observation indicates that PS bead concentration has an impact on the ThT fluorescence intensity. Based on the results in Figure 6.1, two PS bead diameters (108 and 535 nm) were selected to further investigate the effect of PS bead concentration on ThT fluorescence. The 108 and 535 nm PS beads were selected based on the fact that in Figure 6.1, they covered the range of minimum and maximum ThT fluorescence for both concentrations. The concentrations studied are listed in the caption of Figure 6.2.

Figure 6.2 shows that the ThT intensity as a function of concentration is drastically different for the 535 nm PS beads (A) versus the 108 nm PS beads (B). The data for the 535 nm PS beads suggest that even for the highest concentration of PS beads tested, a maximum ThT intensity is not reached. This is in stark contrast to the data for the 108 nm PS beads, which indicate that a maximum ThT is reached. The data in Figure 6.2 also support the hypothesis that bead packing may play a role in the amount of bead surface area for ThT to bind as described in section 6.3.1.

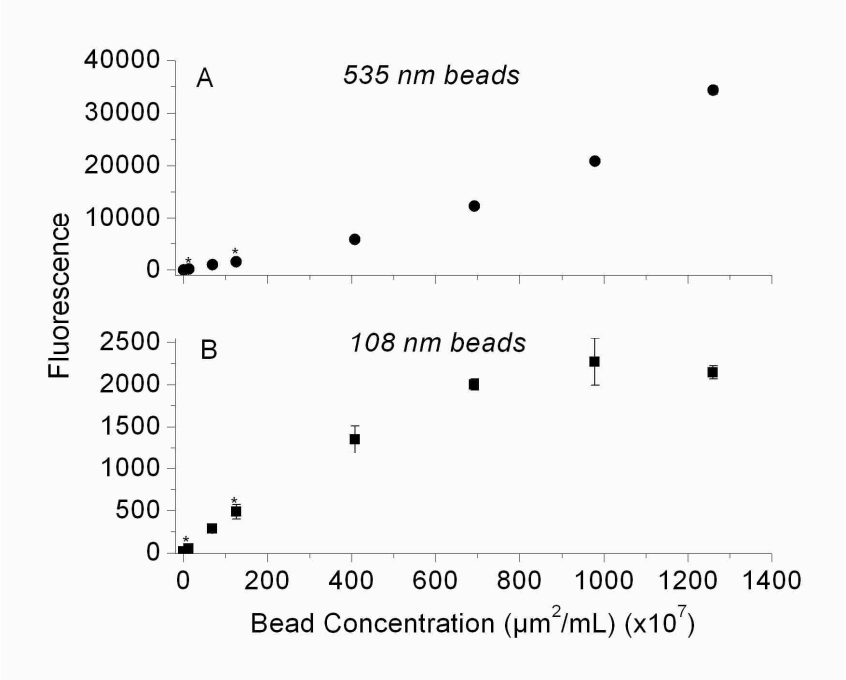

Figure 6.2. Fluorescence of 15 μM ThT in the presence of 535 nm (●) and 108 nm (■) PS beads as a function of bead concentration (μm^2/mL). Bead concentrations are 1.26×10^5, 1.26×10^6, 1.26×10^7, 1.26×10^8, 6.92×10^8, 1.26×10^9, 4.08×10^9, 6.92×10^9, 9.72×10^9, 1.26×10^{10} μm^2/mL. Fluorescence measurements were performed according the procedure described in the experimental section.

6.3.3 ThT Enhancement: PS Beads Are Similar to Aβ

All the data described in sections 6.3.1 and 6.3.2 were collected on a fluorescence plate reader at excitation and emission wavelengths of 440:485 nm. These wavelengths are the enhanced ThT maximum wavelengths described in the literature for the interaction of ThT with amyloid fibrils [63]. It is clear from the plate reader data that PS beads do induce ThT fluorescence at these wavelengths over the range of 108–1072 nm.

Excitation/emission matrix (EEM) data were also collected to determine the enhanced λ_{max} of ThT in the presence of PS beads. For this study, a spectrofluorometer was used, which scans the defined wavelengths of interest using monochromators. This is clearly advantageous over the plate reader, whose wavelengths were rigidly defined by bandpass filters. In addition to indicating the ex:em λ_{max}, another advantage of EEM measurements is that it can indicate whether any additional interesting ex:em fluorescence wavelengths result from the interaction of ThT with PS beads.

Figure 6.3 shows EEMs for unbound 15 μM ThT (A), 15 μM ThT in the presence of Aβ (1-40) fibrils (B), 15 μM ThT in the presence of 1.26×10^8 μm^2/mL 535 nm PS beads (C) 15 μM ThT in the presence of 1.26×10^8 μm^2/mL 108 nm PS beads (D). The Aβ (1-40) fibril sample was confirmed to contain fibrils in another published study [118]. After that study the Aβ sample was frozen at -80°C until thawed for this study. Figure 6.3A shows only a single peak at for ThT at ex:em 332:440 nm. In the presence of Aβ fibril, ThT enhancement is observed with a new ThT peak emerging at ex:em 440:490 nm (Figure 6.3B). These wavelengths are consistent with those reported by LeVine et. al. for Aβ-bound ThT enhancement [63]. Moreover, unbound ThT can also be observed in Figure 6.3B, which indicates that not all the ThT is bound to Aβ. Figures 6.3C and 6.3D illustrate that the 535 and 108 nm PS beads exhibit ThT enhancement at ex:em

405:490 nm. The excitation λ_{max} of ThT in the presence of PS beads (405 nm) is not perfectly aligned with that for Aβ-bound ThT (440 nm). The emission λ_{max} for ThT in the presence of PS beads and Aβ are the same. The EEM data presented in Figure 6.3 clearly demonstrate that PS beads can be a source of interference when studying Aβ aggregates with ThT at ex:em 440:490 nm.

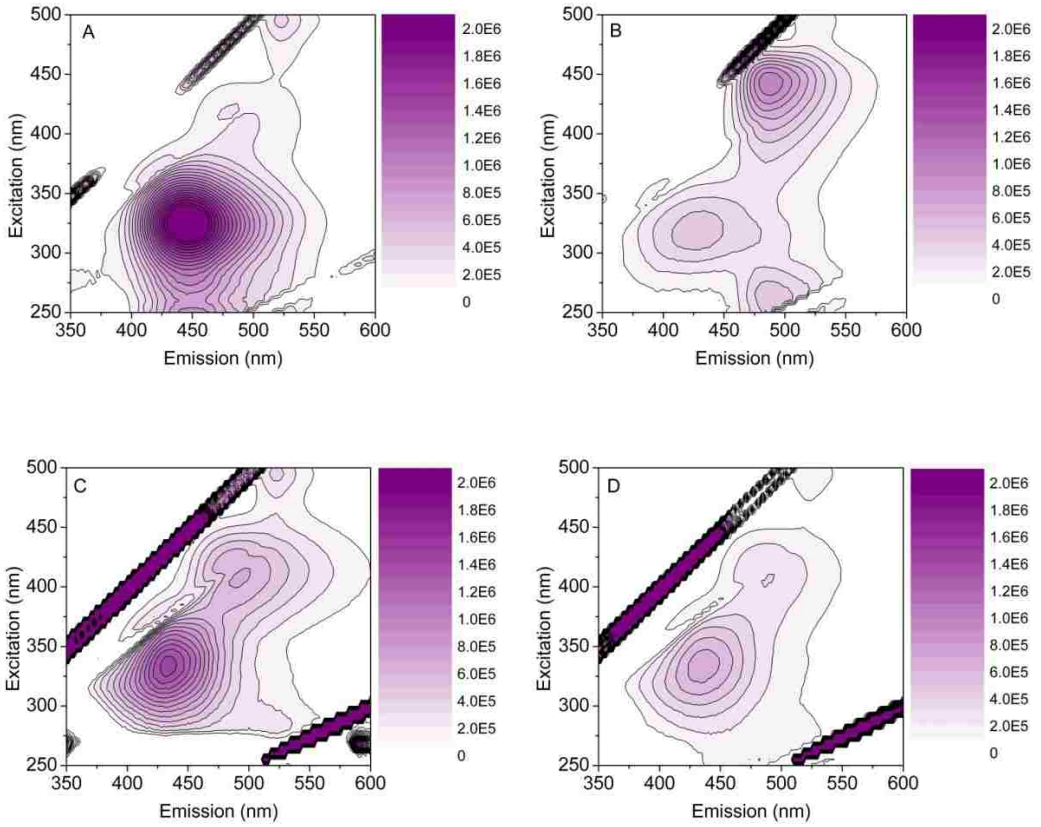

Figure 6.3. Contour plots of EEM of 15 μM ThT (A), 15 μM ThT in the presence of Aβ fibrils (B), and 15 μM ThT in the presence of 1.26×10^8 μm^2/mL 535 nm beads (C), 15 μM ThT in the presence of 1.26×10^8 μm^2/mL 108 nm PS beads (D). All samples were in 10.0 mM tris buffer at pH 7.80. 3.00mL of sample were placed in a in a 1.0 cm quartz cuvette for measurements. Inner filter correction was performed before plotting the data.

6.3.4 Excitation and Emission Scans of ThT as a Function of Bead Concentration

The goal of this part of study was to evaluate the excitation-emission spectra as a function of PS bead concentration at selected wavelengths observed in the contour plots of EEMs

in Figure 6.3. The wavelengths of interested selected from the EEMs where 332 nm, 405 nm, and 440 nm for the excitation and 435 nm and 490 nm for the emission. Emission spectra were collected with the excitation at 332 nm, 405 nm, and 440 nm. Similarly, excitation spectra were collected with the emission at 435 nm and 490 nm. Initially, the goal was to analyze a larger range of concentrations of both 108 nm and 535 nm beads as in microplate reader studies (1.26×10^{5} μm^2/mL to 1.26×10^{10} μm^2/mL). Due to the high inner filter effect at higher concentrations and insignificant change in the fluorescence of ThT at lower concentrations this was not possible. After evaluation of several sets of experiments the range of concentrations studied was between 1.26×10^{7} μm^2/mL and 1.26×10^{8} μm^2/mL for the 535 nm PS beads and between 1.26×10^{8} μm^2/mL and 1.26×10^{9} μm^2/mL for the 108 nm PS beads.

The study of the mixtures of PS beads and 15 μM ThT using a fluorometer showed an increase in fluorescence signal of ThT with the increase in concentration of beads. The data are illustrated in Figure 6.4. It is clear in Figure 6.4 that other than intensity the emission spectra are not affected by concentration, i.e. no additional emission peaks are observed as a function of PS bead concentration

Figure 6.4A shows emission spectra of mixtures of 15 μM ThT and different concentrations of 535 nm PS beads between 1.26×10^{7} μm^2/mL and 1.26×10^{8} μm^2/mL with the excitation at 440 nm. The bead concentration was added in equal steps of 3.88×10^{7} μm^2/mL as discussed in the figure caption. There is an increase in the fluorescence of ThT with the addition of 535 nm beads. The increase in ThT fluorescence as a function of PS bead concentration is plotted in the inset of Figure 6.4A, where the fluorescence value is the apex, or λ_{max} of the emission intensity. An exponential fit provided the highest correlation coefficient ($R^2 = 0.989$) between the ThT fluorescence and PS bead concentration. A linear fit resulted in an $R^2 = 0.957$.

Figure 6.4B shows emission spectra of mixtures of 15 µM ThT and different concentrations of 108 nm diameter beads between 1.26×10^{8} µm^2/mL to 1.26×10^{9} µm^2/mL with the excitation at 440 nm. Note that the concentration of 108 nm PS beads used for the experiment is one order of magnitude higher than the concentration of 535 nm PS beads. This is because initial experiments showed only negligible changes in ThT fluorescence with PS bead concentration. The bead concentration was added in equal steps of 3.88×10^{8} µm^2/mL. The inset of Figure 6.4B shows that the relationship of ThT fluorescence versus PS bead concentration is linear ($R^2 = 0.998$).

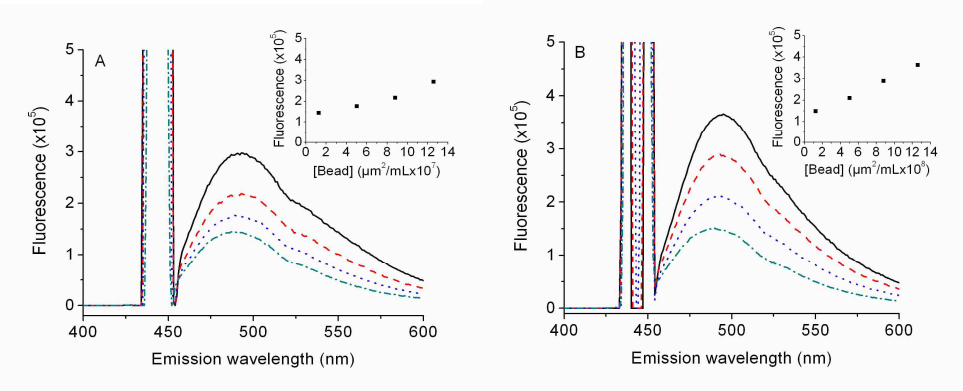

(C) Legend for Figure 6.4 (A) and (B).

Line Style	Concentration of PS Beads (µm^2/mL)	
	535 nm PS Bead	108 nm PS Bead
Dash/Dot	1.26×10^{7}	1.26×10^{8}
Dot	5.03×10^{7}	5.03×10^{8}
Dash	8.80×10^{7}	8.80×10^{8}
Solid	1.26×10^{8}	1.26×10^{9}

Figure 6.4. Fluorescence emission spectra of of 15 µM ThT in the presence of 535 nm PS beads (A) and 108 nm PS beads (B) over a 1 order magnitude range in concentrations (surface area/mL). Excitation was performed at 440 nm. Inner filter correction was performed before plotting the data. For both (A) and (B) the initial mixture of PS beads was prepared in 10 mM tris buffer at pH 7.8 with 15 µM ThT in a 1 cm quartz cuvette. To increase the concentration of PS beads in the cuvette, subsequent additions of PS beads were pipetted directly into the cuvette. For the 535 nm PS beads, equal steps 4.0 µL of 2.91×10^{10} µm^2/mL was added, which equals 3.88×10^{7} µm^2/mL step in concentration. Likewise, for the 108 nm PS beads 4.0 µL of 2.91×10^{11} µm^2/mL was added, which equals 3.88×10^{8} µm^2/mL step in concentration. A legend is provided in (C) below figures (A) and (B), which list the PS bead concentrations. The insets in (A) and (B) plot the intensities of the em λ_{max} versus concentration.

6.4 Conclusions

This work demonstrated that PS beads can induce Thioflavin T fluorescence enhancement similarly to Aβ. Polystyrene beads were used as a model system here because their sizes and concentrations could be carefully controlled. It was shown that the intensity of ThT increases with increasing PS bead diameter, and a maximum fluorescence was reached over the PS bead sizes studied. In general, the magnitude of the ThT intensity increased with increasing concentration of PS beads; however, this relationship is not necessarily linear and depends on both PS bead diameter and PS bead concentration range.

CHAPTER 7

ANALYSIS OF Aβ (1-40) PEPTIDE AGGREGATION BY CAPILLARY ELECTROPHORESIS WITH LASER-INDUCED FLUORESCENCE ANISOTROPY DETECTION

7.1 Introduction

The development and progression of Alzheimer's disease (AD) and other neurodegenerative diseases have been linked to aggregation of amyloidogenic peptides. Soluble monomeric amyloid peptides self-aggregate under physiological conditions to form aggregates ranging vastly in size and structure. The level of neurodegenerative toxicity has been suggested to be related to the size and structure of Aβ aggregates, but it is not clear what size/structure is most toxic. It has also been suggested that the most toxic forms of Aβ are intermediate in size between monomer and fully-formed fibrils [13,27,35,36].

Developing methods to monitor intermediate species between monomers and fully-formed fibrils is extremely challenging. Methods that are commonly used to study monomers or fully-formed fibrils do not work well for studying intermediate-sized structures. For example, mass spectrometry has been used to study monomers, but ionizing aggregates without breaking apart their structures is a problem. Thioflavin T fluorescence is a powerful analytical tool for studying fully-formed fibrils and their rates of formation but is less effective at monitoring Aβ structures that are smaller than fully-formed fibrils, especially monomers. Moreover, a minimum size or structure of Aβ for ThT binding is not clear. Other examples include TEM imaging and light scattering which are effective for studying fully-formed fibrils but less effective for structures smaller than fully-formed fibrils.

An underlying hurdle for Aβ analysis is that multiple methods are needed to study the vast sizes, structures and numbers of Aβ species present in an aggregating Aβ mixture.

Complicating matters further is that intermediates Aβ structures are short-lived transient and dynamic species. Very little is known about these structures because they are unstable relative to fibrils and monomers making it difficult to sample and study.

Capillary electrophoresis (CE) has been shown to be a powerful tool for Aβ analysis [45,77,93,118]. Monomeric and aggregated peptides have been separated by CE-UV for both Aβ (1-40) and Aβ (1-42) isoforms [45,118]. Previous studies in our laboratory [128] and by Kato et al. [113] demonstrated that capillary electrophoresis with laser-induced fluorescence detection could be used study the aggregation of Aβ peptides. Both of these studies used thioflavin T in the separation buffer to label Aβ aggregates. In Chapter 4, it was demonstrated that CE with laser-induced fluorescence (LIF) detection can resolve individual Aβ aggregates using Thioflavin T as a fluorescence probe. In that same chapter, LIF anisotropy (LIFA) was introduced to size characterize the individually detected Aβ aggregates; however, no anisotropy differences were detected for different Aβ aggregates using ThT as a fluorescence probe. Another problem was that the background ThT anisotropy and Aβ aggregate anisotropy were indistinguishable. It was hypothesized that the unpredictable binding ratio and unknown binding mechanism of ThT to Aβ aggregates could have been a partial cause for not observing any anisotropy differences between aggregates and between aggregates and the background.

In this work, a covalently labeled Aβ (1-40) peptide with carboxyfluorescein (FAM) was investigated using CE-LIFA to determine whether different forms of Aβ could be differentiated based on their relative fluorescence anisotropy (FA) values. By using a covalently labeled Aβ peptide, all forms of Aβ from monomers to fully-formed fibrils will be fluorescently labeled. This is distinct from the work in Chapter 4 where ThT was used to noncovalently label some of the Aβ structures in an unpredictable manner. In addition to using covalently labeled Aβ

peptides, this work is distinct from the previous work in Chapter 4 because the FAM-Aβ peptide is sampled and analyzed during its incubation while aggregating over several days. The goal of analyzing the aggregating mixture over time is to attempt to detect transient Aβ species that are intermediate between monomers and fully-formed aggregates.

7.2 Experimental

7.2.1 Chemicals

All solutions were prepared in 18 MΩ water obtained from a Modulab water purification system (United States Filter Corp.; Palm Desert, CA) unless otherwise noted. Phosphate buffered saline (PBS), Tris (hydroxymethyl) aminomethane (Tris) and methanol (99.8%) were purchased from Fisher Scientific (Fair Lawn, NJ). Phosphate buffered saline contained 22.8 mM phosphate, 274 mM NaCl, 5.4 mM KCl and 0.1% NaN_3 at pH 7.4. Tris buffer was prepared at 10.00 mM, and the pH was adjusted to 7.80 with HCl. This Tris buffer was used for all experiments unless otherwise noted. The buffer was filtered through a 0.02 μm filter (Whatman; Hillsboro, OR). Mesityl oxide (MO) was purchased from Alfa Aesar (Ward Hill, MA), and working solutions of MO were prepared in Tris buffer at a concentration of 0.2% (v/v). Coumarin 334 was purchased from Acros Organics (Morris Plains, NJ), and a stock solution was prepared at 1.00 μM in methanol. Working solutions of coumarin 334 were prepared at 100 nM in Tris buffer.

7.2.2 Aβ Sample Preparation and Characterization

Unlabeled Aβ (1-40) peptide was purchased from the W.M Keck Foundation Biotechnology Research Laboratory (Yale University, New Haven CT). Carboxyfluorescein labeled Aβ (1-40), i.e. FAM-Aβ (1-40), was purchased from Anaspec Inc. (Fremont, CA). Each Aβ peptide monomer is covalently labeled with a single carboxyfluorescein on the first aspartic acid (D) on the amine terminus of the peptide chain. Arctic Aβ (1-40) was purchased from

BioSource. Arctic Aβ (shown below) is a variant of the normal Aβ (1-40) peptide by replacement of the glutamic acid (E) at position 22 in the peptide chain with Glycine (G). All peptides were stored with desiccant at -80 °C until used.

```
                1   5   10  15  20  25  30  35  40
FAM-DAEFRHDSGYEVHHQKLVFFAEDVGSNKGAIIGLMVGGVV
```

All monomeric peptide solutions were prepared independently in PBS buffer, and the targeted, total concentration of Aβ used for aggregation studies was 20 to 25 μM [45,118,128]. After the monomeric peptide solutions were prepared, the Aβ monomer concentration of each solution was determined by HPLC-UV. Monomer preparation and analysis have been described in detail previously [45,118]. After the concentrations were determined, the FAM-Aβ peptide was mixed at a mass ratio of 1:4 or 1:1 with either unlabeled Aβ (1-40) or Arctic Aβ (1-40), respectively, to give a final total monomeric equivalent Aβ concentration between 20 and 25 μM. The total volume of each mixture was 1 mL. The mixed monomeric Aβ peptides were then incubated at 37°C and ambient pressure during the aggregation studies.

In order to remove aliquots of sample for analysis during aggregation, the sample was removed from the incubator and lightly vortexed to homogenize the mixture and suspend any aggregates that may have settled to the bottom of the centrifuge tube. A 200 μL aliquot of the sample was removed from the mixture to analyze, and the remaining portion of the mixture was returned to incubator to continue aggregating. The 200 μL aliquot was buffer exchanged from PBS buffer into the Tris buffer at pH 7.80 for CE analysis [59]. To perform the buffer exchange, the sample was placed in a 3000 molecular weight cutoff Microcon filter cartridge and centrifuged at 14,000 rpm (approximately 20,000 g) at 4° C for 60 min. The retained portion of the sample was resuspended in Tris buffer. This process was performed until the theoretical volume % PBS was below 5%, which typically required 3 cycles of centrifuging. Next, the

Microcon filter was inverted into a clean centrifuge tube and spun at 3000 rpm for 1 min to collect the Aβ sample. This sample was transferred to a 200 μL thermowell polypropylene tube (Corning Incorporated; Corning, NY) and put on ice until CE analysis, which was performed approximately 2 hr after completing the buffer exchange.

To minimize photobleaching of the fluorophore-labeled peptide during sample preparation and prior to CE analysis, exposure of samples to ambient light was minimized during the all stages of the sample handling, including incubation, sampling, buffer exchanging and analysis. This was accomplished by keeping the sample container wrapped in aluminum foil when possible and reducing the ambient light.

7.2.3 Capillary Electrophoresis with Laser-Induced Fluorescence Anisotropy Detection

Prior to CE-LIFA, samples were characterized by CE-UV [45,118] using a Beckman Coulter PACE MDQ equipped with a diode array detector. Samples were then analyzed immediately with a lab-constructed CE-LIFA instrument. The LIFA detector used for this work was described in detail previously [128] and is based on a design published by [120]. Excitation was carried out using a polarized diode laser with and excitation wavelength and laser power of 445 nm and 1.63 mW, respectively. For the detection system used in this work, the 490 nm emission bandpass filter used previously for thioflavin T detection [128] was replaced with a 560 nm emission bandpass filter better suited for detection of emission of the fluorescein label. The parallel and perpendicular fluorescence emissions were collected simultaneously by two separate photomultiplier tubes (PMT). The outputs of the PMTs were filtered by 500 Hz low pass RC filters and collected by a National Instrument PCI-6024E DAQ board at a scan rate of 1000 Hz. The fast data collection was necessary for detecting peaks from individual Aβ fibrils that typically have peak widths of 3-15 ms at FWHM [128]. The CE-LIFA data collection was

controlled by a program written with LabView Version 5.0, and the data were analyzed using Origin Pro and Microsoft Excel.

The fluorescent neutral marker (coumarin 334) was injected prior to the Aβ sample injection. This injection order minimized potential interactions between Aβ and the neutral marker because all forms of Aβ detected migrated slower than the neutral marker. Injections conditions are given in the figure captions. The Aβ samples were vortexed prior to every injection to suspend any aggregates that could have settled to the bottom of the sample vial. The electrophoretic potential was applied using a Spellman CZE1000R high-voltage power supply (Hauppauge, NY) at 25.0 kV (417 V/cm). The electrophoretic current was 5-6 μA.

7.2.4 Data Analysis

The dual channels of the detection system allowed the parallel and perpendicular fluorescence emission relative to the polarization of the laser source to be measured simultaneously. The measured fluorescence intensities were used to calculate the fluorescence anisotropy according to Equation 7.1, where r is the fluorescence anisotropy and $I_{\parallel}$ and $I_{\perp}$ are the measured parallel and perpendicular fluorescence intensities relative to the polarization of the excitation source, respectively. The factor G corrects for differences in responses and sensitivities between the two PMTs. For this work, the voltages applied to both PMTs were adjusted so that G was as close to 1 as possible. This was done by using a dilute solution of coumarin 334 (50-100 nM), which is expected to have an FA near 0 because of its small size and fast rotational diffusion rate. After adjusting the G-factor empirically to as close to 1 as possible, some day-to-day variability was observed in the coumarin 334 fluorescence anisotropy values. To correct for this, the average G-factor per day was calculated using Equation 7.2, where the intensities are those from coumarin 334. This G-factor was used in the Equation 7.1 to calculate

the fluorescence anisotropy of all the peaks in the electropherograms from that day.

$$r = \frac{I_{\parallel} - GI_{\perp}}{I_{\parallel} + 2GI_{\perp}} \tag{7.1}$$

$$G = \frac{I_{\parallel}}{I_{\perp}} \tag{7.2}$$

Fast data collection (1000 Hz) was used because of the narrow peak widths due to individual, large Aβ aggregates, which produce peaks that are only ~ 10 ms wide [82,106,128]. The fast data collection causes fast random fluctuations in measured signals. These random fluctuations do not occur equally in both the parallel and perpendicular channels; therefore, the fluorescence anisotropy can be drastically different from one time point to the next based on these random fluctuations. To reduce the impact that the random fluctuations could have on the calculated FA of the narrow (~10 ms) Aβ fibril peaks, the FA was averaged over the FWHM of the fibrils' fluorescence peaks. For broad peaks due to coumarin 334 and Aβ monomer and intermediate peaks, the FA was averaged over 100 ms at the apex of the peak.

7.3 Results and Discussion

Previous studies have demonstrated that CE-LIF with ThT in the separation buffer can be used successfully for analysis of Aβ peptide aggregation [113] and detection of individual Aβ aggregates [128]. Our work also explored the potential of this approach with LIFA detection [128,129]; however, different Aβ aggregates detected with ThT labeling did not exhibit distinct fluorescence anisotropy values. Another limitation of labeling with ThT is that only some larger Aβ aggregates will produce enhanced fluorescence [4,12,63]. In this study, the aggregation of Aβ (1-40) with a covalently attached fluorophore was carried out using CE-LIFA. The objective of this study was to determine if significant differences in FA could be measured for different aggregate types by CE-LIFA. The Aβ (1-40) peptide was labeled with carboxyfluorescein on the

first aspartic acid (D) on the amine terminus of the peptide chain, and all forms of this peptide should produce a fluorescence signal. A mixture of this labeled peptide with unlabeled Aβ (1-40) was analyzed by CE-LIFA at different times during the aggregation process.

7.3.1 Aggregation of Aβ (1-40)

Figures 7.1-7.3 present CE-LIF electropherograms for an aggregating mixture of FAM-Aβ (1-40) and unlabeled Aβ (1-40) mixed at a mass ratio of 1:4 (FAM labeled:unlabeled) at days 0, 4 and 6 during aggregation. Only one data channel (parallel polarization) for the CE-LIFA experiments is plotted in Figures 7.1, 7.2A and 7.3 for clarity. Corresponding electropherograms for the same samples by CE-UV are shown in Appendix A (Figure A.5). The main objective of sampling and analyzing the aggregating Aβ sample at different days was to attempt to detect Aβ aggregates exhibiting distinct FA values intermediate between monomers and fully-formed fibrils. Figure 7.1 shows that on day 0, only the neutral marker peak at 64.0 s and a monomer peak at 94.7 s were observed, as expected. The CE-UV data did not indicate the presence of any aggregated species (Appendix A: Figure A.5A).

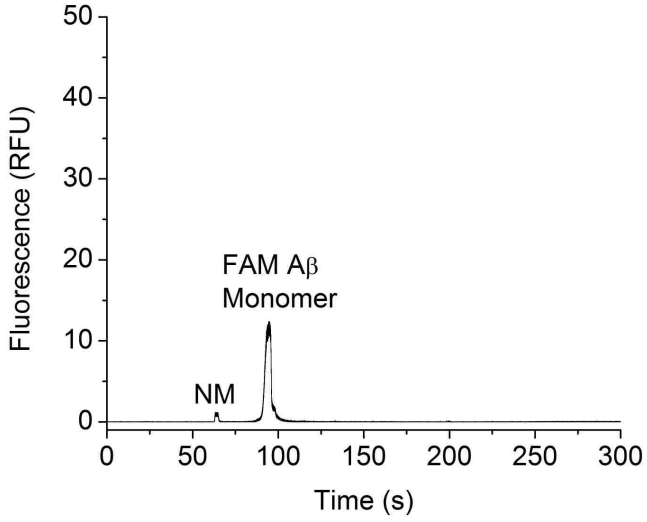

Figure 7.1. CE-LIF electropherogram of a 1:4 mixture of FAM-Aβ (1-40) peptide:Unlabeled Aβ (1-40) peptide sampled on day 0.The main peaks are the neutral marker (NM) peak coumarin 334 at 64.0 s and the FAM-Aβ monomer peak at 94.7 s.

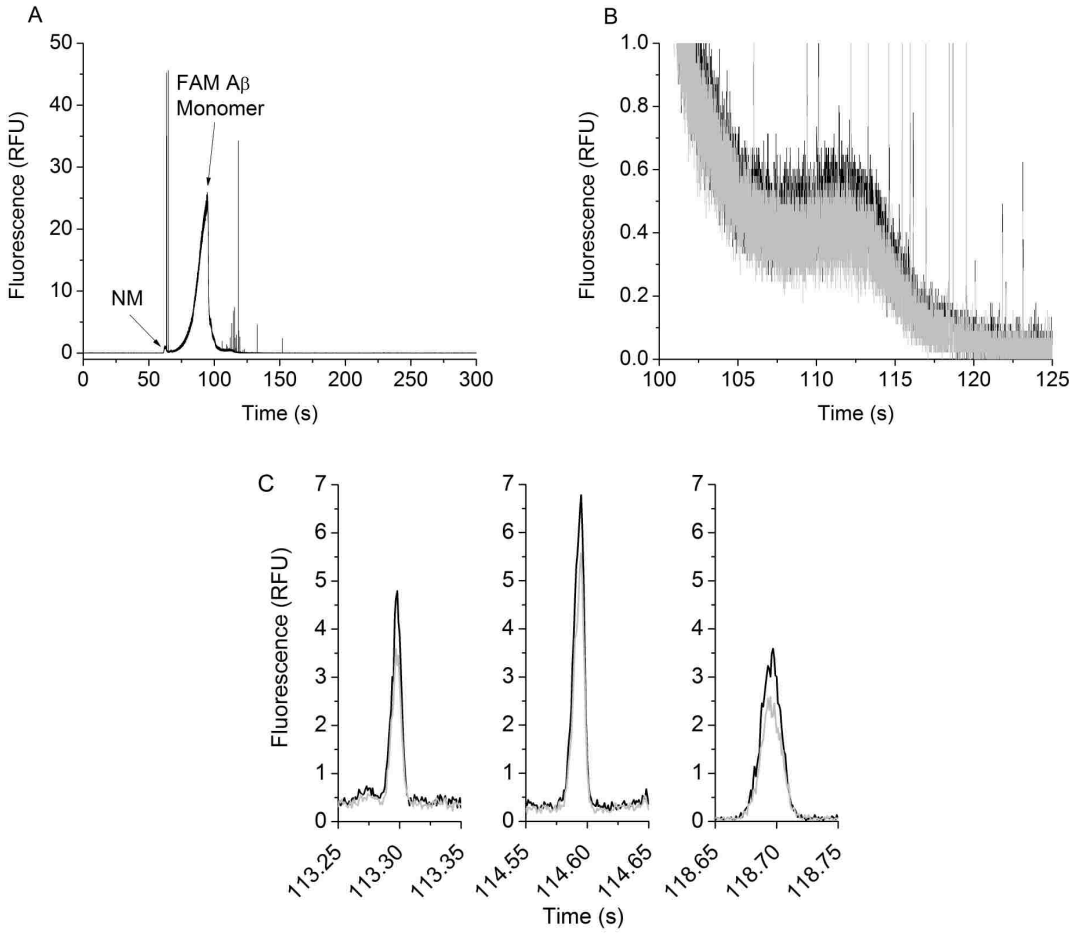

Figure 7.2. CE-LIF electropherogram of a 1:4 mixture of FAM-Aβ (1-40) peptide:Unlabeled Aβ (1-40) peptide sampled on day 4. (A) Single channel data (parallel channel). The neutral marker (NM)and FAM-Aβ (1-40) monomer peaks are labeled. Sharp peaks following the monomer peak are due to large Aβ aggregates. In (B) and (C) the perpendicular and parallel channels are plotted in grey and black, respectively. (B) Expanded view of a broad peak at 112 s thought to be due to an intermediate sized Aβ aggregate. (C) Expanded views of 3 large Aβ aggregate peaks detected individually. The x-axes in (C) are 100 ms for each plot.

The FA value for the monomer peak shown in Figure 1 was 0.019, and the FA value for coumarin 334 was -0.001. The molecular weight of the labeled Aβ monomer, and coumarin 334 are 4689.2 g/mol and 283.3 g/mol, respectively. The measured FA values are consistent with the relative sizes of the two molecules. Fluorescence anisotropy is capable of discerning size differences between different fluorescent species in solution based on their rotational diffusion rates. In general, larger species have smaller rotational diffusion rates and exhibit larger

fluorescence anisotropy values as indicated by the Perrin Equation shown in Equation 7.3, where D is the rotational diffusion coefficient, r_o, is the fundamental anisotropy and τ is the fluorescence lifetime. The fundamental anisotropy is dependent on the angle between the absorption and emission transition dipoles of the fluorophore [69].

$$r = \frac{r_o}{1 + 6D\tau} \tag{7.3}$$

Figure 7.2A shows an electropherogram for the same aggregating mixture sampled on day 4. In Figure 7.2A, the FAM-Aβ monomer peak is at 94.7 s. The day 4 electropherogram includes 12 narrow peaks between 100–120 s with an average FWHM = 12 ms. These peaks are not present in the day 0 sample and are consistent with peaks observed in our earlier studies and attributed to individual Aβ aggregates [128]. That work used ThT in the separation buffer for fluorescence detection.

Figure 7.2B shows one of the most interesting features of this electropherogram, a relatively broad peak (FWHM ~ 2 s) with a migration time of 112 s that was not detected in the day 0 sample. The broad shape of this peak and its migration relative to the monomer peaks suggests that this peak could be to an aggregate peak that is small relative to the structures that can be detected individually as narrow peaks (FWHM =12 ms) [45,118,128]. If this peak is an aggregated form of Aβ (1-40), it should exhibit a FA value greater than that of the monomer peak. Both fluorescence channels are plotted in Figure 7.2B (parallel and perpendicular polarization), and the peak does exhibit fluorescence anisotropy. The average FA value for 5 injections of this sample was 0.063 ± 0.015, while the average value for monomer was 0.018 ± 0.001 (Table 7.1).

Table 7.1. Summary of fluorescence anisotropy results for Aβ mixtures.

Aβ Samples	Coumarin	Monomer	Intermediate	Fibril
FAM:Unlabeled (n = 5)	0.000 ± 0.007	0.018 ± 0.001	0.063 ± 0.015	0.100 ± 0.020 (43 peaks)
FAM:Arctic (n = 3)	0.000 ± 0.002	0.020 ± 0.001	0.095 ±0.002	0.093 ± 0.029 (40 peaks)

FAM:Unlabeled Aβ sample data are averaged from 5 injections
FAM:Arctic Aβ sample data are averaged from 3 injections

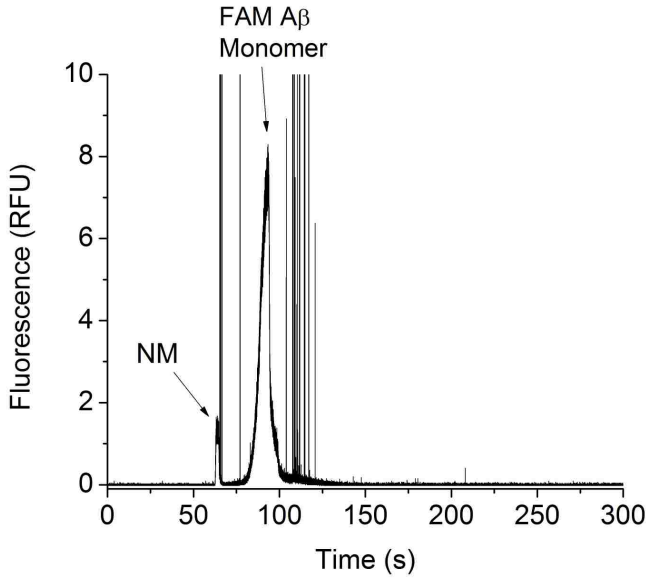

Figure 7.3. CE-LIF electropherogram of a 1:4 mixture of FAM-Aβ (1-40) peptide:Unlabeled Aβ (1-40) peptide sampled on day 6.

This intriguing peak is not present in the electropherogram for the day 6 sample (Figure 7.3). The electropherogram has a monomer peak at 94.4 s and 13 narrow aggregate peaks between 100-120 s. These peaks are similar in shape to the narrow peaks in Figure 7.2A, but they are clearly more intense, on average. These data are consistent with the identification of the broad peak in Figure 7.2A as a relatively small Aβ aggregate, and the narrow peaks in Figures 7.2A and 3 as larger aggregates detected individually. It is not surprising that a small Aβ aggregate would disappear as the aggregation proceeded towards larger structures. The presence

of large aggregates that produce narrow peaks would not be expected at day 0. These peaks increased in number from day 4 (9 peaks averaged from 5 injections) to day 6 (31 peaks averaged from 3 injections), and their intensities increased – consistent with Aβ fibrils that are continuing to grow in size and number.

Figure 7.2C shows parts of the electropherogram from the day 4 sample with both fluorescence channels plotted. Clearly these narrow peaks exhibit significant FA. The average FA value for all 43 of the narrow peaks detected from 5 injections of the day 4 sample was 0.100 ± 0.020 (Table 7.1). These FA data are plotted as a histogram in Figure 7.4A to take advantage of the additional distribution information provided. The FA values for these narrow peaks are larger and distinct compared to the values for the monomer peak and peak shown in Figure 7.2B (Table 7.1). Figure 7.4B is a histogram of the FA of the narrow peaks detected on day 6. The average FA value for all 63 of the narrow peaks detected from 3 injections of the day 6 sample was 0.101 ± 0.023, and a Gaussian distribution is observed.

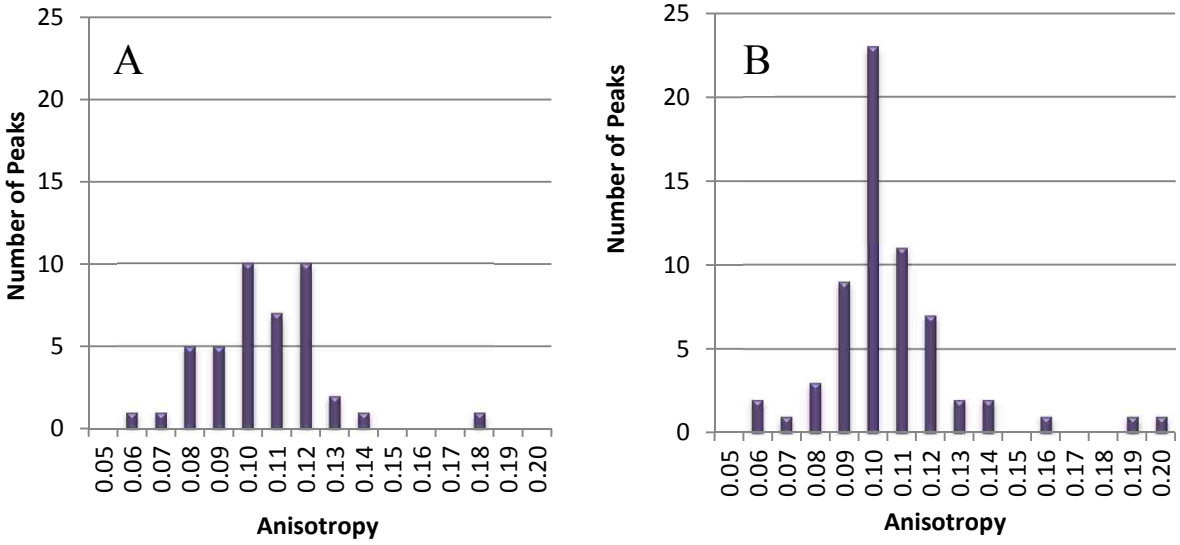

Figure 7.4. Fluorescence anisotropy histograms of narrow peaks detected from the 1:4 mixture of FAM-Aβ (1-40) peptide:Unlabeled Aβ (1-40) peptide sampled on days 4 (A) and day 6 (B). In both (A) and (B), bin = 0.01. In (A), 43 peaks are represented from 5 injections. In (B), 63 peaks are represented from 3 injections.

These experiments were repeated with sampling at days 0, 2, 3 and 6. The primary aim of the increased number of samples taken during the early stages of aggregation was to increase the probability of detecting the apparently transient peak shown in Figure 7.2B. This peak was not observed despite the increase in sampling frequency. The CE-LIFA experiments and corresponding CE-UV experiments did indicate that aggregation to place to form large Aβ aggregates as expected (data not shown). This result is not unexpected. Other reports in the literature indicate the appearance of relatively stable Aβ aggregates of intermediate size indicate that they are short lived, found at low concentration and are not observed in all experiments [83]. At this point it was decided that it would be wise to change to an Aβ aggregation experiment known to produce higher concentrations of more stable intermediate aggregates.

7.3.2 Aggregation of Mixtures of Aβ (1-40) and Arctic Aβ (1-40)

Arctic Aβ is a variant of wild type Aβ where Glu22 is replaced by Gly. This single amino acid mutation has been shown to promote and stabilize the formation of smaller soluble Aβ aggregates, such as oligomers and protofibrils, which are thought to play a pathogenic role in AD [83,105]. Arctic Aβ has been used to study the structure of these species [83,105,130-133]. To further investigate whether intermediate Aβ aggregates between monomers and fully-formed fibrils could be analyzed be CE-LIFA, monomeric FAM-Aβ (1-40) peptide was mixed with monomeric Arctic Aβ (1-40) at a mass ratio of 1:1 to increase the stability of intermediate aggregates; thereby increasing the chance of detecting intermediate species. This Aβ mixture was sampled on days 1, 2, 3, and 6.

Figure 7.5 shows LIF electropherograms from days 2, 3, and 6. The day 1 LIF electropherogram and CE-UV electropherograms for all 4 days are included in Appexdix A (Figures A.6A-E). Compared to the experiments shown in Figures 7.1-7.3, the distance from the

capillary inlet to the detector was increased while using from the same applied potential (417 V/cm) in order to improve the separation resolution.

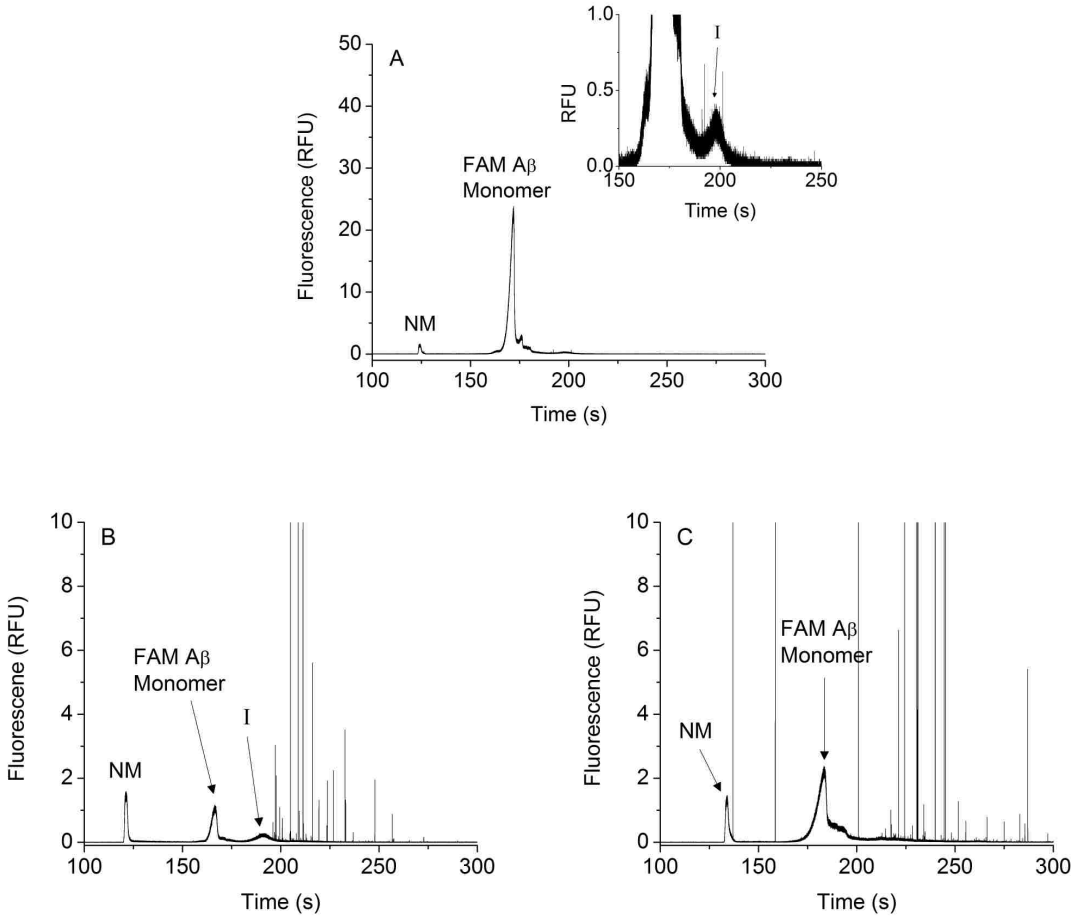

Figure 7.5. Electropherograms of a 1:1 mixture of FAM-Aβ (1-40) peptide:Arctic Aβ peptide sampled on day 2 (A), day 3 (B) and day 6 (C). Peak I is hypothesized to be due to a population of Aβ aggregates that are intermediate in size between monomer and fully-formed fibrils (shown as individually detected narrow peaks).

The FAM-Aβ monomer peak was detected in each electropherogram shown in Figure 7.5 (labeled FAM Aβ Monomer) while the Arctic Aβ monomer was not detected since it was not labeled with a fluorophore. The CE-UV data for the day 1 and day 2 samples (Appendix A: Figure A.6B and A.6C) has peaks for both the Arctic Aβ monomer and FAM-Aβ monomer, at approximately a 1:1 ratio as expected. Intermediate aggregate peaks similar to that in Figure 7.2 were observed for day 1, day 2 and day 6 samples. The CE-UV electropherograms also included

peaks consistent with intermediate aggregates [45,118]. Significant numbers of narrow peaks attributed to larger individual Aβ aggregates are first apparent on day 3 (13 peaks averaged from 3 injections) and increase on day 6 (35 peaks averaged from 3 injections). The average FA value for all 40 of the narrow peaks detected from 3 injections of the day 3 sample was 0.093 ± 0.029 (Table 7.1). Figure 7.6 shows a FA histogram of the narrow peaks detected on day 3. By day 3, the peaks for Arctic Aβ monomer and FAM-Aβ monomer were near or below the CE-UV detection limits though the labeled peptide was still detectable by CE-LIF. Overall these results are consistent with the expected progression of Aβ aggregation.

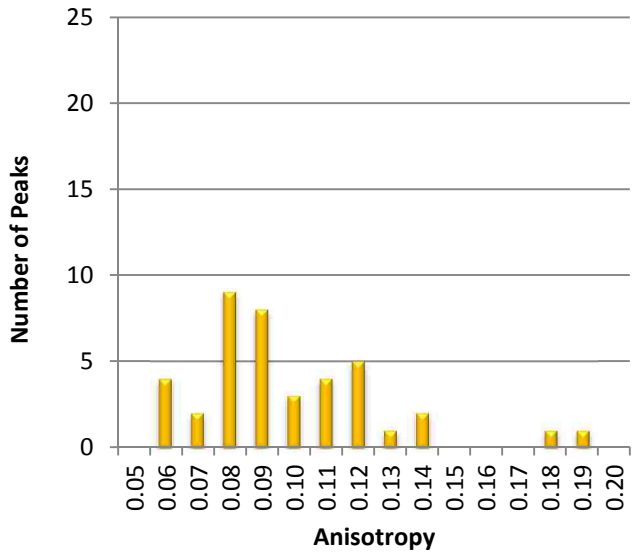

Figure 7.6. . Fluorescence anisotropy histograms of narrow peaks detected from the 1:1 mixture of FAM-Aβ (1-40) peptide:Arctic Aβ (1-40) peptide sampled on day 3 (A). bin = 0.01. 40 peaks are represented from 3 injections.

7.3.3 CE-LIF Anisotropy Analysis of Aβ Peptides

The fluorescence anisotropy data are summarized in Table 7.1. There is a clear increase in the fluorescence anisotropy from monomer to intermediate Aβ peaks and fibrils for both samples. The smaller fluorescence anisotropy for the monomer compared to the intermediate peaks and fibrils is understandable based on fluorescence anisotropy theory because the

monomer is relatively small. The anisotropy of the monomer is greater than that of the coumarin as expected.

It is interesting that the monomer and fibrils, on average, are similar between the two samples taking into account the standard deviation, but the intermediate Aβ peaks' anisotropy values are quite different. The arctic Aβ was used in this work because of it stabilizing effect on intermediate Aβ structures. The data suggest that fluorescence anisotropy can be used to differentiate between intermediates that are potentially different in size and structure.

A relatively high standard deviation of the fibrils' fluorescence anisotropy values is observed in Table 7.1 and Figures 7.4 and 7.6.. Wide variability in the fibrils' fluorescence anisotropy values is understandable since individual fibrils presumably have vastly different sizes and shapes, which would be reflected as differences in fluorescence anisotropy. Plotting the fibrils' anisotropy values versus peak migration time did not result in any discernable trend (data not shown).

7.4 Conclusions

In this work, time-course Aβ aggregation studies were investigated by capillary electrophoresis with laser-induced fluorescence anisotropy detection. By performing the aggregation with fluorescently-labeled Aβ peptides (FAM-Aβ), several forms of Aβ were separated and observed in a single electrophoretic run from monomers to fully-formed fibrils. This data demonstrated that fluorescence anisotropy can be used to differentiate Aβ peaks separated by capillary electrophoresis.

CHAPTER 8

CONCLUSIONS AND FUTURE DIRECTIONS

8.1 Conclusions

The general focus of this dissertation is the analysis of amyloid peptides by capillary electrophoresis (CE) combined with spectroscopic detection. In Chapter 2, a method based on capillary electrophoresis with UV absorbance detection was developed to quantify the concentration of Aβ (1-40) monomer. This method is an alternative to previously established HPLC-UV methods for the same purpose. The advantages of the CE-based method over the HPLC-based method are that the CE-method has faster analysis times, consumes less sample material and achieves lower mass detection limits. The CE method was determined to have a limit of detection of 0.5 μM (19 pg). Chapter 2 also showed that the CE-UV method could be used to indicate whether an Aβ sample preparation would exhibit accelerated aggregation kinetics. This was possible because of the ability of the CE-UV method to separate and detect monomeric and aggregated forms of Aβ (1-40). It is highly significant that open bore CE (i.e. no stationary phase) can separate Aβ aggregates. This is a nontrivial challenge faced by stationary phase-based separation techniques, e.g. LC and gel-based methods.

In Chapter 2, the original goal was to analyze Aβ (1-40) preparations of pure monomer. It was clear from CE results in Chapter 2 that some the preparations contained aggregated forms of Aβ (1-40). Although this was inadvertent, it opened to door to the experiments presented in Chapter 3. In Chapter 3, experiments were designed to analyze various monomeric and aggregated forms of Aβ (1-40) and Aβ (1-42). The CE-UV method described in Chapter 2 was used in Chapter 3 with the exception that the maximum data scan rate allowed by the instrument was used in Chapter 3 (32 Hz versus 4 Hz). The data showed that monomeric and aggregated

forms Aβ peptides were resolved by CE-UV for preparations of both Aβ (1-40) and Aβ (1-42) isoforms. By maximizing the data scan rate, additional sharp peaks were observed in aggregate containing samples. These sharp peaks are believed to be due to fully-formed fibrils, and the broad aggregate peaks are believed to be due to unresolved Aβ intermediate sized aggregates, i.e. oligomers or protofibrils. Aβ seeds are often used to promote aggregation through the elimination of the lag phase associated with the nucleation-dependent growth. Aβ seeds are sonicated Aβ fibrils, where the sonication process breaks up larger fibrils into smaller Aβ fibril fragments that can seed further fibril growth. Aβ (1-40) seeds were also prepared and analyzed by the CE-UV method. Comparing the CE-UV electrophoretic profiles of the Aβ (1-40) seed and Aβ (1-40) fibril samples, fewer sharp peaks, i.e. fibrils, were observed in the seed sample relative to the fibril sample.

The observation of additional sharp peaks in aggregate containing sample shown in CE-UV data in Chapter 3 was largely due to the increase in the data sampling rate from 4 to 32 Hz. It was believed that 32 Hz was still not sufficient for detecting individual Aβ fibrils. In an effort to detect all Aβ fibrils injected into the CE system, a CE-LIFA (laser-induced fluorescence anisotropy) instrument was constructed using a 1000 Hz data sampling rate. This data is presented in Chapter 4. Aβ peptides do not exhibit strong native fluorescence; therefore, the amyloid dye Thioflavin T was used for detecting Aβ fibrils. Thioflavin T was added to the electrophoresis buffer, and labeling the Aβ fibrils with ThT was performed on-column during electrophoresis. The basic CE conditions were held a similar to those in Chapters 1 and 2 as possible. Using the lab-constructed CE-LIFA system, individual Aβ fibrils were resolved and detected as individual peaks. This was shown for Aβ (1-40) and Aβ (1-42) isoforms. These results were validated by analyzing the same Aβ samples by bulk measurements using a

fluorescence plate reader, which is a more common technique used to study Aβ fibrils. The results from the CE and bulk plate reader experiments were consistent.

Chapter 4 also showed that separating Aβ fibrils in the absence of ThT produced sharp peaks due to scattered light albeit careful optical design to eliminate elastic scattering from being detected. Scattered light was also observed in the plate reader study for aggregate-containing samples. It was clear; however, that using ThT resulted in an increase in signal intensity relative to not using ThT. This effect was extremely clear in the case of the Aβ (1-42) monomer sample, which was shown to contain aggregates.

In Chapter 4, LIFA detection was used as a means to characterize individual Aβ fibrils. It was shown in plots of fluorescence anisotropy versus time that no distinction could be made between the fluorescence anisotropy values of the background electrophoresis buffer that contained ThT and the Aβ aggregates, i.e. the fluorescence anisotropy electropherograms looked like noise although there were clearly peaks in the corresponding fluorescence electropherograms. Chapter 5 presented a data treatment method designed to differentiate the fluorescence anisotropy values of the background signal and peaks due to Aβ fibrils. The basis of the data treatment method was the addition of an artificial signal that was equally applied to all fluorescence data points prior to calculating the fluorescence anisotropy. After the data treatment was applied, there were clear fluorescence anisotropy peaks that correspond in time to the fluorescence peaks detected for Aβ aggregates. It was found that increasing the amount of artificial single added to the fluorescence data increased the S/N of the fluorescence anisotropy peaks, but the S/N eventually plateaus as a function of added artificial signal.

In the initial studies of using ThT in the electrophoresis buffer for the on-column labeling and detection of individual aggregates, several sharp peaks mimicking those of Aβ were

observed in the background buffer that included ThT. These peaks were hypothesized to be due to particulate matter in the electrophoresis buffer that were removed by filtering the buffer through a 0.02 μm filter. The potential of particulate matter to enhance ThT similarly to Aβ and produce false positives laid the groundwork for the experiments described in Chapter 6. Chapter 6 describes a spectroscopic investigation of ThT enhancement in the presence of polystyrene (PS) beads. The study showed that ThT enhancement in the presence of PS beads was similar to that of Aβ peptides. Moreover, it is clear in Chapter 6 that ThT enhancement is dependent on both PS bead size and concentration.

In Chapter 7, covalently labeled fluorescent FAM-Aβ (1-40) peptide was mixed with either normal unlabeled Aβ (1-40) or Arctic Aβ (1-40) to produce aggregates. The aggregating Aβ mixtures were sampled over time and analyze by CE-LIFA. The progression of Aβ aggregation was clearly observed from day-to-day CE-LIF data. Aβ monomer, intermediate aggregates and fully-formed fibrils were separated and detected in a single electrophoretic run for some of the days of aggregation. It was determined that these Aβ peaks exhibited different fluorescence anisotropy values.

8.2 Future Directions

Our understanding of amyloid aggregation will continue to depend on developing and improving separation and detection methods. The lab-constructed CE-LIFA instrument used in Chapters 4 and 7 demonstrated, for the first time, the separation of monomers, intermediate aggregates and hundreds of individual fibrils. Moreover, in Chapter 7, the differences in the fluorescence anisotropy values for different forms of Aβ suggested that fluorescence anisotropy may be useful to differentiate Aβ based on size. To continue development work using fluorescence anisotropy as a detection method for Aβ, eliminating scattered light produced from

Aβ fibrils so that the fluorescence anisotropy can be calculated from a pure fluorescence signal will be critical. The magnitude of scattering can be seen in Chapter 4. Reducing scattered light could be accomplished by simply adding multiple notch filters in series.

Eliminating scattered light would be beneficial for fluorescence anisotropy; however, an interesting study would be to modify to the optics of the LIFA system so that one PMT is monitoring light scattering and the other PMT is monitoring fluorescence, i.e. the detection system would not be used to calculate fluorescence anisotropy, but it would provide the magnitude of the scattering under the fluorescence signal for each aggregate. This could be accomplished by replacing the polarizing beam splitter cube with a dichroic shortpass filter, which is essentially a spectral beam splitter. These types of filters are commercially available, e.g. from Edmunds Optics. By using a dichroic shortpass filter, scattered light would pass through the filter and be detected by the PMT that is currently being used to detect perpendicular radiation. This means that the scattering PMT would be scattering at 90° relative to the incidence of the excitation laser radiation on the capillary. The long wavelength of the fluorescence would be reflected by the dichroic shortpass filter and be detected in the PMT currently being used to detect parallel radiation. Another necessary change would be to move the notch filter and fluorescence bandpass filter so that they are between the dichroic shortpass filter and the PMT that is detecting fluorescence. Moreover, it would be necessary to include a scattering bandpass filter between the dichroic shortpass filter and the PMT detecting scattering.

Many researchers are using bulk ThT data to measure amyloid aggregation endpoints and kinetics. Based on the scattering data in Chapter 4, it would be interesting to perform a bulk ThT time-course aggregation study on Aβ but without the ThT. No data in the literature was found that compared bulk scattering to ThT fluorescence of Aβ aggregates in a time-course study.

The time-course aggregation study of FAM-Aβ and unlabeled Aβ presented in Chapter 7 discussed that 1:4 mixture of FAM-Aβ:unlabeled Aβ monomers does not necessarily result in aggregates containing a composition of 1:4 FAM-Aβ:unlabeled Aβ. It would be an interesting study to mix two fluorescently labeled Aβ monomers, which both could absorb radiation from the same excitation source but each would have a unique emission wavelength that could be selectively monitored. This may require custom fluorescent labeling because all the commercially fluorescent Aβ peptides that could be found are fluorescein-based. This means that the emission from the two dyes would be very similar, which makes spectrally separating the emissions extremely difficult or impossible. If suitable dyes become commercially available or if they can be synthesized in lab, changes to the emission optics similar to those described above with the dichroic filter would allow the independent and simultaneous detection of individual aggregates for selective wavelengths. Based on the fluorescence intensity detected from each dye, the ratio of each fluorescently-labeled Aβ incorporated into a single aggregate could be determined. It would be interesting to determine if a correlation exist between the ratio of the starting monomers and the ratio of the monomers incorporated into single aggregates.

REFERENCES

[1] R.N. Rambaran, L.C. Serpell, Amyloid fibrils Abnormal protein assembly, Prion 2 (2008) 112-117.

[2] H. Ecroyd, J.A. Carver, Unraveling the mysteries of protein folding and misfolding, IUBMB Life 60 (2008) 769-774.

[3] J.-C. Rochet, P.T. Lansbury Jr, Amyloid fibrillogenesis: themes and variations, Current Opinion in Structural Biology 10 (2000) 60-68.

[4] H. Naiki, F. Gejyo, Kinetic Analysis of Amyloid Fibril Formation, Method Enzymol. 309 (1999) 305-318.

[5] K. Hasegawa, I. Yamaguchi, S. Omata, F. Gejyo, H. Naiki, Interaction between A beta(1-42) and A beta(1-40) in Alzheimer's beta-amyloid fibril formation in vitro, Biochemistry 38 (1999) 15514-21.

[6] N.l. Carulla, M. Zhou, E. Giralt, C.V. Robinson, C.M. Dobson, Structure and Intermolecular Dynamics of Aggregates Populated during Amyloid Fibril Formation Studied by Hydrogen/Deuterium Exchange, Acc. Chem. Res. 43 (2010) 1072-1079.

[7] A.E. Langkilde, B. Vestergaard, Methods for structural characterization of prefibrillar intermediates and amyloid fibrils, FEBS Letters 583 (2009) 2600-2609.

[8] M. Lindgren, P. Hammarström, Amyloid oligomers: spectroscopic characterization of amyloidogenic protein states, FEBS Journal 277 (2010) 1380-1388.

[9] T. Takahashi, H. Mihara, Peptide and Protein Mimetics Inhibiting Amyloid β-Peptide Aggregation, Acc. Chem. Res. 41 (2008) 1309-1318.

[10] B. O'Nuallain, S. Shivaprasad, I. Kheterpal, R. Wetzel, Thermodynamics of Aβ (1-40) Amyloid Fibril Elongation, Biochemistry 44 (2005) 12709-12718.

[11] T. Ban, D. Hamada, K. Hasegawa, H. Naiki, Y. Goto, Direct Observation of Amyloid Fibril Growth Monitored by Thioflavin T Fluorescence, J. Biol. Chem. 278 (2003) 16462-16465.

[12] M. Biancalana, S. Koide, Molecular mechanism of Thioflavin-T binding to amyloid fibrils, Biochim. Biophys. Acta, Proteins Proteomics 1804 (2010) 1405-1412.

[13] J. Hardy, D.J. Selkoe, Medicine - The amyloid hypothesis of Alzheimer's disease: Progress and problems on the road to therapeutics, Science 297 (2002) 353-356.

[14] D.J. Selkoe, Unraveling the molecular basis of Alzheimer's disease yields novel therapies: a personal retrospective, Journal of Medical Sciences (Sharjah, United Arab Emirates) 2 (2009) 98-107.

[15] G.B. Irvine, O.M. El-Agnaf, G.M. Shankar, D.M. Walsh, Protein aggregation in the brain: The molecular basis for Alzheimer's and Parkinson's diseases, Mol. Med. 14 (2008) 451-464.

[16] X. Cheng, R.B. van Breemen, Mass spectrometry-based screening for inhibitors of beta-amyloid protein aggregation, Anal. Chem. 77 (2005) 7012-7015.

[17] B.J. Alper, W.K. Schmidt, A capillary electrophoresis method for evaluation of Aβ proteolysis in vitro, J. Neurosci. Meth. 178 (2009) 40-45.

[18] J.-F. Wang, R. Lu, Y.-Z. Wang, Regulation of β cleavage of amyloid precursor protein, Neuroscience Bulletin 26 (2010) 417-427.

[19] W.P. Esler, E.R. Stimson, J.R. Ghilardi, H.V. Vinters, J.P. Lee, P.W. Mantyh, J.E. Maggio, In Vitro Growth of Alzheimer's Disease β-Amyloid Plaques Displays First-Order Kinetics†, Biochemistry 35 (1996) 749-757.

[20] S.J. Haugabook, D.M. Yager, E.A. Eckman, T.E. Golde, S.G. Younkin, C.B. Eckman, High throughput screens for the identification of compounds that alter the accumulation of the Alzheimer's amyloid beta peptide (A beta), J. Neurosci. Meth. 108 (2001) 171-179.

[21] R.A. Armstrong, P.L. Lantos, N.J. Cairns, What determines the molecular composition of abnormal protein aggregates in neurodegenerative disease?, Neuropathology 28 (2008) 351-365.

[22] G. Bitan, Structural study of metastable amyloidogenic protein oligomers by photo-induced cross-linking of unmodified proteins, Method Enzymol. 413 (2006) 217-236.

[23] S.A. Funke, E. Birkmann, F. Henke, P. Gortz, C. Lange-Asschenfeldt, D. Riesner, D. Willbold, Single particle detection of Aβ aggregates associated with Alzheimer's disease,

Biochem. Biophys. Res. Commun. 364 (2007) 902-907.

[24] J.D. Lowenson, S. Clarke, A.E. Roher, Chemical modifications of deposited amyloid-beta peptides, Method Enzymol. 309 (1999) 89-105.

[25] G. Bitan, M.D. Kirkitadze, A. Lomakin, S.S. Vollers, G.B. Benedek, D.B. Teplow, Amyloid beta-protein (A beta) assembly: A beta 40 and A beta 42 oligomerize through distinct pathways, P. Natl. Acad. Sci. USA 100 (2003) 330-335.

[26] G. Thorsen, J. Bergquist, A. Westlind-Danielsson, B. Josefsson, Stereoselective Determination of Amino Acids in β-Amyloid Peptides and Senile Plaques, Anal. Chem. 73 (2001) 2625-2631.

[27] M. Austen Brian, E. Paleologou Katerina, A.E. Ali Sumaya, M. Qureshi Mohamed, D. Allsop, M.A. El-Agnaf Omar, Designing peptide inhibitors for oligomerization and toxicity of Alzheimer's beta-amyloid peptide, Biochemistry 47 (2008) 1984-92.

[28] K.L. Sciarretta, D.J. Gordon, S.C. Meredith, Methods in Enzymology, in: I. Kheterpal, and R. Wetzel, (Eds.), Amyloid, Prions, and Other Protein Aggregates, Pt C, Elsevier Academic Press Inc, San Diego, 2006, pp. 273-312.

[29] F.G. De Felice, M.N.N. Vieira, L.M. Saraiva, J.D. Figueroa-Villar, J. Garcia-Abreu, R. Liu, L. Chang, W.L. Klein, S.T. Ferreira, Targeting the neurotoxic species in Alzheimer's disease: inhibitors of Aβ oligomerization, FASEB Journal 18 (2004) 1366-1372, 10 1096/fj 04-1764com.

[30] R. Colombo, A. Carotti, M. Catto, M. Racchi, C. Lanni, L. Verga, G. Caccialanza, E. De Lorenzi, CE can identify small molecules that selectively target soluble oligomers of amyloid β protein and display antifibrillogenic activity, Electrophoresis 30 (2009) 1418-1429.

[31] M.A. Findeis, S.M. Molineaux, Design and testing of inhibitors of fibril formation, Method Enzymol. 309 (1999) 476-488.

[32] C.K. Bett, J.N. Ngunjiri, W.K. Serem, K.R. Fontenot, R.P. Hammer, R.L. McCarley, J.C. Garno, Structure-Activity Relationships in Peptide Modulators of beta-Amyloid Protein Aggregation: Variation in alpha,alpha-Disubstitution Results in Altered Aggregate Size and Morphology, ACS Chem. Neurosci. 1 (2010) 608-626.

[33] M.A. Etienne, J.P. Aucoin, Y. Fu, R.L. McCarley, R.P. Hammer, Stoichiometric

Inhibition of Amyloid β-Protein Aggregation with Peptides Containing Alternating α,α-Disubstituted Amino Acids, J. Am. Chem. Soc. 128 (2006) 3522-3523.

[34] T.A. Lanz, M.J. Karmilowicz, K.M. Wood, N. Pozdnyakov, P. Du, M.A. Piotrowski, T.M. Brown, C.E. Nolan, K.E.G. Richter, J.E. Finley, Q. Fei, C.F. Ebbinghaus, Y.L. Chen, D.K. Spracklin, B. Tate, K.F. Geoghegan, L.F. Lau, D.D. Auperin, J.B. Schachter, Concentration-dependent modulation of amyloid-beta in vivo and in vitro using the gamma-secretase inhibitor, LY-450139, J. Pharmacol. Exp. Ther. 319 (2006) 924-933.

[35] R. Kayed, C.G. Glabe, Conformation-dependent anti-amyloid oligomer antibodies, Method Enzymol. 413 (2006) 326-344.

[36] D.M. Walsh, D.J. Selkoe, Deciphering the Molecular Basis of Memory Failure in Alzheimer's Disease, Neuron 44 (2004) 181-193.

[37] M.S. Shearman, Toxicity of protein aggregates in PC 12 cells: 3-(4, 5-dimethylthiazol-2-yl)-2,5-diphenyltetrazolium bromide assay, Method Enzymol. 309 (1999) 716-723.

[38] X.-Y. Qin, Y. Cheng, J. Cui, Y. Zhang, L.-C. Yu, Potential protection of curcumin against amyloid β-induced toxicity on cultured rat prefrontal cortical neurons, Neurosci. Lett. 463 (2009) 158-161.

[39] M.R. Nilsson, Techniques to study amyloid fibril formation in vitro, Methods 34 (2004) 151-160.

[40] M.G. Zagorski, J. Yang, H. Shao, K. Ma, H. Zeng, A. Hong, Methodological and Chemical Factors Affecting Amyloid β Peptide Amyloidogenicity, Method Enzymol. 309 (1999) 189-204.

[41] M.-S. Lin, L.-Y. Chen, H.-T. Tsai, S.S.S. Wang, Y. Chang, A. Higuchi, W.-Y. Chen, Investigation of the Mechanism of beta -Amyloid Fibril Formation by Kinetic and Thermodynamic Analyses, Langmuir 24 (2008) 5802-5808.

[42] D.B. Teplow, N.D. Lazo, G. Bitan, S. Bernstein, T. Wyttenbach, M.T. Bowers, A. Baumketner, J.-E. Shea, B. Urbanc, L. Cruz, J. Borreguero, H.E. Stanley, Elucidating Amyloid β-Protein Folding and Assembly: A Multidisciplinary Approach, Acc. Chem. Res. 39 (2006) 635-645.

[43] I. Kheterpal, A. Williams, C. Murphy, B. Bledsoe, R. Wetzel, Structural Features of the

Aβ Amyloid Fibril Elucidated by Limited Proteolysis, Biochemistry 40 (2001) 11757-11767.

[44] B. O'Nuallain, A.K. Thakur, A.D. Williams, A.M. Bhattacharyya, S. Chen, G. Thiagarajan, R. Wetzel, Kinetics and thermodynamics of amyloid assembly using a high-performance liquid chromatography-based sedimentation assay, Method Enzymol. 413 (2006) 34-74.

[45] R. Picou, J.P. Moses, A.D. Wellman, I. Kheterpal, S.D. Gilman, Analysis of monomeric Aβ (1-40) peptide by capillary electrophoresis, Analyst 135 (2010) 1631-1635.

[46] A. Lomakin, D.B. Teplow, Quasielastic Light Scattering Study of Amyloid β-Protein Fibril Formation, Protein Pept. Lett. 13 (2006) 247-254.

[47] A. Lomakin, G.B. Benedek, D.B. Teplow, Monitoring protein assembly using quasielastic light scattering spectroscopy, Methods Enzymol. 309 (1999) 429-459.

[48] D.M. Walsh, A. Lomakin, G.B. Benedek, M.M. Condron, D.B. Teplow, Amyloid beta-protein fibrillogenesis - Detection of a protofibrillar intermediate, J. Biol. Chem. 272 (1997) 22364-22372.

[49] A.J. Thompson, T.K. Lim, C.J. Barrow, On-line high-performance liquid chromatography/mass spectrometric investigation of amyloid-beta peptide variants found in Alzheimer's disease, Rapid Commun. Mass Sp. 13 (1999) 2348-2351.

[50] M. Stoeckli, R. Knochenmuss, G. McCombie, D. Mueller, T. Rohner, D. Staab, K.H. Wiederhold, MALDI MS imaging of amyloid, Method Enzymol. 412 (2006) 94-106.

[51] I. Kheterpal, K.D. Cook, R. Wetzel, Hydrogen/Deuterium Exchange Mass Spectrometry Analysis of Protein Aggregates, Method Enzymol. 413 (2006) 140-166.

[52] C. Uetrecht, R.J. Rose, E. van Duijn, K. Lorenzen, A.J.R. Heck, Ion mobility mass spectrometry of proteins and protein assemblies, Chemical Society Reviews 39 (2010) 1633-1655.

[53] D.M. Hartley, D.M. Walsh, C.P. Ye, T. Diehl, S. Vasquez, P.M. Vassilev, D.B. Teplow, D.J. Selkoe, Protofibrillar Intermediates of Amyloid β-Protein Induce Acute Electrophysiological Changes and Progressive Neurotoxicity in Cortical Neurons, J. Neurosci. 19 (1999) 8876-8884.

[54] C. Ha, C.B. Park, Ex Situ Atomic Force Microscopy Analysis of β-Amyloid Self-Assembly and Deposition on a Synthetic Template, Langmuir 22 (2006) 6977-6985.

[55] T.T. Ding, J.D. Harper, Analysis of amyloid-beta assemblies using tapping mode atomic force microscopy under ambient conditions, Method Enzymol. 309 (1999) 510-525.

[56] J. Ryu, H.A. Joung, M.G. Kim, C.B. Park, Surface plasmon resonance analysis of Alzheimer's beta-amyloid aggregation on a solid surface: From monomers to fully-grown fibrils, Anal. Chem. 80 (2008) 2400-2407.

[57] H. LeVine, III, Quantification of β-Sheet Amyloid Fibril Structures with Thioflavin T, Method Enzymol. 309 (1999) 274-284.

[58] M. Chen, K.D. Cook, I. Kheterpal, R. Wetzel, A Triaxial Probe for On-line Proteolysis Coupled with Hydrogen/Deuterium Exchange-Electrospray Mass Spectrometry, J. Am. Soc. Mass Spectrom. 18 (2007) 208-217.

[59] I. Kheterpal, S. Zhou, K.D. Cook, R. Wetzel, Aβ amyloid fibrils possess a core structure highly resistant to hydrogen exchange, P. Natl. Acad. Sci. USA 97 (2000) 13597-13601.

[60] E.J. Nettleton, C.V. Robinson, Probing conformations of amyloidogenic proteins by hydrogen exchange and mass spectrometry, Method Enzymol. 309 (1999) 633-646.

[61] W. Colon, Analysis of protein structure by solution optical spectroscopy, Method Enzymol. 309 (1999) 605-632.

[62] M.R.H. Krebs, E.H.C. Bromley, A.M. Donald, The binding of thioflavin-T to amyloid fibrils: localisation and implications, J. Struct. Biol. 149 (2005) 30-37.

[63] H. Levine III, Multiple ligand binding sites on Aβ (1-40) fibrils, Amyloid 12 (2005) 5-14.

[64] H. Naiki, K. Higuchi, M. Hosokawa, T. Takeda, Fluorometric determination of amyloid fibrils in vitro using the fluorescent dye, thioflavine T, Anal. Biochem. 177 (1989) 244-249.

[65] H. Levine, THIOFLAVINE-T INTERACTION WITH SYNTHETIC ALZHEIMERS-DISEASE BETA-AMYLOID PEPTIDES - DETECTION OF AMYLOID AGGREGATION IN SOLUTION, Protein Sci. 2 (1993) 404-410.

[66] V.I. Stsiapura, A.A. Maskevich, V.A. Kuzmitsky, V.N. Uversky, I.M. Kuznetsova, K.K. Turoverov, Thioflavin T as a Molecular Rotor: Fluorescent Properties of Thioflavin T in Solvents with Different Viscosity, J. Phys. Chem. B 112 (2008) 15893-15902.

[67] R. Khurana, C. Coleman, C. Ionescu-Zanetti, S.A. Carter, V. Krishna, R.K. Grover, R. Roy, S. Singh, Mechanism of thioflavin T binding to amyloid fibrils, J. Struct. Biol. 151 (2005) 229-238.

[68] R. Sabaté, S.J. Saupe, Thioflavin T fluorescence anisotropy: An alternative technique for the study of amyloid aggregation, Biochem. Biophys. Res. Commun. 360 (2007) 135-138.

[69] J.R. Lakowicz, Principles of Fluorescence Spectroscopy, Kluwer Academic/Plenum, New York, 1999.

[70] A. Jan, O. Gokce, R. Luthi-Carter, H.A. Lashuel, The Ratio of Monomeric to Aggregated Forms of Aβ40 and Aβ42 Is an Important Determinant of Amyloid-β Aggregation, Fibrillogenesis, and Toxicity, J. Biol. Chem. 283 (2008) 28176-28189.

[71] H.-W. Klafki, J. Wiltfang, M. Staufenbiel, Electrophoretic Separation of βA4 Peptides (1-40) and (1-42), Anal. Biochem. 237 (1996) 24-29.

[72] S. Betts, M. Speed, J. King, Detection of early aggregation intermediates by native gel electrophoresis and native western blotting, Method Enzymol. 309 (1999) 333-350.

[73] S.N. Bagriantsev, V.V. Kushnirov, S.W. Liebman, K. Indu, W. Ronald, Analysis of Amyloid Aggregates Using Agarose Gel Electrophoresis, Method Enzymol., Academic Press, 2006, pp. 33-48.

[74] J.R. Silveira, A.G. Hughson, B. Caughey, Fractionation of prion protein aggregates by asymmetrical flow field-flow fractionation, Method Enzymol. 412 (2006) 21-33.

[75] D. Rambaldi, A. Zattoni, P. Reschiglian, R. Colombo, E. De Lorenzi, In vitro amyloid Aβ1-42 peptide aggregation monitoring by asymmetrical flow field-flow fractionation with multi-angle light scattering detection, Analytical and Bioanalytical Chemistry 394 (2009) 2145-2149.

[76] D. Brambilla, R. Verpillot, M. Taverna, L. De Kimpe, B. Le Droumaguet, J. Nicolas, M. Canovi, M. Gobbi, F. Mantegazza, M. Salmona, V. Nicolas, W. Scheper, P. Couvreur, K. Andrieux, New Method Based on Capillary Electrophoresis with Laser-Induced Fluorescence

Detection (CE-LIF) to Monitor Interaction between Nanoparticles and the Amyloid-β Peptide, Anal. Chem. 82 (2010) 10083-10089.

[77] P.J. Sweeney, J.G. Darker, W.A. Neville, J. Humphries, P. Camilleri, Electrophoretic Techniques for the Analysis of Synthetic Amyloid β-A4-Related Peptides, Anal. Biochem. 212 (1993) 179-184.

[78] J.P. Landers, Handbook of Capillary Electrophoresis, CRC Press, Boca Raton, 1994.

[79] C.A. Keely, T. Vandegoor, D. McManigill, MODELING FLOW PROFILES AND DISPERSION IN CAPILLARY ELECTROPHORESIS WITH NONUNIFORM ZETA-POTENTIAL, Anal. Chem. 66 (1994) 4236-4242.

[80] R. Weinberger, Practical Capillary Electrophoresis, Academic Press, 2000.

[81] S.P. Radko, A. Chrambach, Separation and characterization of sub-μm- and μm-sized particles by capillary zone electrophoresis, Electrophoresis 23 (2002) 1957-1972.

[82] Y.H. Rezenom, A.D. Wellman, L. Tilstra, C.D. Medley, S.D. Gilman, Separation and detection of individual submicron particles by capillary electrophoresis with laser-light-scattering detection, Analyst 132 (2007) 1215-1222.

[83] H.A. Lashuel, D.M. Hartley, B.M. Petre, J.S. Wall, M.N. Simon, T. Walz, P.T. Lansbury Jr, Mixtures of Wild-type and a Pathogenic (E22G) Form of Aβ40 in Vitro Accumulate Protofibrils, Including Amyloid Pores, J. Mol. Biol. 332 (2003) 795-808.

[84] L. Minati, T. Edginton, M.G. Bruzzone, G. Giaccone, Current Concepts in Alzheimer's Disease: A Multidisciplinary Review, American Journal of Alzheimers Disease and Other Dementias 24 (2009) 95-121.

[85] Y. Nagai, H.A. Popiel, Conformational Changes and Aggregation of Expanded Polyglutamine Proteins as Therapeutic Targets of the Polyglutamine Diseases: Exposed β-Sheet Hypothesis, Current Pharmaceutical Design 14 (2008) 3267-3279.

[86] R. Roychaudhuri, M. Yang, M.M. Hoshi, D.B. Teplow, Amyloid β-Protein Assembly and Alzheimer Disease, J. Biol. Chem. 284 (2009) 4749-4753.

[87] D.M. Walsh, D.J. Selkoe, Aβ Oligomers - a decade of discovery, Journal of Neurochemistry

101 (2007) 1172-1184.

[88] R. Sabaté, M. Gallardo, J. Estelrich, Temperature dependence of the nucleation constant rate in beta amyloid fibrillogenesis, International journal of biological macromolecules 35 (2005) 9-13.

[89] B. O'Nuallain, A.D. Williams, P. Westermark, R. Wetzel, Seeding Specificity in Amyloid Growth Induced by Heterologous Fibrils, J. Biol. Chem. 279 (2004) 17490-17499.

[90] S.S.S. Wang, Y.-T. Chen, P.-H. Chen, K.-N. Liu, A kinetic study on the aggregation behavior of beta -amyloid peptides in different initial solvent environments, Biochem. Eng. J. 29 (2006) 129-138.

[91] S. Sabella, M. Quaglia, C. Lanni, M. Racchi, S. Govoni, G. Caccialanza, A. Calligaro, V. Bellotti, E. De Lorenzi, Capillary electrophoresis studies on the aggregation process of ß-amyloid 1-42 and 1-40 peptides, Electrophoresis 25 (2004) 3186-3194.

[92] E. Varesio, S. Rudaz, K.-H. Krause, J.-L. Veuthey, Nanoscale liquid chromatography and capillary electrophoresis coupled to electrospray mass spectrometry for the detection of amyloid-β peptide related to Alzheimer's disease, J. Chromatogr., A. 974 (2002) 135-142.

[93] R. Verpillot, M. Otto, H. Klafki, M. Taverna, Simultaneous analysis by capillary electrophoresis of five amyloid peptides as potential biomarkers of Alzheimer's disease, J. Chromatogr., A. 1214 (2008) 157-164.

[94] S. Hjerten, K. Elenbring, F. Kilar, J.L. Liao, A.J.C. Chen, C.J. Siebert, M.D. Zhu, CARRIER-FREE ZONE ELECTROPHORESIS, DISPLACEMENT ELECTROPHORESIS AND ISOELECTRIC-FOCUSING IN A HIGH-PERFORMANCE ELECTROPHORESIS APPARATUS, Journal of Chromatography 403 (1987) 47-61.

[95] S.D. Gilman, P.J. Chapman, Measuring electroosmotic flow in microchips and capillaries, Methods Mol. Biol. 339 (2006) 187-201.

[96] D.R. Howlett, K.H. Jennings, D.C. Lee, M.S.G. Clark, F. Brown, R. Wetzel, S.J. Wood, P. Camilleri, G.W. Roberts, Aggregation State and Neurotoxic Properties of Alzheimer Beta-Amyloid Peptide, Neurodegeneration : A Journal for Neurodegenerative Disorders, Neuroprotection, and Neuroregeneration 4 (1995) 23-32.

[97] M. Bodanszki, A. Bodanszki, *The Practice of Peptide Synthesis*, Springer-Verlag, Berlin,

1994.

[98] G. Evin, M.F. Sernee, C.L. Masters, Inhibition of γ-Secretase as a Therapeutic Intervention for Alzheimer's Disease: Prospects, Limitations and Strategies, CNS Drugs 20 (2006) 351-372.

[99] S.S.-S. Wang, A. Becerra-Arteaga, T.A. Good, Development of a Novel Diffusion-Based Method to Estimate the Size of the Aggregated β Species Responsible for Neurotoxicity, Biotechnol. Bioeng. 80 (2002) 50-59.

[100] D.K. Clodfelter, M.A. Nussbaum, J. Reilly, Comparison of free solution capillary electrophoresis and size exclusion chromatography for quantitating non-covalent aggregation of an acylated peptide, J. Pharm. Biomed. Anal. 19 (1999) 763-775.

[101] I. Ali, H.Y. Aboule-Enein, V.K. Gupta, Precision in Capillary Electrophoresis, Analytical Letters 39 (2006) 2345-2357.

[102] F. Foret, S. Fanali, A. Nardi, P. Boček, Capillary zone electrophoresis of rare earth metals with indirect UV absorbance detection, Electrophoresis 11 (1990) 780-783.

[103] M.A. Rodriguez, D.W. Armstrong, Separation and analysis of colloidal/nano-particles including microorganisms by capillary electrophoresis: a fundamental review, J. Chromatogr., B. 800 (2004) 7-25.

[104] R. Kodali, R. Wetzel, Polymorphism in the intermediates and products of amyloid assembly, Current Opinion in Structural Biology 17 (2007) 48-57.

[105] I. Kheterpal, H.A. Lashuel, D.M. Hartley, T. Walz, P.T. Lansbury Jr, R. Wetzel, Aβ Protofibrils Possess a Stable Core Structure Resistant to Hydrogen Exchange, Biochemistry 42 (2003) 14092-14098.

[106] H. Ahmadzadeh, R. Dua, A.D. Presley, E.A. Arriaga, Automated analysis of individual particles using a commercial capillary electrophoresis system, J. Chromatogr., A. 1064 (2005) 107-114.

[107] S.P. Radko, A. Chrambach, Capillary electrophoresis of subcellular-sized particles, J. Chromatogr., B. 722 (1999) 1-10.

[108] S.J. Wood, W. Chan, R. Wetzel, Seeding of Aβ Fibril Formation Is Inhibited by All Three

Isotypes of Apolipoprotein E, Biochemistry 35 (1996) 12623-12628.

[109] J.D. Harper, P.T. Lansbury, Jr., Models of Amyloid Seeding in Alzheimer's Disease and Scrapie: Mechanistic Truths and Physiological Consequences of the Time-Dependent Solubility of Amyloid Proteins, Annu. Rev. Biochem. 66 (1997) 385-407.

[110] H. Levine III, Small molecule inhibitors of Aβ assembly, Amyloid 14 (2007) 185-197.

[111] T. Ban, Y. Goto, Direct Observation of Amyloid Growth Monitored by Total Internal Reflection Fluorescence Microscopy, Method Enzymol. 413 (2006) 91-102.

[112] R. Tycko, Characterization of Amyloid Structures at the Molecular Level by Solid State Nuclear Magnetic Resonance Spectroscopy, Method Enzymol. 413 (2006) 103-122.

[113] M. Kato, H. Kinoshita, M. Enokita, Y. Hori, T. Hashimoto, T. Iwatsubo, T. Toyo'oka, Analytical Method for β-Amyloid Fibrils Using CE-Laser Induced Fluorescence and Its Application to Screening for Inhibitors of β-Amyloid Protein Aggregation, Anal. Chem. 79 (2007) 4887-4891.

[114] Y.-M. Kuo, M.R. Emmerling, C. Vigo-Pelfrey, T.C. Kasunic, J.B. Kirkpatrick, G.H. Murdoch, M.J. Ball, A.E. Roher, Water-soluble Aβ (N-40, N-42) Oligomers in Normal and Alzheimer Disease Brains, J. Biol. Chem. 271 (1996) 4077-4081.

[115] Y.-F. Mok, J. Howlett Geoffrey, Sedimentation velocity analysis of amyloid oligomers and fibrils, Method Enzymol. 413 (2006) 199-217.

[116] T. Frackowiak, T. Baczek, R. Kaliszan, B. Zbikowska, M. Glensk, I. Fecka, W. Cisowski, Binding of an Oxindole Alkaloid from Uncaria Tomentosa to Amyloid Protein (Aβ1-40), Z. Naturforsch., C: J. Biosci. 61 (2006) 821-826.

[117] A. Kishita, S. Nishino, Y. Nishida, Interaction between Cu(II) Compounds and Amyloid β-peptide (1-40) in Solution, Synth. React. Inorg., Met.-Org., Nano-Met. Chem. 35 (2005) 379-383.

[118] R.A. Picou, I. Kheterpal, A.D. Wellman, M. Minnamreddy, G. Ku, S.D. Gilman, Analysis of Aβ (1-40) and Aβ (1-42) monomer and fibrils by capillary electrophoresis, J. Chromatogr., B. 879 (2011) 627-632.

[119] Q.-H. Wan, X.C. Le, Studies of Protein-DNA Interactions by Capillary Electrophoresis/Laser-Induced Fluorescence Polarization, Anal. Chem. 72 (2000) 5583-5589.

[120] R.J. Whelan, R.K. Sunahara, R.R. Neubig, R.T. Kennedy, Affinity Assays Using Fluorescence Anisotropy with Capillary Electrophoresis Separation, Anal. Chem. 76 (2004) 7380-7386.

[121] P. Yang, R.J. Whelan, Y. Mao, A.W.-M. Lee, C. Carter-Su, R.T. Kennedy, Multiplexed Detection of Protein-Peptide Interaction and Inhibition Using Capillary Electrophoresis, Anal. Chem. 79 (2007) 1690-1695.

[122] L. Ye, X.C. Le, J.Z. Xing, M. Ma, R. Yatscoff, Competitive immunoassay for cyclosporine using capillary electrophoresis with laser induced fluorescence polarization detection, J. Chromatogr., B. 714 (1998) 59-67.

[123] D. Allsop, L. Swanson, S. Moore, Y. Davies, A. York, O.M.A. El-Agnaf, I. Soutar, Fluorescence Anisotropy: A Method for Early Detection of Alzheimer β-Peptide (Aβ) Aggregation, Biochem. Biophys. Res. Commun. 285 (2001) 58-63.

[124] K.F. Schrum, J.M. Lancaster, III, S.E. Johnston, S.D. Gilman, Monitoring Electroosmotic Flow by Periodic Photobleaching of a Dilute, Neutral Fluorophore, Anal. Chem. 72 (2000) 4317-4321.

[125] S.D. Gilman, A.G. Ewing, Analysis of Single Cells by Capillary Electrophoresis with On-Column Derivatization and Laser-Induced Fluorescence Detection, Anal. Chem. 67 (1995) 58-64.

[126] X.C. Le, Q.-H. Wan, M.T. Lam, Fluorescence polarization detection for affinity capillary electrophoresis, Electrophoresis 23 (2002) 903-908.

[127] P. Yang, R.J. Whelan, E.E. Jameson, J.H. Kurzer, L.S. Argetsinger, C. Carter-Su, A. Kabir, A. Malik, R.T. Kennedy, Capillary Electrophoresis and Fluorescence Anisotropy for Quantitative Analysis of Peptide-Protein Interactions Using JAK2 and SH2-Bβ as a Model System, Anal. Chem. 77 (2005) 2482-2489.

[128] R. Picou, D.P. Schrum, G. Ku, R.A. Cerqua, I. Kheterpal, S.D. Gilman, Separation and Detection of Individual Aβ Aggregates by Capillary Electrophoresis with Laser-Induced Fluorescence Detection, Anal. Biochem. (Submitted).

[129] R. Picou, S.D. Gilman, A data treatment method for detecting fluorescence anisotropy peaks in capillary electropherograms, Anal. Chim. Acta. (Submitted).

[130] A.R. Lam, D.B. Teplow, H.E. Stanley, B. Urbanc, Effects of the Arctic (E(22)-> G) Mutation on Amyloid beta-Protein Folding: Discrete Molecular Dynamics Study, J. Am. Chem. Soc. 130 (2008) 17413-17422.

[131] A. Lord, A. Gumucio, H. Englund, D. Sehlin, V.S. Sundquist, L. Söderberg, C. Möller, P. Gellerfors, L. Lannfelt, F.E. Pettersson, L.N.G. Nilsson, An amyloid-β protofibril-selective antibody prevents amyloid formation in a mouse model of Alzheimer's disease, Neurobiology of Disease 36 (2009) 425-434.

[132] A. Peralvarez-Marin, L. Mateos, C. Zhang, S. Singh, A. Cedazo-Minguez, N. Visa, L. Morozova-Roche, A. Graslund, A. Barth, Influence of Residue 22 on the Folding, Aggregation Profile, and Toxicity of the Alzheimer's Amyloid beta Peptide, Biophys J 97 (2009) 277-285.

[133] B. Urbanc, M. Betnel, L. Cruz, G. Bitan, D.B. Teplow, Elucidation of Amyloid beta-Protein Oligomerization Mechanisms: Discrete Molecular Dynamics Study, J. Am. Chem. Soc. 132 (2010) 4266-4280.

APPENDIX A: SUPPLEMENTAL FIGURES

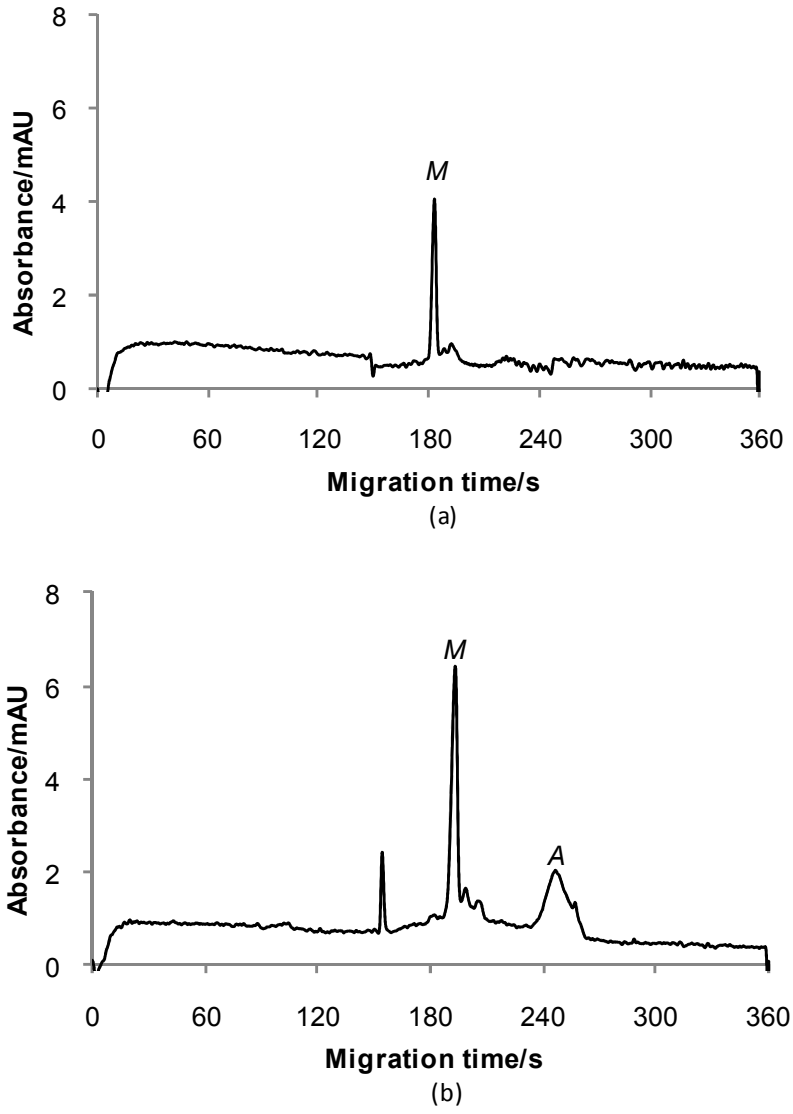

Figure A.1. Aβ (1-40) monomer preparation. Same plot as Figure 2.2 except plotted in time and showing the entire electrophoretic run (360 s or 5 min).

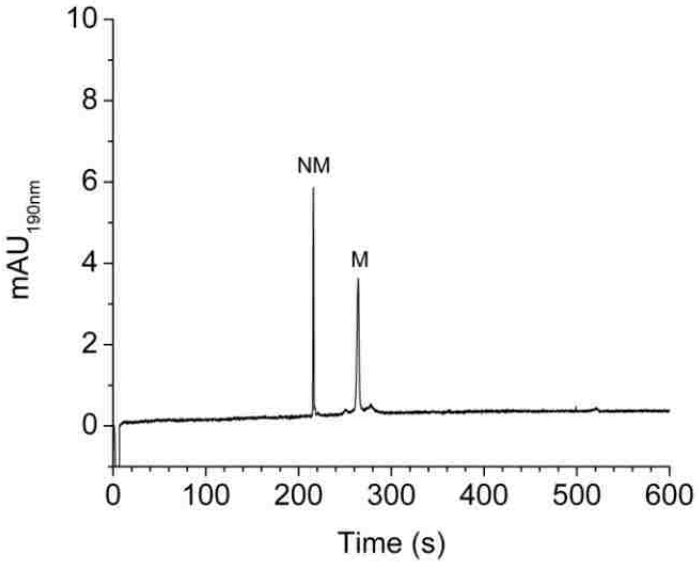

Figure A.2. Electropherogram of Aβ (1-40) monomer with UV absorbance detection (190 nm). The sample was the same as that used for Figure 4.3. The capillary (ID = 50 μm, OD = 366 μm) had a total length of 63.0 cm. The detection window was 53.0 cm from the inlet end. The neutral marker (NM) was injected for 2.0 s at 0.3 psi followed by the Aβ injection for 5.0 s at 0.5 psi. The separation potential was 25.0 kV (397 V/cm). The peaks at 216 s and 264 s are due to the neutral marker and Aβ (1-40) monomer, respectively. The small peaks near the Aβ monomer peak are thought to be due to Aβ synthetic impurities.

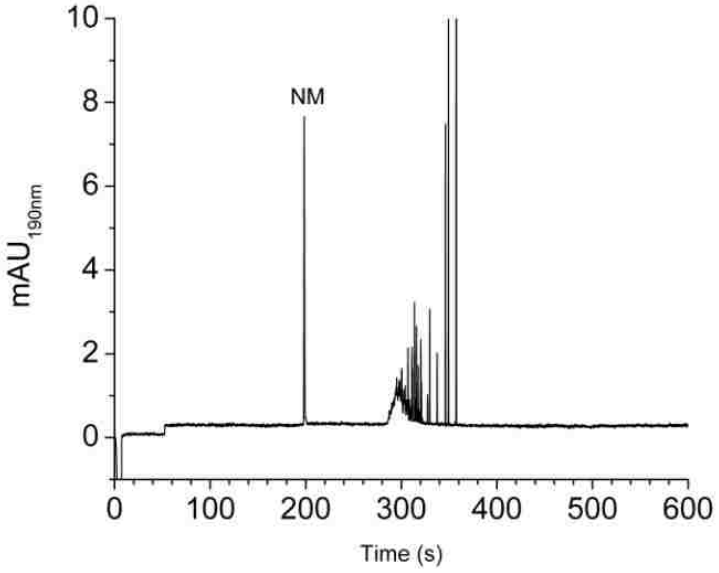

Figure A.3. Electropherogram of Aβ (1-42) fibril with UV absorbance detection at 190 nm. The sample was the same as that used for Figure 4.6. The experimental conditions are the same as in Figure A.2. The peaks at 200 s and 280–360 s are due to the neutral marker and Aβ (1-42) aggregates, respectively.

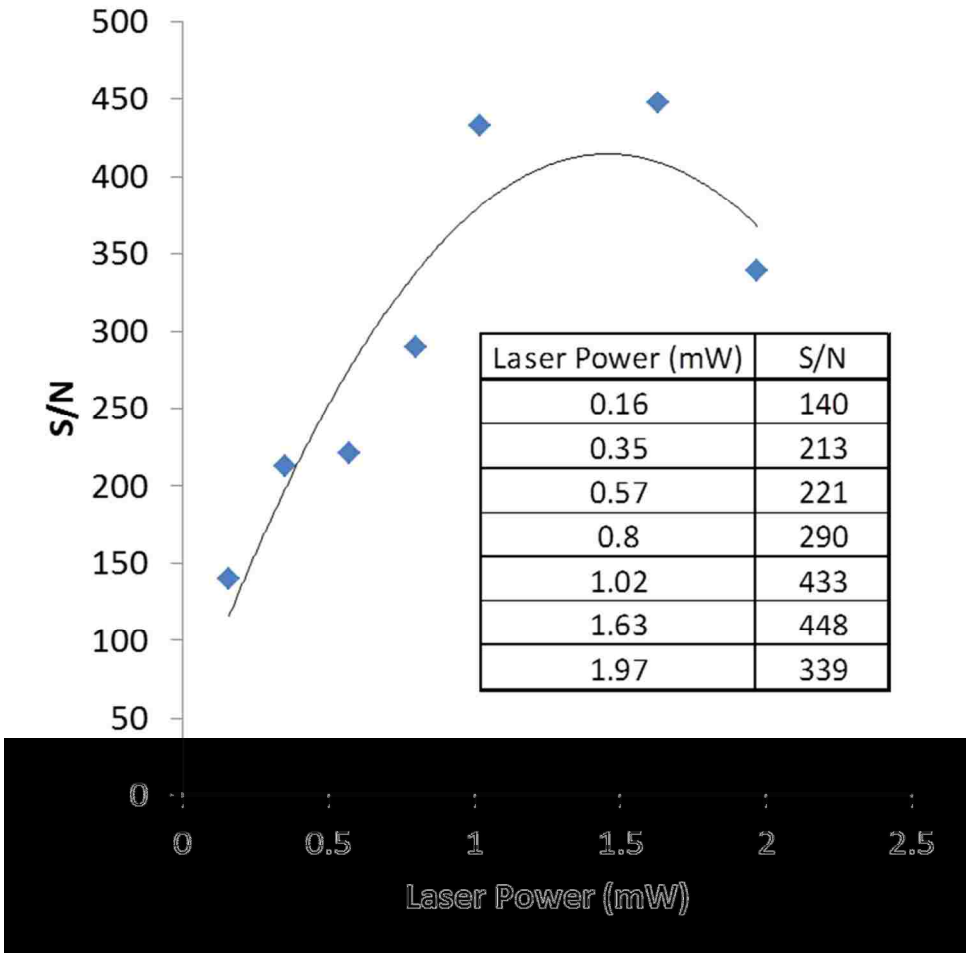

Laser Power (mW)	S/N
0.16	140
0.35	213
0.57	221
0.8	290
1.02	433
1.63	448
1.97	339

Figure A.4. Optimizing laser power for maximum S/N of a 2.5 μM FAM-Aβ (1-40) sample. Seven laser powers tested (values shown in embedded table). The laser power was not tunable. Each laser power was adjusted with neutral density filter(s). The laser power was measured with a power meter. The black curve is there to guide the eye.

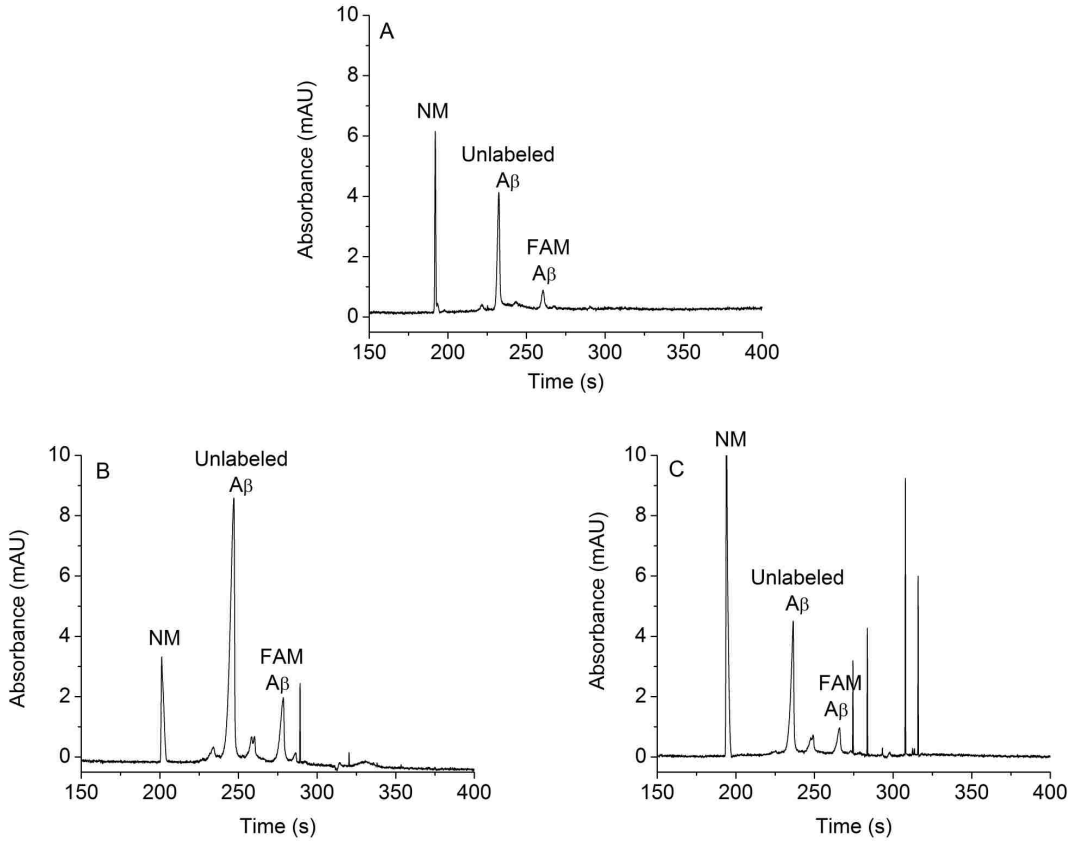

Figure A.5. CE-UV **e**lectropherograms of a 1:4 mixture of FAM-Aβ (1-40) peptide: Unlableled Aβ (1-40) peptide sampled on day 0 (A), day 4 (B) and day 6 (C).

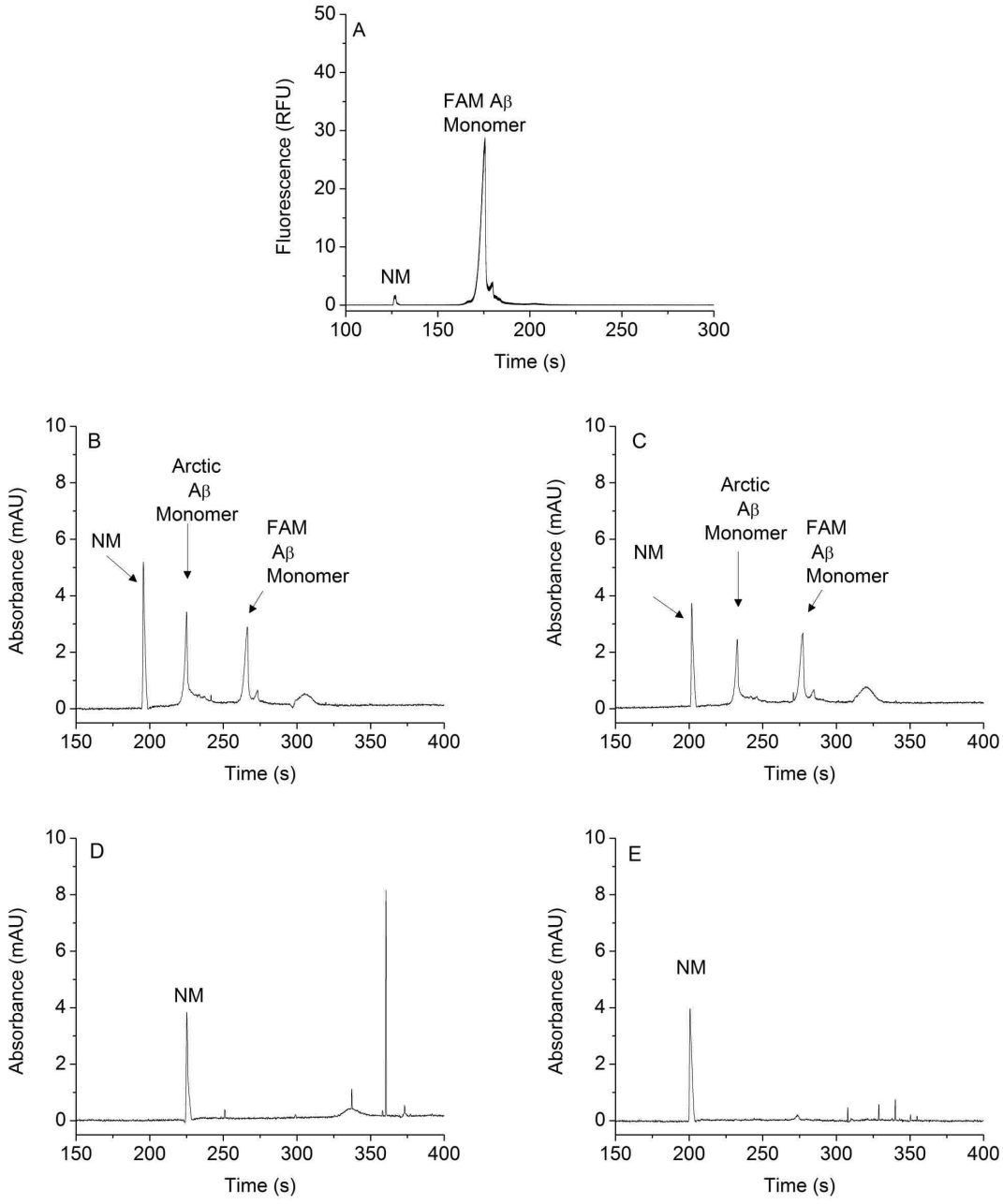

Figure A.6. (A) CE-LIF electropherogram of the FAM-Aβ (1-40) peptide:Arctic Aβ (1-40) peptide analyzed on day 1 of aggregation. (B-E) CE-UV electropherograms of the sample FAM-Aβ (1-40) peptide:Arctic Aβ (1-40) peptide mixture shown in (A) analyzed on day 1 (B), day 2 (C), day 3 (D) and day 6 (E).

APPENDIX B: LETTERS OF PERMISSION

Ryan Picou <rpicou3@tigers.lsu.edu>

RE: Website Email: Copyright Permission

CONTRACTS-COPYRIGHT (shared) <Contracts-Copyright@rsc.org> **Mon, May 16, 2011 at 8:27 AM**
To: Ryan Picou <rpicou3@tigers.lsu.edu>

Dear Dr Picou

The Royal Society of Chemistry (RSC) hereby grants permission for the use of your paper(s) specified below in the printed and microfilm version of your thesis. You may also make available the PDF version of your paper(s) that the RSC sent to the corresponding author(s) of your paper(s) upon publication of the paper(s) in the following ways: in your thesis via any website that your university may have for the deposition of theses, via your university's Intranet or via your own personal website. We are however unable to grant you permission to include the PDF version of the paper(s) on its own in your institutional repository. The Royal Society of Chemistry is a signatory to the STM Guidelines on Permissions (available on request).

Please note that if the material specified below or any part of it appears with credit or acknowledgement to a third party then you must also secure permission from that third party before reproducing that material.

Please ensure that the thesis states the following:

Reproduced by permission of The Royal Society of Chemistry

and include a link to the paper on the Royal Society of Chemistry's website.

Please ensure that your co-authors are aware that you are including the paper in your thesis.

Regards

Gill Cockhead

Contracts & Copyright Executive

Gill Cockhead (Mrs), Contracts & Copyright Executive

Royal Society of Chemistry, Thomas Graham House

Science Park, Milton Road, Cambridge CB4 0WF, UK

Tel +44 (0) 1223 432134, Fax +44 (0) 1223 423623

http://www.rsc.org

-----Original Message-----
From: Ryan Picou [mailto:rpicou3@tigers.lsu.edu]
Sent: 16 May 2011 13:56
To: CONTRACTS-COPYRIGHT (shared)
Subject: Website Email: Copyright Permission

To: Contracts

This Email was sent from the following RSC.ORG page:

I am preparing my Ph.D. dissertation at Louisiana State Univeristy and would like to my publication listed below in my dissertation.

"Analysis of monomeric Abeta (1-40) peptide by capillary electrophoresis"

Can you please grant me permission or assist me in determining who could grant me this permission?

Thank you for your time.

Ryan Picou

Membership No. :

DISCLAIMER:

ELSEVIER LICENSE
TERMS AND CONDITIONS

Oct 11, 2011

This is a License Agreement between Ryan A Picou ("You") and Elsevier ("Elsevier") provided by Copyright Clearance Center ("CCC"). The license consists of your order details, the terms and conditions provided by Elsevier, and the payment terms and conditions.

All payments must be made in full to CCC. For payment instructions, please see information listed at the bottom of this form.

Supplier	Elsevier Limited The Boulevard,Langford Lane Kidlington,Oxford,OX5 1GB,UK
Registered Company Number	1982084
Customer name	Ryan A Picou
Customer address	10170 Hillmont Ave Baton Rouge, LA 70810
License number	2765961156703
License date	Oct 11, 2011
Licensed content publisher	Elsevier
Licensed content publication	Journal of Chromatography B
Licensed content title	Analysis of Aβ (1-40) and Aβ (1-42) monomer and fibrils by capillary electrophoresis
Licensed content author	Ryan A. Picou,Indu Kheterpal,Amber D. Wellman,Madhavi Minnamreddy,Ginger Ku,S. Douglass Gilman
Licensed content date	15 March 2011
Licensed content volume number	879
Licensed content issue number	9-10
Number of pages	6
Start Page	627
End Page	632
Type of Use	reuse in a thesis/dissertation
Portion	full article
Format	both print and electronic
Are you the author of this Elsevier article?	Yes
Will you be translating?	No
Order reference number	

Title of your thesis/dissertation	ANALYSIS OF AMYLOID BETA (Aβ) PEPTIDES BY CAPILLARY ELECTROPHORESIS AND LASER-INDUCED FLUORESCENCE ANISOTROPY DETECTION
Expected completion date	Dec 2011
Estimated size (number of pages)	160
Elsevier VAT number	GB 494 6272 12
Permissions price	0.00 USD
VAT/Local Sales Tax	0.0 USD / 0.0 GBP
Total	0.00 USD
Terms and Conditions	

INTRODUCTION

1. The publisher for this copyrighted material is Elsevier. By clicking "accept" in connection with completing this licensing transaction, you agree that the following terms and conditions apply to this transaction (along with the Billing and Payment terms and conditions established by Copyright Clearance Center, Inc. ("CCC"), at the time that you opened your Rightslink account and that are available at any time at http://myaccount.copyright.com).

GENERAL TERMS

2. Elsevier hereby grants you permission to reproduce the aforementioned material subject to the terms and conditions indicated.

3. Acknowledgement: If any part of the material to be used (for example, figures) has appeared in our publication with credit or acknowledgement to another source, permission must also be sought from that source. If such permission is not obtained then that material may not be included in your publication/copies. Suitable acknowledgement to the source must be made, either as a footnote or in a reference list at the end of your publication, as follows:

"Reprinted from Publication title, Vol /edition number, Author(s), Title of article / title of chapter, Pages No., Copyright (Year), with permission from Elsevier [OR APPLICABLE SOCIETY COPYRIGHT OWNER]." Also Lancet special credit - "Reprinted from The Lancet, Vol. number, Author(s), Title of article, Pages No., Copyright (Year), with permission from Elsevier."

4. Reproduction of this material is confined to the purpose and/or media for which permission is hereby given.

5. Altering/Modifying Material: Not Permitted. However figures and illustrations may be altered/adapted minimally to serve your work. Any other abbreviations, additions, deletions and/or any other alterations shall be made only with prior written authorization of Elsevier Ltd. (Please contact Elsevier at permissions@elsevier.com)

6. If the permission fee for the requested use of our material is waived in this instance, please be advised that your future requests for Elsevier materials may attract a fee.

7. Reservation of Rights: Publisher reserves all rights not specifically granted in the combination of (i) the license details provided by you and accepted in the course of this licensing transaction, (ii) these terms and conditions and (iii) CCC's Billing and Payment terms and conditions.

8. License Contingent Upon Payment: While you may exercise the rights licensed immediately upon issuance of the license at the end of the licensing process for the transaction, provided that you have disclosed complete and accurate details of your proposed use, no license is finally effective unless and until full payment is received from you (either by publisher or by CCC) as provided in CCC's Billing and Payment terms and conditions. If full payment is not received on a timely basis, then any license preliminarily granted shall be deemed automatically revoked and shall be void as if never granted. Further, in the event that you breach any of these terms and conditions or any of CCC's Billing and Payment terms and conditions, the license is automatically revoked and shall be void as if never granted. Use of materials as described in a revoked license, as well as any use of the materials beyond the scope of an unrevoked license, may constitute copyright infringement and publisher reserves the right to take any and all action to protect its copyright in the materials.

9. Warranties: Publisher makes no representations or warranties with respect to the licensed material.

10. Indemnity: You hereby indemnify and agree to hold harmless publisher and CCC, and their respective officers, directors, employees and agents, from and against any and all claims arising out of your use of the licensed material other than as specifically authorized pursuant to this license.

11. No Transfer of License: This license is personal to you and may not be sublicensed, assigned, or transferred by you to any other person without publisher's written permission.

12. No Amendment Except in Writing: This license may not be amended except in a writing signed by both parties (or, in the case of publisher, by CCC on publisher's behalf).

13. Objection to Contrary Terms: Publisher hereby objects to any terms contained in any purchase order, acknowledgment, check endorsement or other writing prepared by you, which terms are inconsistent with these terms and conditions or CCC's Billing and Payment terms and conditions. These terms and conditions, together with CCC's Billing and Payment terms and conditions (which are incorporated herein), comprise the entire agreement between you and publisher (and CCC) concerning this licensing transaction. In the event of any conflict between your obligations established by these terms and conditions and those established by CCC's Billing and Payment terms and conditions, these terms and conditions shall control.

14. Revocation: Elsevier or Copyright Clearance Center may deny the permissions described in this License at their sole discretion, for any reason or no reason, with a full refund payable to you. Notice of such denial will be made using the contact information provided by you. Failure to receive such notice will not alter or invalidate the denial. In no event will Elsevier or Copyright Clearance Center be responsible or liable for any costs, expenses or damage incurred by you as a result of a denial of your permission request, other than a refund of the amount(s) paid by you to Elsevier and/or Copyright Clearance Center for denied

permissions.

LIMITED LICENSE

The following terms and conditions apply only to specific license types:

15. **Translation**: This permission is granted for non-exclusive world **English** rights only unless your license was granted for translation rights. If you licensed translation rights you may only translate this content into the languages you requested. A professional translator must perform all translations and reproduce the content word for word preserving the integrity of the article. If this license is to re-use 1 or 2 figures then permission is granted for non-exclusive world rights in all languages.

16. **Website**: The following terms and conditions apply to electronic reserve and author websites:
Electronic reserve: If licensed material is to be posted to website, the web site is to be password-protected and made available only to bona fide students registered on a relevant course if:
This license was made in connection with a course,
This permission is granted for 1 year only. You may obtain a license for future website posting,
All content posted to the web site must maintain the copyright information line on the bottom of each image,
A hyper-text must be included to the Homepage of the journal from which you are licensing at http://www.sciencedirect.com/science/journal/xxxxx or the Elsevier homepage for books at http://www.elsevier.com , and
Central Storage: This license does not include permission for a scanned version of the material to be stored in a central repository such as that provided by Heron/XanEdu.

17. **Author website** for journals with the following additional clauses:

All content posted to the web site must maintain the copyright information line on the bottom of each image, and
he permission granted is limited to the personal version of your paper. You are not allowed to download and post the published electronic version of your article (whether PDF or HTML, proof or final version), nor may you scan the printed edition to create an electronic version,
A hyper-text must be included to the Homepage of the journal from which you are licensing at http://www.sciencedirect.com/science/journal/xxxxx , As part of our normal production process, you will receive an e-mail notice when your article appears on Elsevier's online service ScienceDirect (www.sciencedirect.com). That e-mail will include the article's Digital Object Identifier (DOI). This number provides the electronic link to the published article and should be included in the posting of your personal version. We ask that you wait until you receive this e-mail and have the DOI to do any posting.
Central Storage: This license does not include permission for a scanned version of the material to be stored in a central repository such as that provided by Heron/XanEdu.

18. **Author website** for books with the following additional clauses:
Authors are permitted to place a brief summary of their work online only.
A hyper-text must be included to the Elsevier homepage at http://www.elsevier.com

All content posted to the web site must maintain the copyright information line on the bottom of each image
You are not allowed to download and post the published electronic version of your chapter, nor may you scan the printed edition to create an electronic version.
Central Storage: This license does not include permission for a scanned version of the material to be stored in a central repository such as that provided by Heron/XanEdu.

19. **Website** (regular and for author): A hyper-text must be included to the Homepage of the journal from which you are licensing at http://www.sciencedirect.com/science/journal/xxxxx. or for books to the Elsevier homepage at http://www.elsevier.com

20. **Thesis/Dissertation**: If your license is for use in a thesis/dissertation your thesis may be submitted to your institution in either print or electronic form. Should your thesis be published commercially, please reapply for permission. These requirements include permission for the Library and Archives of Canada to supply single copies, on demand, of the complete thesis and include permission for UMI to supply single copies, on demand, of the complete thesis. Should your thesis be published commercially, please reapply for permission.

21. **Other Conditions**:

v1.6

If you would like to pay for this license now, please remit this license along with your payment made payable to "COPYRIGHT CLEARANCE CENTER" otherwise you will be invoiced within 48 hours of the license date. Payment should be in the form of a check or money order referencing your account number and this invoice number RLNK500643466.
Once you receive your invoice for this order, you may pay your invoice by credit card. Please follow instructions provided at that time.

Make Payment To:
Copyright Clearance Center
Dept 001
P.O. Box 843006
Boston, MA 02284-3006

For suggestions or comments regarding this order, contact RightsLink Customer Support: customercare@copyright.com or +1-877-622-5543 (toll free in the US) or +1-978-646-2777.

Gratis licenses (referencing $0 in the Total field) are free. Please retain this printable license for your reference. No payment is required.

VITA

Ryan Andrew Picou was born in Houma, Louisiana. The grade schools he attended were Bourg Elementary, Montegut Middle and South Terrebonne High. After graduating high school in 2001, he studied chemistry at Nicholls State University in Thibodaux, Louisiana, where he earned a Bachelor of Science degree in chemistry in 2005. He then attended Louisiana State University, where he is pursuing a doctorate degree in chemistry.